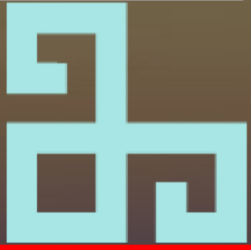


ISSN 1694-7398
e-ISSN

www.journals.manas.edu.kg

June 2019

Volume 7, Issue 1



MJEN

*MANAS
JOURNAL OF
ENGINEERING*



BISHKEK



ISSN: 1694- 7398
e-ISSN: 1694- 7398
Year: 2019
Volume: 7
Issue: 1
<http://journals.manas.edu.kg>
journals@manas.edu.kg

PUBLICATION PERIOD

Manas Journal of Engineering (MJEN) is published twice year, MJEN is a peer reviewed journal.

OWNERS Kyrgyz - Turkish Manas University
Prof. Dr. Sebahattin BALCI
Prof. Dr. Asilbek KULMIRZAYEV

EDITOR Prof. Dr. Ali Osman SOLAK

ASSOCIATE EDITOR Prof. Dr. Fahreddin ABDULLAYEV

FIELD EDITORS

Prof. Dr. Asilbek ÇEKKEEV	(Mathematics, Topology)
Prof. Dr. Anarkül URDALETOVA	(Mathematics)
Prof. Dr. İbrahim İlker ÖZYİĞİT	(Biotechnology, Molecular Biology and Genetics)
Prof. Dr. Osman TUTKUN	(Chemistry and Chemical Engineering)
Assoc. Prof. Dr. Anarseyit DEYDİEV	(Food Engineering, Food Technology)
Assoc. Prof. Dr. Gülbübü KURMANBEKOVA	(Biology, Biochemistry)
Assoc. Prof. Dr. Raimbek SULTANOV	(Computer Engineering, Information Technology)
Asist. Prof. Dr. Emil OMURZAKOĞLU	(Nanoscience, Nanotechnology, Nanomaterials)
Asist. Prof. Dr. Rita İSMAİLOVA	(Computer Engineering, Information Technology)

EDITORIAL BOARD

Prof. Dr. Ali Osman SOLAK	(Chemistry)
Prof. Dr. Selahattin GÜLTEKİN	(Chemical Engineering)
Prof. Dr. Zarlík MAYMEKOV	(Environmental and Ecological Engineering)
Prof. Dr. Coşkan ILICALI	(Food Engineering)
Prof. Dr. Ulan BİRİMKULOV	(Computer Engineering)
Prof. Dr. Fahreddin ABDULLAEV	(Applied Mathematics and Informatics)
Assoc. Prof. Dr. Tamara KARAŞEVA	(Physics)

EDITORIAL ASSISTANTS Assit. Prof. Dr.Rita İSMAİLOVA
Dr. Ruslan ADİL AKAI TEGİN
Jumagul NURAKUN KYZY

CORRESPONDENCE ADDRESS

Kyrgyz Turkish Manas University
Mira Avenue 56 Bishkek, KYRGYZSTAN
URL: <http://journals.manas.edu.kg>
e-mail: journals@manas.edu.kg
Tel : +996 312 492763- Fax: +996 312 541935



Contents

<i>Vuslat Sarıkaya Osman Tutkun Kurmancan Kaparova</i>	<i>Separation of chromium and nickel ions by supported liquid membranes using TOA as carrier</i>	<i>1-6</i>
<i>Iredia D. Erhunmwun Monday J. Omoregie</i>	<i>Determination of the temperature distribution in a rectangular cooling fin using the finite element method</i>	<i>7-12</i>
<i>Hava Çavuşoğlu Vatansever Ayşegül Ersoy Meriçboyu</i>	<i>Production of antibacterial polyvinylpyrrolidone nanofibers containing silver nanoparticles via electrospinning method</i>	<i>13-23</i>
<i>Jamila Smanalieva Zhyldyzai Ozbekova Asylbek Kulmyrzaev Peter Fischer</i>	<i>Investigation of fatty acid composition, thermal and rheological behavior of yak, cow and horse fats</i>	<i>24-33</i>
<i>Tarih Eren Babür Kemal Kaan Tekinşen Ümit Gürbüz</i>	<i>Some quality qualifications of cooked meat sous vide in the storage process</i>	<i>34-41</i>
<i>Gizem Eker Sanlı Busra Tandogan</i>	<i>Determination of soil pollution derived from polychlorinated biphenyls (PCBs) in Bursa: spatial and temporal variations</i>	<i>42-51</i>
<i>Asan Omuraliev Ella Abylaeva</i>	<i>Two-dimensional parabolic problem with a rapidly oscillating free term</i>	<i>52-59</i>
<i>Dağıstan Şimşek Burak Oğul</i>	<i>Solutions of the system of maximum difference equations</i> $x_{n+1} = \max \left\{ \frac{1}{x_{n-1}}, \frac{y_n}{x_n} \right\}; y_{n+1} = \max \left\{ \frac{1}{y_{n-1}}, \frac{x_n}{y_n} \right\}$	<i>60-67</i>

Separation of chromium and nickel ions by supported liquid membranes using TOA as carrier

Vuslat Sarıkaya¹, Osman Tutkun^{2,*}, Kurmancan Kaparova³

¹ Sakarya University, Faculty of Science, 54187 Adapazarı, Türkiye

^{2,*} Kyrgyz-Turkish Manas University, Dep. Chem. Engineering, Bishkek, Kyrgyzstan. tutkun@sakarya.edu.tr, ORCID: 0000-0001-6585-9228.

³ Kyrgyz-Turkish Manas University, Dep. Chem. Engineering, Bishkek, Kyrgyzstan.

ABSTRACT

The extensive use of chromium in leather tanning, metallurgy, electroplating and other industries has resulted in the release of aqueous chromium to the subsurface at numerous sites. Cr (VI) has received considerable attention owing to its extensive industrial applications and has long been recognised as a toxic substance due to its strong oxidising potential and the ease with which it can cross the biological membranes. In recent years the application of various solvent extraction technologies to the removal and concentration of chromium have been widely studied; chemical precipitation, ion exchange, reverse osmosis, diffusion dialysis, adsorption, liquid membrane technique are some of the alternatives that have been reported in the literature. Recently supported liquid membrane (SLM) extraction is an alternative to conventional solvent extraction due to its advantages like high selectivity, operational simplicity, low solvent inventory, low energy consumption, zero effluent discharge and combination of extraction and stripping into one single unit. In this work the selective separation of chromium from acidic media, containing the mixtures of chromium and nickel by SLM was investigated using TOA (tri-octylamine) as carrier. The liquid membrane was consisted of the desired concentration of an extractant (TOA), a modifier (TBP), and a diluent (chloroform, kerosene, cyclohexane). The membrane support was microporous hydrophobic polypropylene Celgard 2500. Such parameters as, the solvent type, feed solution pH, extractant (TOA) concentration, modifier (TBP) concentration and temperature were experimentally studied and the optimum conditions were determined. The permeation coefficients (P) and the initial fluxes of chromium (J_0) were calculated. Separation factors of chromium over nickel was calculated from the experimental measurements.

ARTICLE INFO

Research article

Received: 24.04.2019

Accepted: 20.05.2019

Keywords:

Supported liquid membranes, chromium-nickel separation, tri-octylamine (TOA), TBP, solvent extraction

*Corresponding author

1. Introduction

The extensive use of chromium in leather tanning, metallurgy, electroplating and other industries has resulted in the release of aqueous chromium to the subsurface at numerous sites. Cr (VI) has received considerable attention owing to its extensive industrial applications and has long been recognised as a toxic substance due to its strong oxidising potential and the ease with which it can cross the biological membranes. In recent years the application of various solvent extraction technologies to the removal and concentration of chromium have been widely studied; chemical precipitation, ion exchange, reverse osmosis, diffusion dialysis, adsorption,

liquid membrane technique are some of the alternatives that have been reported in the literature [1].

Recently supported liquid membrane (SLM) extraction is emerging as an alternative to conventional solvent extraction due to its advantages like high selectivity, operational simplicity, low solvent inventory, low energy consumption, zero effluent discharge and combination of extraction and stripping into one single unit.

In this work the selective separation of chromium from acidic media, containing the mixtures of chromium and nickel by SLM was investigated using TOA (tri-octylamine) as carrier. The liquid membrane was consisted of the desired

concentration of an extractant (TOA), a modifier (TBP), and a diluent (chloroform, kerosene, cyclohexane). The membrane support was microporous hydrophobic polypropylene Celgard 2500. Such parameters as, the solvent type, feed solution pH, extractant (TOA) concentration, modifier (TBP) concentration and temperature were experimentally studied and the optimum conditions were determined. The permeation coefficients (P) and the initial fluxes of chromium (J_0) were calculated. Separation factors of chromium over nickel was calculated from the experimental measurements.

2. Experimental

2.1. Chemicals

As ion carrier of chromium, TOA (Merck) was used. $K_2Cr_2O_7$, $NiSO_4 \cdot 6H_2O$, NaOH, chloroform, xylene, n-decanol, TBP are of analytical grade (Merck) and all the stock solutions for chromium and nickel were prepared by dissolving the salts in distilled water.

2.2. Flat-sheet supported liquid membrane preparation and measurements

The permeation coefficient (P) and initial flux (J_0), from C-t curves, were calculated from Eqs. (1) and (2) :

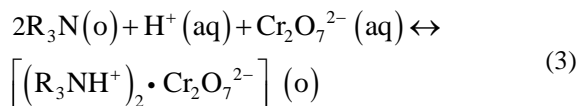
$$\ln \frac{C}{C_0} = - \frac{A\varepsilon}{V_F} P t \quad (1)$$

$$J_0 = - \left(\frac{dC}{dt} \right)_0 \left(\frac{V_F}{A\varepsilon} \right) \quad (2)$$

where V_F is the volume of the feed phase, ε is the porosity of membrane support, C and C_0 are the concentrations of cobalt in the feed phase at elapsed time and time zero, respectively, and t is the elapsed time. $(dC/dt)_0$ is the slope at $t = 0$, V_F is the volume of the feed solution. A is the membrane area.

Amines are the general reagents among the extractants which form ion-pairs and known as basic extractant types, and extract metal ions according to an ion association principle. The chemical reactions occurring on the feed and stripping side of membrane are given below :

Feed side reaction:



If the complex formed, as shown in Eq. 3, diffuses through the membrane toward the strip side, the stripping reaction for the complex with an alkaline solution is expressed by Eq. 4:

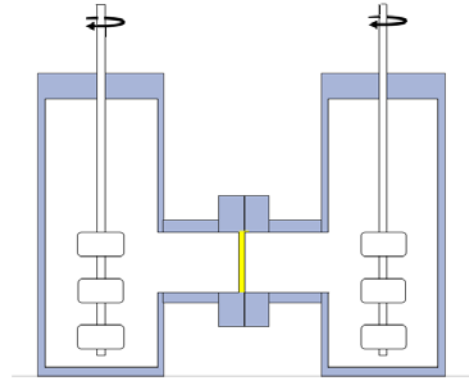
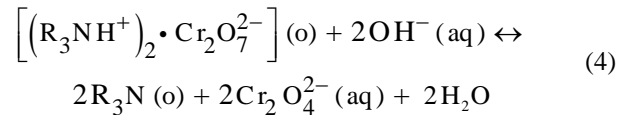


Figure 1. Schematic diagram of experimental apparatus.

Competitive transport of the equimolar and non-equimolar mixture of Cr and Ni ions across the SLM from the aqueous solutions were studied using a two-compartment permeation cell, made from a pyrex glass, with flat-sheet membranes of 12.56 cm^2 area (A), as shown schematically in Fig. 1. In all experiments the supports used for the liquid membranes were microporous hydrophobic polypropylene Celgard 2500 (Celgard Inc., USA) $25 \mu\text{m}$ thick, $0.209 \mu\text{m} \times 0.054 \mu\text{m}$ pore size and 55 % porosity. The support was soaked for 18 hours in a membrane solution of the desired composition, then leaving them to drip for a few seconds before being placed in the SLM cell. TBP was used as a modifier to improve the membrane performance. The volumes of both aqueous feed and strip phases were 250 mL. Various feed solutions were prepared by adding both chromium and nickel salts to study the effect of feed composition. The feed and stripping phases were mechanically stirred at the desired mixing speeds at $20 \pm 1^\circ\text{C}$ to avoid concentration polarisation conditions at the membrane interfaces and in the bulk of the solutions. During the transport experiments in SLM system, the samples of feed and strip phases (about 1 mL) were periodically removed for determination of Cr and Ni concentration by atomic absorption spectroscopy (Shimadzu 6701GF, Japan). The feed phase pH measurements were determined with a Schott model CG840 pH meter (Germany). Membrane permeabilities were determined by monitoring chromium and nickel concentrations in the feed phase as a function of time.

3. Results and discussion

3.1. Effect of diluent

The influence of the diluent on both the stability and efficiency of supported liquid membranes for the transport of metal ions has been reported [2-5]. Experiments were carried out for separation and extraction of chromium from the

aqueous solutions. The results obtained indicate that TOA with TBP is a more effective carrier for chromium in chloroform than others as indicated in Fig. 2.

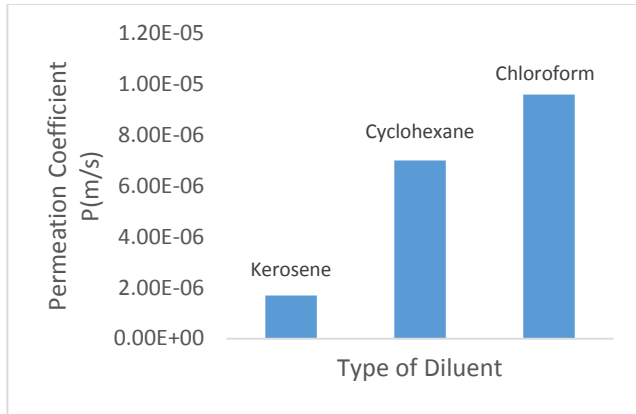


Figure 2. The effect of diluent (Extractant (TOA): 5 % w/w; TBP: 20 w/w %; Feed phase: 500 mg/L Cr^{6+} ; 500 mg/L Ni^{2+} ; Feed soln.pH: 0.5; Feed stirring speed: 1200 min^{-1} ; Strip phase stirring speed: 1200 min^{-1} ; Strip solution: 2 w/w % NaOH; Temp.: 20°C; Membrane support: Celgard 2500)

3.2. Effect of feed solution pH

In order to assess the role of the pH on separation of chromium from the equimolar and nonequimolar mixtures of chromium and nickel, pH variation studies in the range of 0.5-5 were carried out, as indicated in Fig. 3. As seen from Fig. 3, the permeation coefficient decreased from 2.77×10^{-5} to 0.34×10^{-5} m/s with increase of pH from 0.5 to 5.0. The increase in proton concentration, that is a decrease in pH, will lead to increased formation of the complex, $(R_3NH^+)_2 \cdot Cr_2O_7^{2-}$ that causes to increase the diffusional resistance and hence the permeation coefficient decreases [5]. On the other hand, the decrease in the coefficient with the increase in pH can be explained by the fact that the concentration of the protonated tertiary amine, R_3NH^+ decreases due to the less availability of proton and thus the adduct, $(R_3NH^+)_2 \cdot Cr_2O_7^{2-}$ concentration will decrease, as described by Eq. 3. As a result, the flux will decrease.

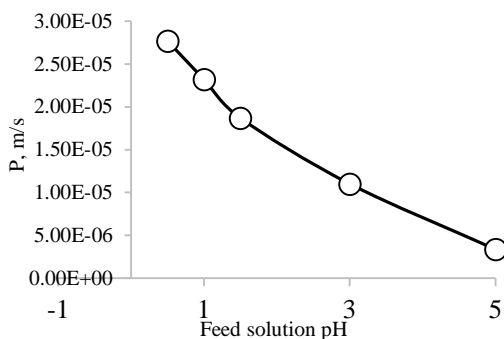


Figure 3. Effect of feed pH on Cr permeation coefficient (Diluent (Chloroform): 75 % w/w; Extractant (TOA): 5 % w/w; TBP: 20

w/w %; Feed phase: 500 mg/L Cr^{6+} ; 500 mg/L Ni^{2+} ; Feed stirring speed: 1200 min^{-1} ; Strip phase stirring speed: 1200 min^{-1} ; Strip solution: 2 w/w % NaOH; Temp.: 20°C; Membrane support: Celgard 2500)

3.3. Effect of TOA concentration.

As shown in Eq. (3), the chromium extraction and thereby the transport rates are dependent the carrier concentration. In order to understand the effect of carrier (TOA) concentration on the transport of chromium, the experiments were carried out at varying concentration of TOA. As shown in Fig. 4, the permeation coefficient increases with increasing carrier concentration. In facilitated transport, the metal ion transport is expected to increase with the carrier concentration which is in conformity with the behaviour at least at lower concentration range.

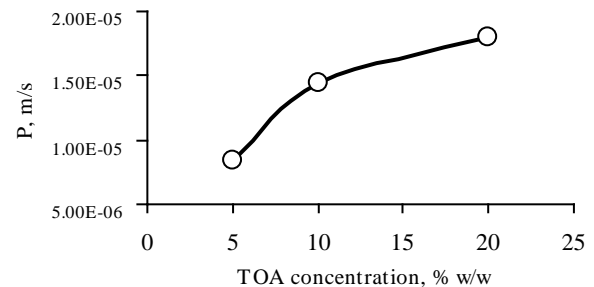


Figure 4. Effect of carrier (TOA) concentration on the permeation coefficient (Diluent (Chloroform): 55-95 %; Feed phase: 500 mg/L Cr^{6+} ; 500 mg/L Ni^{2+} ; Feed soln.pH: 0.5; Feed stirring speed: 1200 min^{-1} ; Strip stirring speed: 1200 min^{-1} ; Strip soln: 2 w/w % NaOH; Temperature: 20°C; Membrane support: Celgard 2500).

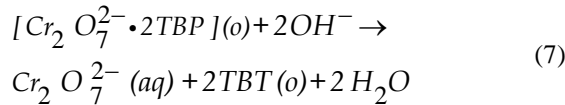
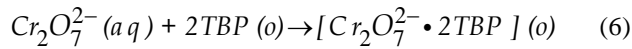
3.4. Synergistic effect of solvation extractant (TBP).

The combination of amines and neutral or solvation extractants was studied in a potential extracting system for metal ions [6]. TBP variation studies in the range of 0-40 % w/w were carried out, as indicated in Fig. 5. Fig. 5 shows that there is a synergic effect, from which the flux of cobalt, J_o is increased when carriers are used. The increase in TBP concentration increases the Cr flux since the complex diffusivity, as described by Eq. (5), in the membrane phase increases due to a decrease in the membrane viscosity [7]. According to Marcus [8], however, an adduct between the complex of Eq. (6) a neutral ligand, like TBP, could also be formed in the SLM. This view is also supported by Biswas and Basu [9] that the nature of the extracted adduct in presence of combined extractant can be expected to be $[(R_3NH^+)_2 \cdot Cr_2O_7^{2-} \cdot B]$, B represents neutral extractant. Thus, the effect of B, may be described in terms of the replacement of water molecules from $[(R_3NH^+)_2 \cdot Cr_2O_7^{2-} \cdot xH_2O]$. This leads an adduct formation which is responsible for the enhanced extraction into the organic phase. However, De Haas et al. [10] give the

extraction and stripping reactions for TBP by Eqs. (6) and (7), respectively.

$$D = kT / \eta \quad (5)$$

where D : diffusion coefficient, η : viscosity and, T : temperature.



From Fig. 3 it can be seen that the value of the flux increases up to 25 % w/w TBP in the membrane and then it decreases. The increase in TBP concentration, in fact, causes the viscosity of membrane solution, having TOA as extractant, to decrease and thus the Cr flux increases up to a certain level that the membrane solution becomes saturated or viscous again.

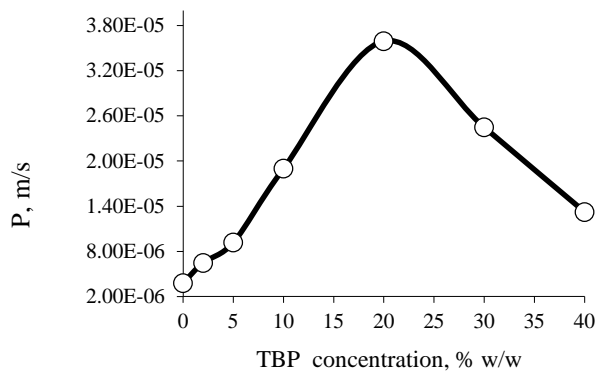


Figure 5. Synergistic effect of neutral or solvation extractant (TBP) conc. on permeation coefficient (Diluent (Chloroform): 55-95 %; Extractant (TOA): 5 %; Feed phase: 500 mg/L Cr^{6+} ; 500 mg/L Ni^{2+} ; Feed soln.pH: 0.5; Feed stirring speed: 1200 min^{-1} ; Strip stirring speed: 1200 min^{-1} ; Strip soln: 2 w/w % NaOH; Temperature: 20°C; Membrane support: Celgard 2500).

3.5. Effect of strip phase (NaOH) concentration.

The strength of the strip phase for the transported Cr (VI) could have a significant effect on the efficiency and selectivity of the Cr (VI) transport. The stripping efficiency of the sodium hydroxide solution in the receiving phase was studied in the range 0-10 % w/v (0-2.5 M). The results are shown in Fig. 6. The figure indicates that with increase in concentration of NaOH, the permeation of chromium increases up to 5 % NaOH concentration and decreases after that. This may be due to the saturation of the driving force for diffusion through the SLM owing to an increase of chromium complexes concentration at the membrane-strip interface, as reported also elsewhere [11].

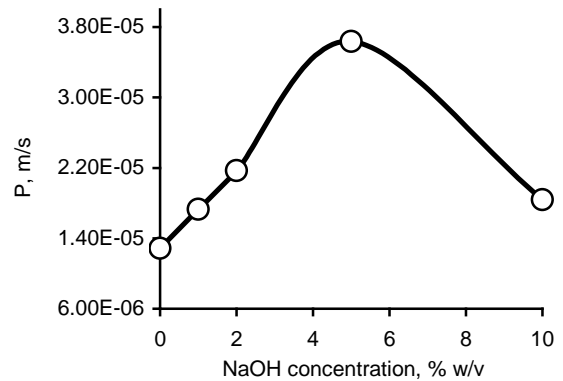


Figure 6. Synergistic effect of neutral or solvation extractant (TBP) conc. on permeation coefficient (Diluent (Chloroform): 55-95 %; Extractant (TOA): 5 %; Feed phase: 500 mg/L Cr^{6+} ; 500 mg/L Ni^{2+} ; Feed soln.pH: 0.5; Feed stirring speed: 1200 min^{-1} ; Strip stirring speed: 1200 min^{-1} ; Strip soln: 2 w/w % NaOH; Temperature: 20°C; Membrane support: Celgard 2500).

3.6. Effect of system temperature.

The chromium permeation through SLM was also examined against temperature, between 25°C and 50°C, as shown in Fig. 7. From Fig. 7, the Cr permeation or flux increases with the increase of temperature. The increase in temperature causes the complex diffusivity in the membrane phase to increase and the membrane viscosity to decrease, as given in Eq. 5, and thus the Cr flux increases. This indicates that the diffusional resistance to mass transfer is of prime importance.

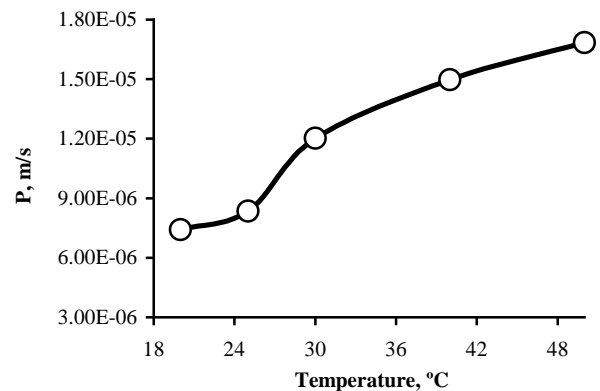


Figure 7. Effect of temperature on permeation coefficient (Diluent (Chloroform): 90 %; Extractant (TOA): 5 %; Feed phase: 500 mg/L Cr^{6+} ; 500 mg/L Ni^{2+} ; Feed soln. pH: 2; Feed stirring speed: 1200 min^{-1} ; Strip stirring speed: 1200 min^{-1} ; Strip soln: 2 w/w % NaOH; Membrane support: Celgard 2500).

3.7. Optimum conditions.

The following results were obtained from examining the experimental parameters :

- Diluent: Chloroform

- Feed solution pH: 0.5
- Feed solution stirring rate: 1200 min⁻¹
- Stripping solution stirring rate: 1200 min⁻¹
- Extractant (TOA) concentration: 10 % w/w
- Neutral or solvation extractant (TBP) concentration: 20 %
- Temperature: 50°C
- Stripping solution: 2 % w/w NaOH
- Polymer support: Celgard 2500 ($\epsilon = 0.55$; $\Phi = 0.29 \times 0.054 \mu\text{m}$; $\delta = 25 \mu\text{m}$)

3.8. Membrane selectivity.

Under the optimum conditions, the effect of feed concentration, both equimolar and non-equimolar, on the extraction rate or separation of chromium over nickel have been experimentally studied. The separation factors, $\alpha_{Cr/Ni}$, Eq. 8, of Cr over Ni, based on the initial feed composition, have been determined for 8 hours, under the optimum conditions, and shown for the both equimolar and non-equimolar feed mixtures in Table 1.

Table 1. Separation factors, $\alpha_{Cr/Ni}$ of Cr over Ni, based on the initial feed solutions, under the optimum conditions.

Equimolar feed mixtures,	$\alpha_{Cr/Ni}$	Nonequimolar feed mixtures,	$\alpha_{Cr/Ni}$
100 mg/L Cr + 100 mg/L Ni	8.0	100 mg/L Cr + 1000 mg/L Ni	43.4
200 mg/L Cr + 200 mg/L Ni	18.3	200 mg/L Cr + 1000 mg/L Ni	50.2
500 mg/L Cr + 500 mg/L Ni	27.6	400 mg/L Cr + 1000 mg/L Ni	71.7
700 mg/L Cr + 700 mg/L Ni	36.3	600 mg/L Cr + 1000 mg/L Ni	44.8
1000 mg/L Cr + 1000 mg/L Ni	28.0	800 mg/L Cr + 1000 mg/L Ni	34.8

$$\alpha_{Cr/Ni} = \frac{(C_{Cr}/C_{Ni})_{strip}}{(C_{Cr}/C_{Ni})_{feed,o}} \quad (8)$$

The concentration-time profiles of Cr (VI) and Ni transport for equimolar feed mixtures of 2000 mg/L each, was also studied over a time period of 46 hours, in the optimum conditions, as depicted in Fig. 8. From Fig. 8, it is confirmed that under the optimum conditions, almost all Cr (VI) was transported from the feed phase into the receiving phase. On the other hand, the selective separation of chromium from nickel is reasonably possible, as indicated in Fig. 8.

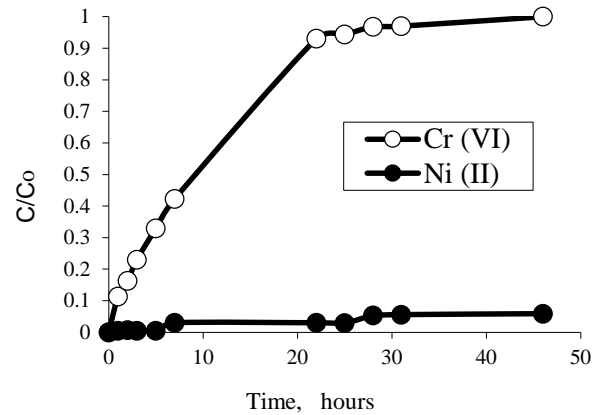


Figure 8. Relative transport rates of Cr and Ni through Celgard 2500 membrane containing 10 % TOA and 20 % TBP in chloroform (Feed phase: 2000 mg/L Cr⁶⁺; 2000 mg/L Ni²⁺; optimum conditions).

4. Conclusions

Supported liquid membrane process using TOA plus TBP to extract and separate Cr from the acidic feed solutions has been studied. From this study the following conclusions can be drawn:

- The optimum conditions are determined experimentally as stated above.
- At the optimum conditions, the extraction of chromium is achieved with the efficiencies of 97.6 % and 57.1 % for the equimolar feed mixtures of 200 mg/L Cr + 200 mg/L Ni, and 700 mg/L Cr + 700 mg/L Ni, respectively, within 8 hours, and the separation factors of Cr over Ni are 18.3 and 36.3. For nonequimolar feed mixtures of 100 mg/L Cr + 1000 mg/L Ni, and 800 mg/L Cr + 1000 mg/L Ni, the extraction efficiencies of cobalt are 100.0 % and 66.4 %, respectively, and the separation factors of Cr are 43.4 and 34.8 in 8 hrs.
- The extraction rate of cobalt increases with the increase of system temperature. The initial mass flux of Cr increased from 3.79×10^{-6} kg/m²s to 9.25×10^{-6} kg/m²s, as the temperature increased from 20°C to 50°C. The separation factor $\alpha_{Cr/Ni}$ also increases from 21.3 to 27.8 in 8 hours. It also shows that the diffusional resistance in the liquid membrane phase is of a great importance.

References

- [1]. Kongolo K., Mwena M.D., Banza A.N., Gock E., "Cobalt and Zinc Recovery from Copper Sulphate Solution by Solvent Extraction", Miner. Eng. 16, (2003), 1371-1374.

- [2]. Kumbasar R.A., Tutkun O., "Separation and Concentration of Gallium from Acidic Leach Solutions Containing Various Metal Ions by Emulsion Type of Liquid Membranes Using TOPO as Mobile Carrier", *Hydrometallurgy*, 75 (1-4), (2004), 111-121.
- [3]. Molinari R., Drioli E., Pantano G., "Stability and Effect of Diluents in Supported Liquid Membranes for Cr (III), Cr (VI) and Cd (II) Recovery", *Sep. Sci. Technol.* 24 (12-13), (1989), 1015-1032.
- [4]. El Aamrani F.Z., Kumar A., Beyer L., Cortina J.L., Sastre A.M., "Uphill Permeation Model of Gold (III) and Its Separation from Base Metals Using Thiourea Derivatives as Ionophores Across a Liquid Membrane", *Hydrometallurgy*, 50, (1998), 315-324.
- [5]. Sastre A.M., Kumar A., Shukla J. P., Singh R. K., "Uphill Permeation Model of Gold (III) and Its Separation From Base Metals Using Thiourea Derivatives as Ionophores Across a Liquid Membrane", *Sep. Purif. Methods*, 27, (1998), 213-298.
- [6]. Gaikwad A.G., "Synergetic Transport of Europium Through a Contained Supported Liquid Membrane Using Trioctylamine and Tributyl Phosphate as Carriers", *Talanta*, 63, (2004), 917-926.
- [7]. Campderros M.E., Marchese J., *Hydrometallurgy*, "Transport of Niobium (V) Through a TBP-Alamine 336 Supported Liquid Membrane from Chloride Solutions", 61 (2001), 89-95.
- [8]. Marcus A.S., *Ion Exchange and Solvent Extraction of Metal Complexes*, New York: Interscience, (1969).
- [9]. Biswas S., Basu S., "Synergic Extraction of Uranium (VI) by Combination of Tri-iso-octylamine and Neutral Donors", *Radioanal. Nucl. Chem.*, 242 (1), (1998), 387-394
- [10]. De Haas K.S., Brink P.A., Crowther P., "Solvent Extraction of Iron, Cobalt and Nickel from Thiocyanate Melts", *Inorg. Nucl. Chem.* 33 (12), (1971), 4301-4309.
- [11]. Venkateswaran P., Palanivelu K., "Recovery Of Lead (II) From Aqueous Solutions by Flat Sheet Supported Liquid Membrane: Batch Experimental Studies and Transport Modeling", *Hydrometallurgy*, 78, (2005), 107-115.

Determination of the temperature distribution in a rectangular cooling fin using the finite element method

Iredia D. Erhunmwun^{1,*}, Monday J. Omoregie²

^{1,*}Department of Production Engineering, University of Benin, Benin City, Nigeria. iredia.erhunmwun@uniben.edu, ORCID: 0000-0002-0497-8220

² Department of Quantity Surveying, Faculty of Environmental Science, University of Benin, P.M.B. 1154, Benin City, Nigeria. monday.omoregie@uniben.edu

ABSTRACT

This paper involves the use of the Galerkin finite element method to determine the temperature distribution in a rectangular cooling fin. The governing equation is a one-dimensional second order differential equation. The result shows that the temperature at the tip of the rectangular cooling fin which was 100°C and begins to drop as it proceeds to the other end of the rectangular cooling fin which is 61.5518°C at 0.1m. The result obtained from the finite element solutions when compared with the analytical solution, shows that the accuracy was very high with the highest percentage error of 0.000432875. It can be stated that the finite element solution is an accurate method for determining the temperature distribution in a rectangular cooling fin.

ARTICLE INFO

Research article

Received: 18.04.2019

Accepted: 16.05.2019

Keywords:

Cooling fins,
heat transfer,
finite element method,
analytical solution.

*Corresponding author

1. Introduction

Rectangular fins are used to remove heat from the surface of a body by conduction along the fins and convection from the surface of the fins into the surroundings. Fins are the most effective instrument for increasing the rate of heat transfer. As we know, they increase the area of heat transfer and cause an increase in the transferred heat amount. A complete review on this topic is presented by Kraus et al. [1]. Fins are widely used in many industrial applications such as air conditioning, refrigeration, automobile, chemical processing equipment and electrical chips.

Although there are various types of the fins, but the rectangular fin is widely used among them, probably, due to simplicity of its design and its easy manufacturing process. For ordinary fins problem, the thermal conductivity assumes to be constant, but when temperature difference between the tip and base of the fin is large, the effect of the temperature on thermal conductivity must be considered. Also, it is very realistic that to consider the heat generation in the fin (due to electric current or etc.) as a function of temperature. Domairi and Fazeli [2] used the least squares method for predicting the performance of a longitudinal fin with temperature-dependent

internal heat generation and thermal conductivity and they compared their results by Homotopy Perturbation Method (HPM), Variational Iteration Method (VIM) and double series regular perturbation method and found that the least squares method was a simpler method.

Razani and Ahmadi [3] considered circular fins with an arbitrary heat source distribution and a nonlinear temperature-dependent thermal conductivity and obtained the results for the optimum fin design. Unal [4] conducted an analytical study of a rectangular and longitudinal fin with temperature-dependent internal heat generation and temperature-dependent heat transfer coefficient. Another study about this issue (convective fin with both temperature dependent thermal conductivity and internal heat generation) was performed by Shouman [5]. Kundu [6] had solved a problem about thermal analysis and optimization of longitudinal and pin fins of uniform thickness subject to fully wet, partially wet and fully dry surface conditions. Domairry and Fazeli [7] solved the nonlinear straight fin differential equation by the Homotopy Analysis Method (HAM) to evaluate the temperature distribution and fin efficiency. Also, temperature distribution for annular fins with temperature-dependent thermal conductivity was studied by Ganji et al. [8] using HPM. The

effects of temperature-dependent thermal conductivity of a moving fin with considering the radiation losses have been studied by Aziz and Kaani [9]. Furthermore, Bouaziz and Aziz [10] introduced a double optimal linearization method (DOLM) to get a simple and accurate solution for the temperature distribution in a straight rectangular convective–radiative fin with temperature-dependent thermal conductivity. Inc [11] used HAM to obtain the efficiency of straight fin with temperature dependent thermal conductivity.

The concept of Differential Transformation Method (DTM) was firstly introduced by Ghafoori et al. [12] which was used to solve both linear and nonlinear initial value problems in electric circuit analysis. This method can be applied directly for linear and nonlinear differential equations without requiring linearization, discretization or perturbation and this is the main benefit of this method. Ghafoori, et al. [13] used the DTM for solving the nonlinear oscillation equation. Abdel-Halim Hassan [14] applied DTM for different systems of differential equations and he discussed the convergence of this method in several examples of linear and nonlinear systems of differential equations. Recently, analytical methods were used for solving the heat transfer through the porous fins with different geometries [15-19]. It is obvious that a number of researchers seem not to have analyzed the temperature distribution in a rectangular cooling fin. But none has attempted to use the finite element method. Hence, this paper using the finite element analysis tends to fill this gap.

2. Methodology

Consider a rectangular cooling fin. The governing equation (i.e. balance of energy) is

$$-\frac{d^2T}{dx^2} + \frac{\beta}{ka}(T - T_\infty) = 0 \tag{1}$$

where T is the temperature, k is the thermal conductivity, β is the film coefficient, a is the thickness and T_∞ is the temperature of the surrounding fluid (i.e., ambient temperature) [20].

Eq. 1 was derived by approximating the true physical situation. Therefore, the assumptions are:

- i. The temperature is a function of the x direction alone
- ii. No heat is lost from the end or from the edges
- iii. The heat flux at the surface is given by $q_x = h(T - T_a)$, where h is a constant and T depends on x [21].

The boundary conditions of the problem are

$$T(0) = T_w \quad (\text{wall temperature}) \tag{2}$$

$$\left(kA \frac{dT}{dx} \right) \Big|_{x=L} = 0 \tag{3}$$

2.1. Solution

The equations can be recast in the residual form as:

$$-\frac{d^2T}{dx^2} + \frac{\beta T}{ka} - \frac{\beta T_\infty}{ka} = 0 \tag{4}$$

In the analysis involving Finite Element method, the governing equation can only be solved if it is in order one. But the governing equation for the temperature distribution in a rectangular cooling fin is in order two, so, the need to weaken the governing equation to order one. Therefore, the weak form of eq. 4 is as shown in eq. 5.

$$\int_{x_A}^{x_B} \frac{\partial w}{\partial x} \frac{\partial T}{\partial x} dx + \frac{\beta}{ka} \int_{x_A}^{x_B} w T dx - \frac{\beta T_\infty}{ka} \int_{x_A}^{x_B} w dx - w Q_A - w Q_B = 0 \tag{5}$$

This is followed by the introduction of the interpolation functions to enable us derive the finite element model. The weak form in eq. 5 requires that the approximation chosen for T should be at least quadratic in x so that there are no terms in eq. 5 that are identically zero. Since the primary variable is simply the function itself, the Lagrange family of interpolation functions is admissible. We proposed that T is the approximation over a typical finite element domain by the expression:

$$T(x) = \sum_{j=1}^n T_j \psi_j^e(x) \quad \text{and} \quad w = \psi_i^e(x) \tag{6}$$

In Galerkin’s weighted residual method, the weighting functions are chosen to be identical to the trial functions as shown in eq. 6.

Substituting eq. 6 into eq. 5 and simplifying, eq. 5 reduces to eq. 7.

$$\sum_{j=1}^n T_j(x) \int_{x_A}^{x_A+h} \frac{\partial \psi_i}{\partial x} \frac{\partial \psi_j}{\partial x} dx + \sum_{j=1}^n T_j(x) \frac{\beta}{ka} \int_{x_A}^{x_A+h} \psi_i \psi_j dx - \frac{\beta T_\infty}{ka} \int_{x_A}^{x_A+h} \psi_i dx - w Q_A - w Q_B = 0 \tag{7}$$

$$\text{where } x_B = x_A + h \tag{8}$$

Eq. 7 is the developed finite element model. This is then used to generate the elemental matrices.

Eq. 7 can be written in the condensed form as:

$$[K_{ij}^e] \{T_j^e\} + \frac{\beta}{ka} \{M_{ij}^e\} \{T_j^e\} = \frac{\beta T_\infty}{ka} \{f_i^e\} + \{Q_i^e\} \tag{9}$$

$$\text{where } K_{ij}^e = \int_{x_A}^{x_A+h} \frac{\partial \psi_i^e(x)}{\partial x} \frac{\partial \psi_j^e(x)}{\partial x} dx \tag{10}$$

$$M_{ij}^e = \int_{x_A}^{x_A+h_e} \psi_i^e(x) \psi_j^e(x) dx \tag{11}$$

$$f_i^e = \int_{x_A}^{x_A+h_e} \psi_i^e dx \tag{12}$$

$$\psi_2(x) = \frac{4x}{h_e} \left(1 - \frac{x}{h_e}\right) \tag{14}$$

$$\psi_3(x) = -\frac{x}{h_e} \left(1 - \frac{2x}{h_e}\right) \tag{15}$$

Hence, the one-dimensional Lagrange quadratic interpolation function for Equation becomes

$$\psi_1(x) = \left(1 - \frac{x}{h_e}\right) \left(1 - \frac{2x}{h_e}\right) \tag{13}$$

where h_e = Elemental length of the rectangular cooling fin

To evaluate the K_{ij} , f_i and M_{ij} matrices, we substitute eq. 13-15 accordingly into eq. 10, 11 and 12 respectively, we have;

$$K^e = \frac{1}{3h_e^3} \begin{bmatrix} 7h_e^2 - 24h_e\xi_A + 48\xi_A^2 & -8(h_e^2 - 3h_e\xi_A + 12\xi_A^2)h_e^2 + 48\xi_A^2 & \\ -8(h_e^2 - 3h_e\xi_A + 12\xi_A^2) & 16(h_e^2 + 12\xi_A^2) & -8(h_e^2 + 3h_e\xi_A + 12\xi_A^2) \\ h_e^2 + 48\xi_A^2 & -8(h_e^2 + 3h_e\xi_A + 12\xi_A^2)7h_e^2 + 24h_e\xi_A + 48\xi_A^2 & \end{bmatrix} \tag{16}$$

$$M^e = \frac{1}{30h^3} \begin{bmatrix} 4h^4 - 30h^3\xi_A + 90h^2\xi_A^2 - 120h\xi_A^3 + 120\xi_A^4 & 2h^4 - 60h^2\xi_A^2 + 120h\xi_A^3 - 240\xi_A^4 & -h^4 + 30h^2\xi_A^2 + 120\xi_A^4 \\ 2h^4 - 60h^2\xi_A^2 + 120h\xi_A^3 - 240\xi_A^4 & 16h^4 + 480\xi_A^4 & 2h^4 - 60h^2\xi_A^2 - 120h\xi_A^3 - 240\xi_A^4 \\ -h^4 + 30h^2\xi_A^2 + 120\xi_A^4 & 2h^4 - 60h^2\xi_A^2 - 120h\xi_A^3 - 240\xi_A^4 & 4h^4 + 30h^3\xi_A + 90h^2\xi_A^2 + 120h\xi_A^3 + 120\xi_A^4 \end{bmatrix} \tag{17}$$

$$f^e = \begin{Bmatrix} \frac{h_e - x_A + \frac{2x_A^2}{h_e}}{6} \\ \frac{2(h_e^2 - 6x_A^2)}{3h_e} \\ \frac{h_e + x_A + \frac{2x_A^2}{h_e}}{6} \end{Bmatrix} \tag{18}$$

Assembly of the Matrix using four elements

The assembled K^e matrix is given as:

$$[K^e] = \frac{1}{3h_e} \begin{bmatrix} 7 & -8 & 1 & 0 & 0 & 0 & 0 & 0 & 0 \\ -8 & 16 & -8 & 0 & 0 & 0 & 0 & 0 & 0 \\ 1 & -8 & 38 & -80 & 49 & 0 & 0 & 0 & 0 \\ 0 & 0 & -80 & 208 & -128 & 0 & 0 & 0 & 0 \\ 0 & 0 & 49 & -128 & 230 & -344 & 193 & 0 & 0 \\ 0 & 0 & 0 & 0 & -344 & 784 & -440 & 0 & 0 \\ 0 & 0 & 0 & 0 & 193 & -440 & 614 & -800 & 433 \\ 0 & 0 & 0 & 0 & 0 & 0 & -800 & 1744 & -944 \\ 0 & 0 & 0 & 0 & 0 & 0 & 433 & -944 & 511 \end{bmatrix} \tag{19}$$

The assembled M^e matrix is given as:

$$M^e = \frac{h}{30} \begin{bmatrix} 4 & 2 & -1 & 0 & 0 & 0 & 0 & 0 & 0 \\ 2 & 16 & 2 & 0 & 0 & 0 & 0 & 0 & 0 \\ -1 & 2 & 68 & -178 & 149 & 0 & 0 & 0 & 0 \\ 0 & 0 & -178 & 496 & -418 & 0 & 0 & 0 & 0 \\ 0 & 0 & 149 & -418 & 1628 & -3118 & 2039 & 0 & 0 \\ 0 & 0 & 0 & 0 & -3118 & 7696 & -5038 & 0 & 0 \\ 0 & 0 & 0 & 0 & 2039 & -5038 & 10508 & -16738 & 9989 \\ 0 & 0 & 0 & 0 & 0 & 0 & -16738 & 38896 & -23218 \\ 0 & 0 & 0 & 0 & 0 & 0 & 9989 & -23218 & 138964 \end{bmatrix} \tag{20}$$

The assembled f^e matrix is given as:

$$f^e = \frac{h_c}{6} \begin{Bmatrix} 1 \\ 4 \\ 2 \\ 4 \\ 4 \\ 2 \\ 4 \\ 4 \\ 1 \end{Bmatrix} \quad (21)$$

Eq. 19, 20 and 21 are substituted into eq. 9 to obtain the temperature distribution in the rectangular cooling fin. But the assembled matrix cannot be solved directly. But with the introduction of either the boundary condition or initial conditions or a combination of both the initial and boundary conditions, the nodal values of the parameter (Temperature) can be determined.

3. Results

In other to solve this problem analytically, we recast eq. 1, 2 and 3 by introducing the following non-dimensional quantities;

$$\theta = \frac{T - T_\infty}{T_w - T_\infty}; \quad \xi = \frac{x}{L}; \quad N = \sqrt{\left(\frac{\beta L^2}{ka}\right)} \quad (22)$$

Therefore, eq. 1, 2 and 3 becomes respectively

$$-\frac{d^2\theta}{d\xi^2} + N^2\theta = 0 \quad (23)$$

$$\theta(0) = 1 \quad (24)$$

$$\left(\frac{d\theta}{d\xi}\right)_{\xi=1} = 0 \quad (25)$$

The analytical solution of the problem is given in eq. 26

$$\theta = \cosh N\xi - (\tanh N)\sinh N\xi \quad (26)$$

The data used in analysing this problem are given thus:

$$\beta = 35W / m^2 \text{ } ^\circ C, \quad k = 170W / m \text{ } ^\circ C, \quad T_0 = 100^\circ C, \\ T_\infty = 20^\circ C, \quad L = 100mm, \quad t = 1mm$$

4. Discussion

The Finite Element solutions obtained in this problem can be used to determine the temperature distribution in a rectangular cooling fin. This is as a result of substituting the appropriate values of the domains and boundary conditions into the formulated coefficient matrix equations. The results are represented in the Table 1 for both the Finite Element Solution and the analytical solution.

Table 1. Comparison between FEM solution and analytical solution.

Length (m)	T °C (FEM Solution)	T °C (Analytical Solution)	% ERROR
0.0000	100.0000	100.0000	0.0000
0.0125	89.8610	89.8614	4.3288E-04
0.0250	81.6539	81.6537	-3.1399E-04
0.0375	75.1120	75.1120	9.4111E-05
0.0500	70.0259	70.0255	-5.5540E-04
0.0625	66.2302	66.2301	-1.5269E-04
0.0750	63.6037	63.6032	-7.0786E-04
0.0875	62.0604	62.0602	-2.8332E-04
0.1000	61.5519	61.5514	-7.6003E-04

The graph of the finite element solution and the analytical solution converges as shown in Figure 1 which shows a decline in temperature as the length of the fin increases.

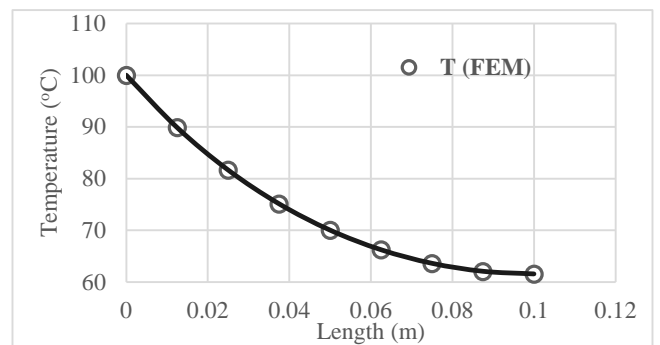


Figure 1. A graph of Temperature and Length of fin for FEM and analytical solution.

Figure 1 shows that the temperature at the tip of the rectangular cooling fin is 100°C and begins to drop as it proceeds to the other end of the rectangular cooling fin which is 61.5518°C at 0.1m. As a result of the decrease in temperature from one end of the cooling fin to the other, more heat is released into the surrounding air thereby raising the ambient temperature (T∞). This increase in the ambient temperature (T∞) has a direct relationship with the temperature in the rectangular cooling fin. This means that the higher the ambient temperature (T∞), the higher the temperature in the rectangular cooling fin. This is shown in Figure 2.

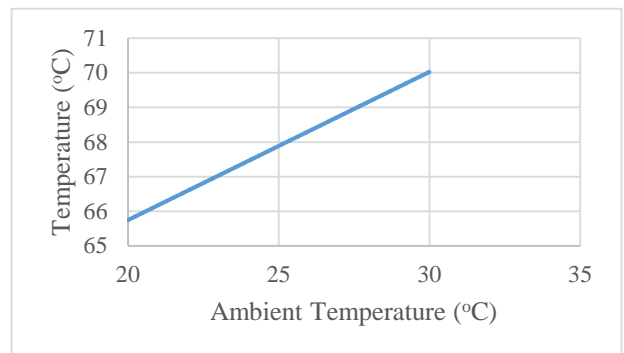


Figure 2. A graph of fin temperature against ambient temperature.

A mathematical model was developed keeping other parameters constant to show the relationship between the fin temperature and the ambient temperature. The model developed is as shown in eq. 27.

$$T = 0.4282T_{\infty} + 57.18 \quad (27)$$

It was observed that the model fits in well with a coefficient of determination (R^2) of 100%. This shows that the ambient temperature was able to account for 100% of the variation in the temperature of the rectangular cooling fin.

5. Conclusion

In this paper, the Galerkin finite element method has been used to determine the temperature distribution in a rectangular cooling fin. The results shows that finite element method is a more reliable and accurate method for determining the temperature distribution in a rectangular cooling fin successfully.

References

- [1]. Kraus A.D., Aziz A., Welty J.R. *Extended Surface Heat Transfer* John Wiley, New York, (2002).
- [2]. Aziz A., Bouaziz M.N. "A least squares method for a longitudinal fin with temperature dependent internal heat generation and thermal conductivity". *Energy Convers Manag*, 52, (2011), 2876-2882.
- [3]. Razani A., Ahmadi G. "On optimization of circular fins with heat generation". *J Frankl Inst*, 303 (2), (1977), 211-218.
- [4]. Unal H.C. "Temperature distributions in fins with uniform and non-uniform heat generation and non-uniform heat transfer coefficient". *International Journal of Heat and Mass Transfer*, 30 (7), (1987), 1465-1477.
- [5]. Shouman AR. "Nonlinear heat transfer and temperature distribution through fins and electric elements of arbitrary geometry with temperature dependent properties and heat generation". NASA technical note, TN D-4257, (1968).
- [6]. Kundu B. "Performance and optimum design analysis of longitudinal and pin fins with simultaneous heat and mass transfer: unified and comparative investigations". *Appl Therm Eng*, 27, (2007), 976-987.
- [7]. Domairry G., Fazeli M. "Homotopy analysis method to determine the fin efficiency of convective straight fins with temperature-dependent thermal conductivity". *Commun Nonlinear Sci Numer Simul*, 14, (2009), 489-499.
- [8]. Ganji D.D., Ganji Z.Z., Ganji H.D. "Determination of temperature distribution for annual fins with temperature-dependent thermal conductivity by HPM". *Therm Sci*, 15, (2011), 111-115.
- [9]. Aziz A., Khani F. "Convection–radiation from a continuously moving fin of a variable thermal conductivity". *J Frankl Inst*, 348, (2011), 640-651.
- [10]. Bouaziz M.N., Aziz A. "Simple and accurate solution for convective–radiative fin with temperature dependent thermal conductivity using double optimal linearization". *Energy Convers Manag*, 51, (2010), 2776-2782.
- [11]. Mustafa Inc, "Application of homotopy analysis method for fin efficiency of convective straight fins with temperature-dependent thermal conductivity". *Math Comput Simul*, 79, (2008), 189-200.
- [12]. Zhou J.K. "Differential Transformation Method and its Application for Electrical Circuits". Hanzhong University press, Wuhan, China, (1986).
- [13]. Ghafoori S., Motevalli M., Nejad M.G., Shakeri F., Ganji D.D., Jalaal M. "Efficiency of differential transformation method for nonlinear oscillation: comparison with HPM and VIM". *Curr Appl Phys*, 11, (2011), 965-971.
- [14]. Abdel-Halim Hassan I.H. "Application to differential transformation method for solving systems of differential equations". *Appl Math Model*, 32, (2008), 2552-2559.
- [15]. Hatami M., Ganji D.D. "Thermal behavior of longitudinal convective–radiative porous fins with different section shapes and ceramic materials (SiC and Si3N4)". *Ceram Int*, 40, (2014), 6765-6775.
- [16]. Hatami M., Ganji D.D. "Thermal and flow analysis of microchannel heat sink (MCHS) cooled by Cu–water nanofluid using porous media approach and least square method". *Energy Convers Manag*, 78, (2014), 347-358.
- [17]. Hatami M., Ganji D.D. "Investigation of refrigeration efficiency for fully wet circular porous fins with variable sections by combined heat and mass transfer analysis". *International Journal of Refrigeration*, 40, (2014), 140-151.
- [18]. Hatami M., Ganji D.D. "Thermal performance of circular convective-radiative porous fins with different section shapes and materials". *Energy Convers Manag*, 76, (2013), 185-193.
- [19]. Hatami M., Hasanpour A., Ganji D.D. "Heat transfer study through porous fins (Si3N4 and Al) with temperature-dependent heat generation". *Energy Convers Manag*, 74, (2013), 9-16.

[20]. Reddy J.N. An Introduction to the Finite Element Method, Second Edition, McGraw-Hill, Texas, (1993).

[21]. Bird R.B., Stewart W.E., Lightfoot E.N. "Transport Phenomena" Second Edition, John Wiley & Sons, Inc, New York, (2002), 310.

Production of antibacterial polyvinylpyrrolidone nanofibers containing silver nanoparticles via electrospinning method

Hava Çavuşoğlu Vatansver^{1,*}, Ayşegül Ersoy Meriçboyu²

^{1,*}Istanbul Technical University, Faculty of Chemical and Metallurgical Engineering, Department of Chemical Engineering, Istanbul, Turkey, hava.cavusoglu@gmail.com, ORCID: 0000-0003-1687-1276

² Istanbul Technical University, Faculty of Chemical and Metallurgical Engineering, Department of Chemical Engineering, Istanbul, Turkey, ORCID: 0000-0002-2254-0863

ABSTRACT

Since polymeric nanofibers find extensive usage in medical applications, the risks associated with bacterial contamination must be taken into account. In this study, the production of antibacterial polyvinylpyrrolidone (PVP) nanofibers containing silver nanoparticles (AgNPs) was achieved. For this production, AgNPs with the average diameters ranging from 5.69 nm to 14.83 nm were synthesized and characterized firstly. Then, the properties of the nanofibers produced via electrospinning method were investigated by means of scanning electron microscopy (SEM) and X-ray diffraction (XRD) techniques. The effect of AgNPs on the conductivity of electrospinning solutions were investigated. The stability of nanofiber mats were determined to show the crosslinking efficiency. Finally, antimicrobial tests against three types of microorganisms (*E. coli*, *S. aureus* and *A. niger*) were carried out according to zone of inhibition method. Antimicrobial test results proved that nanofibers containing AgNPs show inhibition against *E.coli* and *S. aureus*, while neat nanofibers not. Additionally, any antifungal activity was not observed against *A. niger*.

ARTICLE INFO

Research article

Received: 03.04.2019

Accepted: 25.04.2019

Keywords:

Silver nanoparticles, polyvinylpyrrolidone, electrospinning, nanofibers.

*Corresponding author

1. Introduction

Nanotechnology provides an opportunity for production of nanomaterials which can be in the form of metal, ceramic, polymeric or composite with at least one external dimension in the nanoscale or having internal or surface structure in the nanoscale [1]. As the size decreases to nanoscale, surface to volume ratio increases and hence surface atom fraction increases and quantum effect becomes important. Consequently, the properties of nanomaterials such as optical, electrical, mechanical, chemical, magnetic improve and differ from their atomic-molecular or bulk counterparts [1, 2].

Polymeric nanofibers have novel properties due to their large specific surface area, small pore size, high porosity, flexibility and improved mechanical structure [3]. Highly enhanced surface area, continuous and interconnected porous network of nanofiber mats provide efficient fluid absorption, adequate space for cell attachment, transportation of gases, nutrients or drugs, which are important properties in biomedical usage [3, 4]. Nanofibers

can be produced by variety of methods such as drawing, template synthesis, phase separation, self-assembly and electrospinning which are based on physical, chemical, thermal and electrostatic techniques [5]. Among these methods, electrospinning is the most attractive because of enabling easy and rapid fabrication of continuous fibers with diameters ranging from tens of nanometers to microns along with the advantages of easy set-up, cost effectiveness, allowing diameter control and variety of material usage [5-7].

Electrospinning technique uses electrostatic forces in order to form nanofibers from liquid polymer solutions or melt [6]. In this technique, the pendant drop which is fed to the nozzle gets charged by applying high voltage and it forms a liquid jet after electrostatic force overcomes surface tension. The jet elongates and dries through solvent evaporation due to undergoing physical instabilities under the electrical field and solid nanofibers are deposited on the collector at the end [6-8]. Morphology and diameter of nanofibers can be controlled by changing the electrospinning parameters which are solution parameters (e.g. concentration, molecular

weight, viscosity, surface tension), process parameters (e.g. applied voltage, tip to collector distance, flow rate) and ambient parameters (e.g. humidity and temperature) [9].

Since polymeric nanofibers are notably used in medical areas, the risks associated with bacterial growth or infection must be prevented [3, 10, 11]. Electrospun nanofibers can be converted to outstanding antimicrobial materials via functionalization of the nanofibrous matrix by addition of AgNPs [10, 12]. AgNPs have remarkable physico-chemical properties such as high thermal and electrical conductivity, chemical stability and catalytic activity [13]. Beside of these properties, AgNPs have broad-spectrum antimicrobial effect to many type of bacteria, fungi, and virus despite their low toxicity, they exhibit biocidal effect via multiple mechanism, and release Ag^+ ions slowly, these properties make them strong antimicrobial agent for various biomedical applications [14-17]. Silver nanoparticles can be synthesized with many methods which are mainly classified under three groups as physical, chemical and biological [18]. Chemical reduction method has widely usage which allow to synthesize nanoparticles with various size and shape [18-20]. In this method, reduction of Ag^+ ions to Ag^0 is generally carried out in aqueous or solvent medium containing metal precursor, reducing agent and stabilizer by applying heat and using catalyst, if necessary. [20, 21]. As an alternative to the classical heating that causes an increase in reaction time and thermal gradients in the reaction medium, microwave irradiation provides rapid and uniform heating in order to produce small and monodispersed nanoparticles by accelerating the reaction [22, 23].

As reported in the literature, antibacterial electrospun nanofibers containing silver nanoparticles were prepared with different types of polymers such as polyacrylonitrile (PAN) [12], poly(butylene succinate) (PBS) [24], chitosan [25], polyvinyl alcohol/chitosan blend [26], nylon 6 [27], polycaprolactone (PCL) [28], chitosan/poly(ethylene oxide) blend [29], gelatin [30]. Being a hydrophilic, biocompatible, soluble in water and various solvents, non-toxic and a good compounding properties as well as a good dispersant, polyvinylpyrrolidone (PVP) has been used to form nanofibers alone or blending with different polymers in order to improve spinnability and/or introduction of AgNPs to the matrix [24, 31-33]. In this study, PVP nanofibers containing AgNPs were produced via electrospinning method for potential usage in biomedical applications. In this context, AgNPs were synthesized from AgNO_3 salt in ethanolic solutions of low molecular weight PVP and the effect of PVP concentration on the AgNPs synthesis process was investigated firstly. Then, the effect of electrospinning solution composition on the neat and AgNPs containing PVP nanofiber structures were determined and compared in detail. Finally, antimicrobial properties of neat and AgNPs containing nanofibers were tested against *E. coli*, *S. aureus* and *A. niger*.

2. Materials and methods

2.1. Materials

For the synthesis of AgNPs silver nitrate (AgNO_3) was used as silver precursor and PVP ($\text{C}_6\text{H}_9\text{NO}$)_n with the average molecular weight of 40000 was used as stabilizing agent. On the other hand PVP with the average molecular weight of 360000 was used for the preparation of electrospinning solution. Avoiding any confusion in the text, PVP with the average molecular weight of 40000 and 360000 were written as L-PVP and H-PVP, respectively. Ethanol ($\text{C}_2\text{H}_5\text{OH}$) was used as reducing agent for the synthesis of AgNPs and also solvent for PVP. All chemicals mentioned above were analytical grade and used directly without further purification.

2.2. Synthesis of AgNPs

For the synthesis of AgNPs, 1% (w/v) L-PVP solution was prepared first by dissolving 0.15 g L-PVP in 15 mL ethanol and kept on a magnetic stirrer at room temperature for 24 h. Then, AgNO_3 was added with a PVP/ AgNO_3 weight ratio (R) of 10 and 50 and the solution was stirred until ensuring complete dissolution. Resultant solution was placed into a domestic microwave oven operating 2450 MHz frequency and treated at different conditions which were given in Table 1. To prevent intense boiling of the solution microwave irradiation was carried out discontinuously.

Table 1. Conditions applied for AgNPs synthesis in microwave.

R	Microwave power (W)	Irradiation time (s)
10	180	30
	180	60
	600	30
	600	60
50	180	30
	180	60
	600	30
	600	60

R = PVP/ AgNO_3 weight ratio

To investigate the effect of polymer concentration on the properties of synthesized AgNPs, 5%, 7.5% and 10% (w/v) L-PVP/ethanol solutions were also prepared. The addition of AgNO_3 salt to these colourless solutions with a constant R value of 50, a change in the colour from yellow to brown was observed which indicates the AgNPs formation in the solution. Because of this observation microwave treatment was not applied to these solutions.

2.3. Preparation of Electrospinning Solution

Electrospinning was firstly applied to the L-PVP solutions containing AgNPs but densely accumulated nanofiber mats cannot be produced because of their low viscosity. In order to solve this problem, viscous H-PVP solutions were prepared by dissolving different amounts of H-PVP in ethanol with continuous stirring for 24 h. Then,

electrospinning solutions having different compositions as given in Table 2 were prepared by mixing H-PVP solutions with the same volume of L-PVP solutions and stirring them for 1 h.

Table 2. Composition of the electrospinning solutions.

Total PVP conc. % (w/v)	Concentration % (w/v) of the solutions		^a Amount of AgNO ₃ (%)
	L-PVP	H-PVP	
5	1	9	1
5	1	9	0
10	1	19	0.5
10	1	19	0
5	5	5	1
5	5	5	0
7.5	7.5	7.5	1
7.5	7.5	7.5	0
10	10	10	1
10	10	10	0

^a With respect to the total PVP

2.4. Production of Nanofibers

Electrospinning device (Nanospinner 24-XP, Inovenso) based on a bottom-up spinning technique was used to produce nanofibers. Electrospinning solutions were transferred to a 5 mL plastic syringe which was connected to syringe pump and flow rate was set as 3.5 mL/h. Constant voltage of 18 kV was applied to form an electrical field at the distance of 16.5 cm between tip of syringe and grounded plate wrapped with aluminium foil. During nanofiber production process relative humidity was kept lower than 60% because of the highly hygroscopic nature of the polymer.

Nanofibrous mats were exposed to thermal treatment at different conditions (150°C for 3 h, 175°C for 2 h and 200°C for 2 h) in order to prevent their solubility in water and other solvents.

2.5. Characterization of AgNPs and Nanofibers

Dynamic light scattering (DLS) technique was used to determine the size of AgNPs via Nano-flex particle size analyzer. The UV-visible spectra of the AgNPs solution was measured with a Hach Lange-DR 5000 spectrophotometer to confirm AgNPs formation. The morphology of the electrospun nanofibrous mats was investigated by scanning electron microscopy (SEM, FEI Nova NanoSEM 450). The average fiber diameter and the standard deviation were calculated using Image-J software program from 50 randomly selected measurements for each SEM images. The crystalline structure of nanofibers containing AgNPs was determined by X-ray diffraction analyzer (XRD, Rigaku).

2.6. Antimicrobial Activity Test

Antimicrobial properties of the thermally treated nanofiber mats against three types of microorganism were tested with zone of inhibition method. In this method, *Escherichia coli* (*E. coli*) as a gram-negative bacteria, *Staphylococcus aureus* (*S. aureus*) as a gram-positive bacteria and *Aspergillus niger* (*A. niger*) as a fungus were inoculated to selective agar. Then, samples were placed on the middle of the petri dishes and incubated for 24 h. At the end of this period, the resulted zone of inhibition around the sample was observed.

3. Results and discussion

3.1. Synthesis and Characterization of AgNPs

Fig. 1 shows the appearances of 1% L-PVP solutions obtained after AgNPs synthesis in microwave at different conditions as indicated in Table 1. It is clearly seen that L-PVP-EtOH solutions which were colourless initially, turned to a hardly visible yellow colour after dissolution of AgNO₃ and gradually darkened with increasing microwave power and irradiation time. AgNPs have different colours depending on the particle size and the shape through absorption and scattering effects resulted from strong interaction between light and nanoparticles [21, 34]. Colour change to yellow-brown is a physical evidence of the formation of AgNPs in solutions [12, 24, 32, 35, 36]. Considering the changes in colours of solutions, it is deduced that 180 W microwave power was not adequate to reduce Ag⁺ ions. Therefore, microwave oven should be operated at 600 W for AgNPs synthesis in 1% L-PVP solutions.

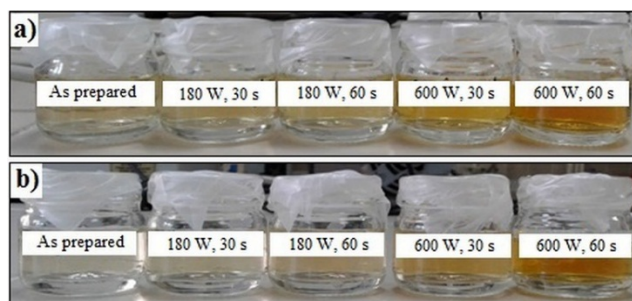


Figure 1. 1% L-PVP solutions containing AgNO₃ with the ratio of $R = 10$ (a) and $R = 50$ (b).

Ethanol is a proper solvent for nanoparticle synthesis due to its ability of reduction of strongly electropositive metal ions and having high dielectric losses which enable to heat under microwave irradiation [22, 37]. On the other hand, PVP is one of the most used stabilizing agent in the synthesis of silver nanoparticles [38]. Being an amphiphilic non-ionic polymer, PVP has a structure of consisting of hydrophilic amide groups in its pyrrolidone rings and hydrophobic polyvinyl backbone. Thus, PVP provides steric stabilization by binding nanoparticle surface due to the high affinity of N and O atoms for silver ions and nanoparticles while polymer

chain surrounds the nanoparticle surface to prevent agglomeration [20, 39-41]. Moreover, the ability of this polymer to reduce metal ions has also been known [24]. The studies in which the effects of molecular weight of PVP on AgNPs synthesis were investigated have shown that increase in molecular weight resulted to increase in nanoparticle size [42, 43]. This was explained by the effective interaction with silver ions in the case of lower molecular weight PVP which has shorter molecules resulting increased number of polymer chains in the medium [42, 43].

As shown in Fig. 2, the colours of the solutions having L-PVP concentrations of 5%, 7.5% and 10% and R value of 50 were changed significantly right after the dissolution of AgNO₃ without any microwave treatment. It was also observed that the solutions turned to a darker colour with increasing the amount of silver ions in the solution. It was reported that the reduction rate of silver ions in PVP-EtOH solutions increases with the increase in PVP and AgNO₃ concentration and temperature; moreover, the reaction time decreases significantly with increasing the amount of PVP in the solution [41]. Chen et al. synthesized AgNPs via mixing AgNO₃-EtOH solution with the same volume of PVP-EtOH solution and they observed that increasing the concentration of PVP accelerates the reaction and increasing concentration of AgNO₃ leads to increase the number of AgNPs formed [40].



Figure 2. 5%, 7.5% and 10% L-PVP solutions containing AgNO₃ with the ratio of R = 50.

In the present study formation of AgNPs was also confirmed by measuring the absorption spectra of 7.5% L-PVP solution having R value of 50. As shown in Fig. 3 an absorption band at 414 nm was observed which is attributed to characteristic surface plasmon resonance (SPR) of spherical AgNPs [24, 35]. Collective oscillation of conduction electrons on nanoparticle surfaces after exposed to light at specific wavelengths leads to exhibition of SPR [21, 34].

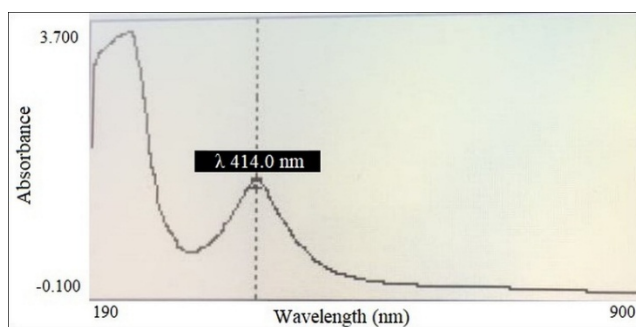


Figure 3. Absorption spectra of 7.5% L-PVP solution having R = 50 value.

Mean particle diameters and size distributions of AgNPs were measured with DLS analysis and the results were given in Table 3 and Fig. 4. It was found that the mean particle diameters of AgNPs synthesized in 1% L-PVP solutions ranged from 9.72 nm to 14.83 nm. The mean particle size of AgNPs obtained at the same microwave operation conditions for different R values were found very close to each other (Table 3). Increasing the microwave power from 180 W to 600 W caused a small decrease in particle diameter and an increase in standard deviation. Fig. 4 demonstrates the particle size distributions of AgNPs synthesized from 1% L-PVP solutions at 180 W (Fig. 4a-d) and 600 W (Fig. 4e-h) microwave power. The graphs in Fig. 4a-d confirm that AgNPs have narrow size distributions and standard deviation. By evaluating the DLS measurement results and the colour changes of 1% L-PVP solutions simultaneously, it can be concluded that 180 W microwave power was not adequate for complete reduction of Ag⁺ ions in the solution.

Table 3. DLS results of AgNPs synthesized in 1% L-PVP solutions.

R	Microwave power (W)	Irradiation time (s)	Mean particle diameter (nm)	Standard deviation (nm)
10	180	30	12.70	2.42
	180	60	14.83	2.69
	600	30	11.90	3.37
	600	60	10.88	3.25
50	180	30	13.71	2.32
	180	60	14.29	2.49
	600	30	9.72	2.56
	600	60	10.25	3.26

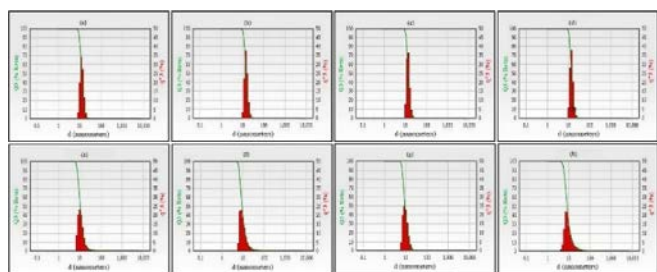


Figure 4. Size distributions of 1% L-PVP solutions operated at 180 W for (a) $R = 10-30$ s, (b) $R = 10-60$ s, (c) $R = 50-30$ s, (d) $R = 50-60$ s, 600 W for (e) $R = 10-30$ s, (f) $R = 10-60$ s, (g) $R = 50-30$ s, (h) $R = 50-60$ s.

Table 4 and Fig. 5 summarize DLS measurement results obtained for the solutions with 5%, 7.5%, 10% L-PVP concentrations and R value of 50. In respect to these results, AgNPs in the concentrated L-PVP solutions dispersed in two regions as low and high diameter but most of the particles clustered around lower sizes. As given in Table 4; 98.9% of the AgNPs synthesized in 5% L-PVP solution have 5.69 nm mean diameter, 94.5% of the AgNPs synthesized in 7.5% L-PVP solution have 7.4 nm mean diameter and 84% of the AgNPs synthesized in 10% L-PVP solutions have 7.47 nm mean diameter.

Table 4. DLS results of AgNPs synthesized in 5, 7.5 and 10% L-PVP solutions.

R	L-PVP conc. % (w/v)	Mean particle diameter (nm)	Percentage of mean particle diameter in solution (%)
	5	5.69	98.9
		237.7	1.1
50	7.5	7.4	94.5
		334	5.5
	10	7.47	84
		416	16

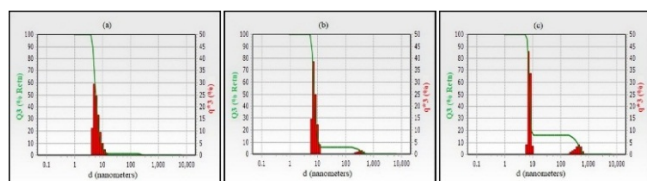


Figure 5. Size distributions of AgNPs synthesized in (a) 5%, (b) 7.5% and (c) 10% L-PVP solutions.

In the previous works it was observed that, the mean diameter of AgNPs decreased by increasing concentration of PVP at constant concentration of AgNO_3 [40, 41]. This phenomena was explained as the formation of high number of nuclei because of increasing the rate of spontaneous nucleation in the presence of PVP [40]. In this study, while the mean diameters of AgNPs synthesized in 1% L-PVP solutions ranged between 9.72-14.83 nm, this value decreased to 5.69 nm in 5% L-PVP solution. By further increasing L-PVP concentration to 7.5% and 10%, mean

diameters became almost constant as 7.4 nm and 7.47 nm, respectively. As a result, increasing concentration of L-PVP gets particle diameter smaller up to a definite size, which is accordance with the study of Chen et al. [40].

3.2. Production of Nanofibers

3.2.1. Effect of the PVP Content of Electrospinning Solution on Nanofiber Structure

In order to investigate the effect of electrospinning solution composition on nanofiber structure various solutions containing different amounts of L-PVP and H-PVP as given in Table 2 were prepared as described in experimental section and used for neat nanofiber production. SEM images of the nanofibers produced from these solutions were given in Fig. 6.

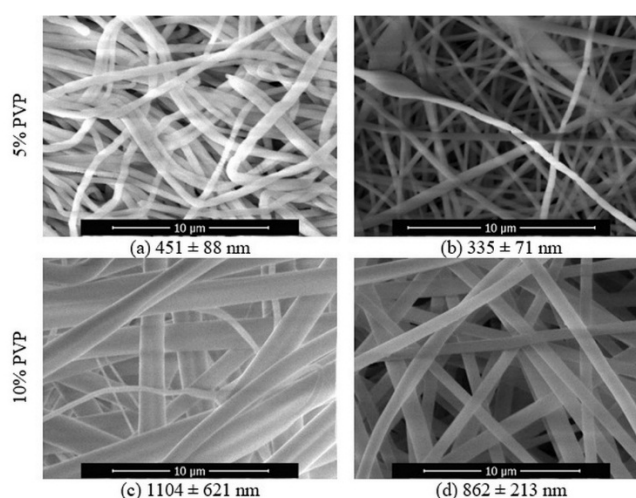


Figure 6. SEM images of nanofibers produced from 5% and 10% PVP solutions with compositions of (a) 1% L-PVP + 9% H-PVP, (b) 5% L-PVP + 5% H-PVP, (c) 1% L-PVP + 19% H-PVP, (d) 10% L-PVP + 10% H-PVP.

Fig. 6 shows that all the solutions are suitable to form nanofibers but somewhat different morphologies. The nanofibers produced from 1% L-PVP + 9% H-PVP solution (Fig. 6a) are not smooth and they also tend to accumulate over each other. On the other hand, the nanofibers produced from 5% L-PVP + 5% H-PVP solution (Fig. 6b) are smooth and separated from each other but have a beaded structure. Similar problems as in the nanofibers produced from 1% L-PVP + 9% H-PVP solution can also be seen in the nanofibers produced from 1% L-PVP + 19% H-PVP solution (Fig. 6c). The nanofibers produced from 10% L-PVP + 10% H-PVP solution have long, bead free and uniform structure (Fig. 6d). Since molecular weight of polymer indicates the entanglement of polymer chains, while low molecular weight polymers tend to form beads, smooth fibers can be obtained from the same concentration of higher molecular weight ones [44]. The high content of L-PVP in 5% L-PVP + 5% H-PVP solution compared with 1% L-PVP + 9% H-

PVP solution lead to decrease in solution viscosity and consequently occurrence of bead-on-string structure.

If the mean diameters of the nanofibers given in Fig. 6 are compared, it can be seen that nanofibers produced from 10% PVP solutions have thicker diameters than 5% PVP solutions. Indeed, increase in nanofiber diameter with increasing polymer concentration is an expected result. Furthermore, when the nanofibers produced from 5% and 10% PVP solutions are evaluated within themselves, it is obvious that the solutions having same ratio of L-PVP and H-PVP have thinner fiber diameter. Increasing the content of H-PVP in the solutions leads to increase solution viscosity, which favours the formation of thicker fibers.

By considering all these observation and results, another electrospinning solution with 7.5% PVP content was prepared by mixing same volume of 7.5% L-PVP and 7.5% H-PVP solutions. The SEM image of electrospun nanofiber produced from this solution was shown in Fig. 7. As depicted from Fig. 7 beaded structure was eliminated by increasing the PVP concentration from 5% to 7.5%; furthermore, more uniform and smooth fibers were formed. Mean diameter of the nanofibers produced from 7.5% PVP solution was measured as 605 ± 137 nm which is between the mean diameters of nanofibers produced from 10% PVP solution (856 ± 213 nm) and 5% PVP solution (335 ± 71 nm).

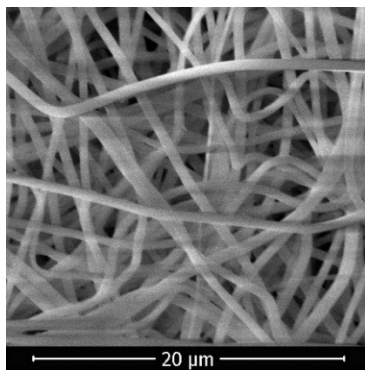


Figure 7. SEM images of nanofibers produced from 7.5% PVP solution.

3.2.2. Effect of the AgNPs Content of Electrospinning Solution on Nanofiber Structure

SEM images of the AgNPs containing nanofibers produced from the electrospinning solutions having the composition as indicated in Table 2 were given in Fig. 8.

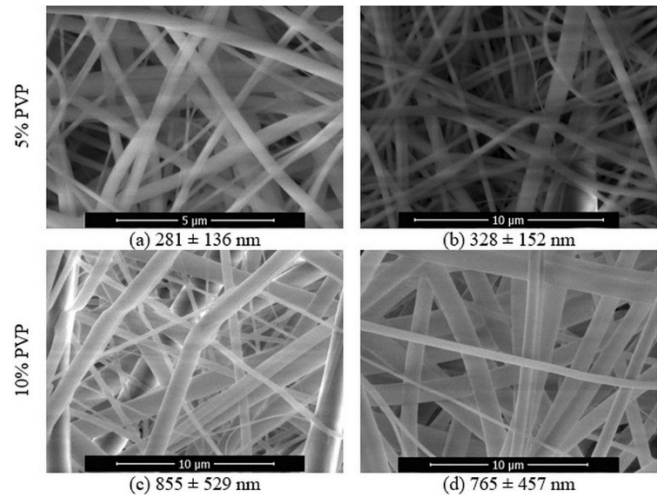


Figure 8. SEM images of AgNPs containing nanofibers produced from electrospinning solutions with compositions of (a) 1% L-PVP + 9% H-PVP + 1% AgNO₃, (b) 5% L-PVP + 5% H-PVP + 1% AgNO₃, (c) 1% L-PVP + 19% H-PVP + 0.5% AgNO₃, (d) 10% L-PVP + 10% H-PVP + 1% AgNO₃.

Nanofibers produced from 1% L-PVP + 9% H-PVP + 1% AgNO₃ solution have more smooth, long and isolated form (Fig. 8a) as compared with the nanofibers produced from 1% L-PVP + 9% H-PVP solution (Fig. 6a), but size distribution became larger while mean diameter decreasing. On the other hand, bead-on string structure of nanofibers produced from 5% L-PVP + 5% H-PVP + 1% AgNO₃ solution retained this structure but showing heterogeneity despite having similar mean diameter as seen in Fig. 8b. Similarly, existence of AgNPs reduced the diameter of nanofibers produced from 10% PVP solutions and increased their heterogeneity. Additionally, SEM images of AgNPs containing nanofibers produced from 7.5% PVP solution were given in Fig. 9. As expected, the mean diameter decreased from 605 ± 137 nm to 550 ± 212 nm with widened size distribution by the addition of AgNPs.

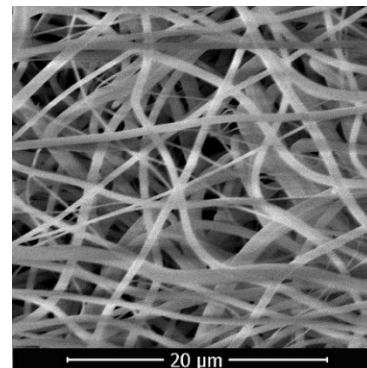


Figure 9. SEM images of AgNPs containing nanofibers produced from 7.5% PVP solution.

The changes observed in the diameter and size distribution of nanofibers containing AgNPs can be attributed to increase in the conductivity of the electrospinning solutions by AgNPs addition. Conductivity values of different

electrospinning solutions were measured with Multiparameter (Mettler Toledo S470 SevenExcellence) and the results were given in Table 5. As can be seen from Table 5, the conductivity values are found higher for electrospinning containing AgNPs. Hwang and Jeong was reported that AgNPs are more strongly affected by the electrical field produced during the electrospinning process than the polymer and hence the polymer is drawn and stretched by AgNPs resulting in formation of thinner nanofibers [33].

Table 5. Conductivity values of different electrospinning solutions.

Total PVP conc. % (w/v)	Concentration % (w/v) of the solutions		^a Amount of AgNO ₃ (%)	Conductivity (μS/cm)
	L-PVP	H-PVP		
5	5	5	1	53.2
	5	5	0	10.6
7.5	7.5	7.5	1	58.1
	7.5	7.5	0	12.2
10	10	10	1	61.3
	10	10	0	13.9

^a With respect to the total PVP

3.2.3. Effect of Thermal Treatment

PVP nanofibers can be crosslinked by photo-crosslinking process via UV-irradiation [33, 45] or thermal treatment between 150 and 200 °C [46]. In the present study, nanofibers were heated at 150, 175 and 200 °C to determine the optimum thermal treatment temperature. Then, the thermal treatment efficiency was determined by observing the solubility of nanofibers, which were cut into squares of 1 cm², in deionize water for 24 h.

Firstly, AgNPs containing and neat nanofibers produced from 1% L-PVP + 19% H-PVP solutions were heated at 150 °C for 3 h according to the procedure described of Wang et al. [32]. After immersing of these nanofiber mats in deionized water for 24 h, it was observed that while neat nanofiber mat dissolved, AgNPs containing nanofiber mat generally maintained its structure but tended to disintegration. Since the thermal treatment applied at 150 °C for 3 h was not adequate to crosslink of the nanofiber mats, thermal treatment procedure reported by Jin et al. [47] was applied for both 175 °C and 200 °C temperatures. Weight losses determined for the thermally treated nanofiber mats after contact with deionized water for 24 h were given in Table 6. According to these results, when temperature increased from 175 °C to 200 °C, weight losses of AgNPs containing nanofiber mats reduced proportionally with the increasing PVP concentration. If we compare the weight loss values of AgNPs containing and neat nanofibers produced from 10% PVP solutions, it was found that AgNPs containing nanofibers are more stable than neat nanofibers.

Thus, it can be concluded that the addition of AgNPs in nanofiber structure makes crosslinking process easy.

Table 6. Weight losses of thermally treated nanofiber mats after contact with deionized water for 24 h.

Total PVP conc. % (w/v)	Concentration % (w/v) of the solutions		^a Amount of AgNO ₃ (%)	Weight loss (%)	
	L-PVP	H-PVP		175 °C	200 °C
5	1	9	1	55.37	7.33
5	5	5	1	29.55	17.14
10	10	10	1	9.79	9.65
10	10	10	0	41.54	15.87

^a With respect to the total PVP

Based on these results, AgNPs containing and neat nanofibers produced from 7.5% PVP solutions were thermally treated at 200 °C and SEM images of these nanofibers were shown in Fig. 10. Mean diameter of neat nanofibers was measured as 605 ± 137 nm and 618 ± 109 nm before and after thermal treatment, respectively. On the other hand mean diameter of AgNPs containing nanofibers rose from 550 ± 212 nm to 606 ± 231 nm after thermal treatment. These slight changes occurred in fiber diameter are in the range of standard deviations of the as-spun nanofibers. It shows that thermal treatment has negligible effect on morphology as well as fiber diameter. Meanwhile, weight losses of these neat and AgNPs containing nanofibers were found as 22% and 12%, respectively.

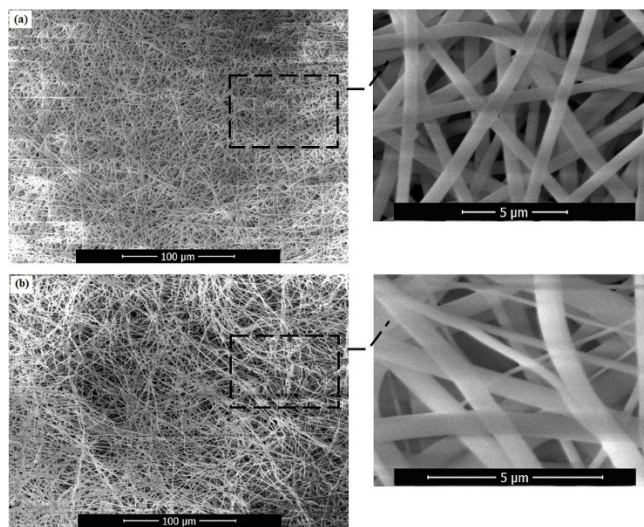


Figure 10. (a) neat, (b) AgNPs containing nanofibers produced from 7.5% PVP solution after thermal treatment at 200 °C for 2 h.

3.2.4. XRD Analysis

XRD diffraction analysis of the AgNPs containing nanofibers produced from 7.5% PVP solutions before and after thermal treatment at 200 °C for 2 h was given in Fig. 11. For both fiber mats peaks were observed at 2θ values of

around 44.5° , 64.5° and 85° which were associated with (200), (220) and (222) planes of face centered cubic form of Ag [32]. Similarly, Fransis et al. synthesized silver nanoparticles in the size of about 5 nm which is obtained from a peak at (200) plane in the XRD pattern and it was further confirmed with TEM analysis [48].

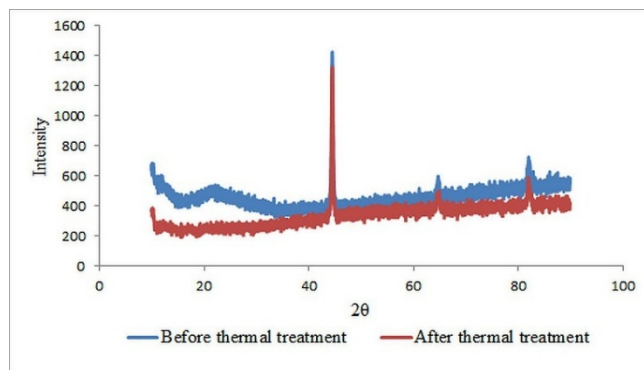


Figure 11. XRD patterns of AgNPs containing nanofibers produced from 7.5% PVP solutions before and after thermal treatment.

3.3. Antimicrobial Activity

Although silver and silver compounds have been used for antimicrobial purposes since ancient times, the mechanism of the action of silver has not been clarified exactly [49-51]. However, antimicrobial effects of silver ions are based on the interaction between metal ions and electron donor functional groups (such as thiol, carboxylate, phosphate, hydroxyl, amines etc.), which results in binding of silver ions with proteins and nucleic acids [16, 52]. Most commonly emphasized mechanisms of silver nanoparticles to bacteria are comprise of (1) release of free silver ions gradually cause to damage in ATP production and DNA replication, (2) reactive oxygen species generation from both silver ions and nanoparticles and (3) direct cell membrane damage by silver nanoparticles [16, 17].

Antimicrobial properties of neat and AgNPs containing thermal treated nanofibers produced from 7.5% PVP solutions were investigated against *E. coli*, *S. aureus* and *A. niger* and the results were demonstrated in Fig. 12. As can be seen from Fig. 12, while neat nanofiber mats allowed microbial growth on their surfaces for all types (Fig. 12a-c); AgNPs containing nanofiber mats inhibited the *E. coli* and *S. aureus* growth by forming small zones of inhibition around their surroundings (Fig. 12d-e). Nevertheless, no antifungal activity was observed against *A. niger*.

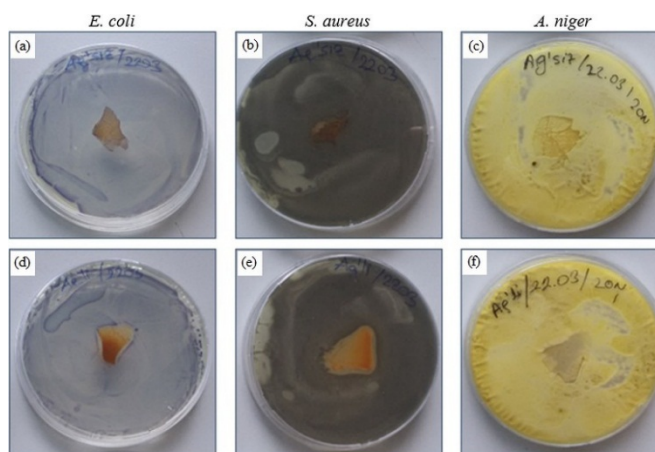


Figure 12. Zone of inhibition test against *E. coli*, *S. aureus* and *A. niger*. (a-c) neat nanofibers, (d-f) AgNPs containing nanofibers.

4. Conclusion

In the line of the aim that preparation of antibacterial polymeric nanofibers for biomedical applications, PVP nanofibers containing AgNPs were successfully produced by electrospinning method. To reduction of Ag^+ ions to Ag^0 atoms, microwave treatment was applied for 1% L-PVP solutions; any microwave treatment was not necessary to produce AgNPs for 5%, 7.5% and 10% L-PVP solutions because of increased reaction rate by increasing L-PVP amount in the solution. Microwave treatment at 180 W was not sufficient to reduce the Ag^+ ions in 1% L-PVP solutions. DLS results showed that all the AgNPs solutions have an average particles size ranging from 5.69 nm to 14.83 nm together with a trend as decreasing size by increasing the L-PVP concentration to a certain point. The UV spectrum of the AgNP solution in 7.5% L-PVP solution confirmed the AgNPs formation clearly.

H-PVP was used to obtain required solution viscosity for the electrospinning process to form a densely accumulated nanofiber mats. SEM images showed that increase in polymer concentration and H-PVP ratio in the electrospinning solution lead to increase in nanofiber diameters. Based on these results, optimum amount of total PVP was determined as 7.5% PVP solution prepared by mixing L-PVP and H-PVP solutions with the same concentration. Existence of AgNPs in the electrospinning solution was resulted a decrease in the nanofiber diameter due to increasing conductivity of electrospinning solution. PVP nanofibers containing AgNPs were effectively crosslinked by thermal treatment at 200°C . Furthermore, XRD patterns of the nanofibers gave (200), (220) and (222) crystal faces of AgNPs. Disk diffusion test results showed that while neat PVP nanofibers allowed microbial growing on their surface; AgNPs containing nanofibers formed a small zone of inhibition against *E. coli* and *S. aureus*.

However, both neat and AgNPs containing nanofibers showed no antifungal effect.

References

- [1]. Dolez P.I., "Nanomaterials definitions, classifications, and applications" in *Nanoengineering: Global Approaches to Health and Safety Issues*, P. I. Dolez, Ed. Amsterdam: Elsevier, (2015), 3-40.
- [2]. de Mello Donegá C., "The nanoscience paradigm: "Size Matters!"," in *Nanoparticles: Workhorses of Nanoscience*, C. de Mello Donegá, Ed. Berlin, Heidelberg: Springer, (2014), 1-12.
- [3]. Van Der Schueren L., De Clerck K., "Nanofibrous textiles in medical applications" in *Handbook of Medical Textiles*, V. T. Bartels, Ed. Oxford: Woodhead Publishing, (2011), 547-566.
- [4]. Pisignano D., *Polymer Nanofibers: Building Blocks for Nanotechnology*. Cambridge, UK: Royal Society of Chemistry, (2013).
- [5]. Beachley V., Wen X., "Polymer nanofibrous structures: Fabrication, biofunctionalization, and cell interactions", *Progress in Polymer Science*, 35 (7), (2010), 868-892. doi:10.1016/j.progpolymsci.2010.03.003
- [6]. Wang L., Ryan A. J., "Introduction to electrospinning" in *Electrospinning for Tissue Regeneration*, L. A. Bosworth and S. Dowres, Eds. Oxford, Cambridge: Woodhead Publishing, (2011), 3-33.
- [7]. Fang J., Niu H., Lin T., Wang X., "Applications of electrospun nanofibers", *Chinese Science Bulletin*, 53 (15), (2008), 2265-2286. doi:10.1007/s11434-008-0319-0
- [8]. Baji A., Mai Y.W., Wong S.C., Abtahi M., Chen P., "Electrospinning of polymer nanofibers: Effects on oriented morphology, structures and tensile properties", *Composites Science and Technology*, 70 (5), (2010), 703-718. doi:10.1016/j.compscitech.2010.01.010
- [9]. Bhardwaj N., Kundu S. C., "Electrospinning: A fascinating fiber fabrication technique", *Biotechnology Advances*, 28 (3), (2010), 325-347. doi:10.1016/j.biotechadv.2010.01.004
- [10]. Gao Y., Bach Truong Y., Zhu Y., Louis Kyratzis I., "Electrospun antibacterial nanofibers: Production, activity, and in vivo applications", *Journal of Applied Polymer Science*, 131 (18), (2014), 40797. doi:10.1002/app.40797
- [11]. Burger C., Hsiao B. S., Chu B., "Nanofibrous materials and their applications", *Annual Review of Materials Research*, 36 (1), (2006), 333-368. doi:10.1146/annurev.matsci.36.011205.123537
- [12]. Shi Q., Vitchuli N., Nowak J., Caldwell J.M., Breidt F., "Durable antibacterial Ag/polyacrylonitrile (Ag/PAN) hybrid nanofibers prepared by atmospheric plasma treatment and electrospinning", *European Polymer Journal*, 47 (7), (2011), 1402-1409. doi:10.1016/j.eurpolymj.2011.04.002
- [13]. Tran Q.H., Nguyen V.Q., Le A.T., "Silver nanoparticles: synthesis, properties, toxicology, applications and perspectives", *Advances in Natural Sciences: Nanoscience and Nanotechnology*, 4, (2013), 033001. doi:10.1088/2043-6262/4/3/033001
- [14]. Ge L., Li Q., Wang M., Ouyang J., Li X., "Nanosilver particles in medical applications: synthesis, performance, and toxicity", *International Journal of Nanomedicine*, 9 (1), (2014), 2399-2407. doi:10.2147/IJN.S55015
- [15]. Yu S., Yin Y., Liu J., "Silver nanoparticles in the environment", *Environmental Science-Processes & Impacts*, 15 (1), (2013), 78-92. doi:10.1039/c2em30595j
- [16]. Dallas P., Sharma V. K., Zboril R., "Silver polymeric nanocomposites as advanced antimicrobial agents: Classification, synthetic paths, applications, and perspectives", *Advances in Colloid and Interface Science*, 166 (1-2), (2011), 119-135. doi:10.1016/j.cis.2011.05.008
- [17]. Marambio-Jones C., Hoek E.M.V., "A review of the antibacterial effects of silver nanomaterials and potential implications for human health and the environment", *Journal of Nanoparticle Research*, 12 (5), (2010), 1531-1551. doi:10.1007/s11051-010-9900-y
- [18]. Irvani S., Korbekandi H., Mirmohammadi S.V., Zolfaghari B., "Synthesis of silver nanoparticles: chemical, physical and biological methods", *Journal of Research in Pharmaceutical Sciences*, 9 (6), (2014), 385-406.
- [19]. León-Silva S., Fernández-Luqueño F., López-Valdez F., "Silver nanoparticles (AgNP) in the environment: a review of potential risks on human and environmental health", *Water, Air & Soil Pollution*, 227 (9), (2016), 306. doi:10.1007/s11270-016-3022-9
- [20]. Tan K., Cheong K., "Advances of Ag, Cu, and Ag-Cu alloy nanoparticles synthesized via chemical reduction route", *Journal of Nanoparticle Research*, 15 (4), (2013), 1537. doi:10.1007/s11051-013-1537-1
- [21]. Abbasi E., Milani M., Fekri Aval S., Kouhi M., Akbarzadeh A. et al., "Silver nanoparticles: Synthesis methods, bio-applications and properties", *Critical Reviews in Microbiology*, 42 (2), (2016), 173-180. doi:10.3109/1040841X.2014.912200

- [22]. Tsuji M., Hashimoto M., Nishizawa Y., Kubokawa M., Tsuji T., "Microwave-assisted synthesis of metallic nanostructures in solution", *Chemistry-A European Journal*, 11 (2), (2005), 440-452. doi:10.1002/chem.200400417
- [23]. Banach M., Pulit-Prociak J., "Synthesis, characteristics, and biocidal activity of silver nanoparticles" in *Fabrication and Self-Assembly of Nanobiomaterials*, A. M. Grumezescu, Ed. William Andrew Publishing, 2016, pp. 367-399.
- [24]. Tian L., Wang P., Zhao Z., Ji J., "Antimicrobial activity of electrospun poly(butylene succinate) fiber mats containing PVP-capped silver nanoparticles", *Applied Biochemistry and Biotechnology*, 171 (7), (2013), 1890-1899. doi:10.1007/s12010-013-0461-2
- [25]. Liu Y., Liu Y., Liao N., Cui F., Park M. et al., "Fabrication and durable antibacterial properties of electrospun chitosan nanofibers with silver nanoparticles", *International Journal of Biological Macromolecules*, 79, (2015), 638-643. doi:10.1016/j.ijbiomac.2015.05.058
- [26]. Abdelgawad A. M., Hudson S. M., Rojas O. J., "Antimicrobial wound dressing nanofiber mats from multicomponent (chitosan/silver-NPs/polyvinyl alcohol) systems", *Carbohydrate Polymers*, 100, (2014), 166-178. doi:10.1016/j.carbpol.2012.12.043
- [27]. Montazer M., Malekzadeh S.B., "Electrospun antibacterial nylon nanofibers through in situ synthesis of nanosilver: Preparation and characteristics", *Journal of Polymer Research*, 19 (10), (2012), 9980. doi:10.1007/s10965-012-9980-8
- [28]. Augustine R., Kalarikkal N., Thomas S., "Electrospun PCL membranes incorporated with biosynthesized silver nanoparticles as antibacterial wound dressings", *Applied Nanoscience*, 6 (3), (2016), 337-344. doi:10.1007/s13204-015-0439-1
- [29]. An J., Zhang H., Zhang J., Zhao Y., Yuan X., "Preparation and antibacterial activity of electrospun chitosan/poly(ethylene oxide) membranes containing silver nanoparticles", *Colloid and Polymer Science*, 287 (12), (2009), 1425-1434. doi:10.1007/s00396-009-2108-y
- [30]. Rujitanaroj P., Pimpha N., Supaphol P., "Wound-dressing materials with antibacterial activity from electrospun gelatin fiber mats containing silver nanoparticles", *Polymer*, 49 (21), (2008), 4723-4732. doi:10.1016/j.polymer.2008.08.021
- [31]. Jin W., Lee H.K., Jeong E. H., Park W.H., Youk J.H., "Preparation of polymer nanofibers containing silver nanoparticles by using poly(N-vinylpyrrolidone)", *Macromolecular Rapid Communications*, 26 (24), (2005), 1903-1907. doi:10.1002/marc.200500569
- [32]. Wang S., Bai J., Li C., Zhang Y., Zhang J., "Ag nanoparticle-embedded one-dimensional β -CD/PVP composite nanofibers prepared via electrospinning for use in antibacterial material", *Colloid and Polymer Science*, 290 (7), (2012), 667-672. doi:10.1007/s00396-011-2581-y
- [33]. Hwang S., Jeong S., "Electrospun nano composites of poly(vinyl pyrrolidone)/nano-silver for antibacterial materials", *Journal of Nanoscience and Nanotechnology*, 11 (1), (2011), 610-613. doi:10.1166/jnn.2011.3243
- [34]. Shenashen M.A., El-Safty S.A., Elshehy E.A., "Synthesis, morphological control, and properties of silver nanoparticles in potential applications", *Particle and Particle Systems Characterization*, 31 (3), (2014), 293-316. doi:10.1002/ppsc.201300181
- [35]. Pal A., Shah S., Devi S., "Microwave-assisted synthesis of silver nanoparticles using ethanol as a reducing agent", *Materials Chemistry and Physics*, 114 (2-3), (2009), 530-532. doi:10.1016/j.matchemphys.2008.11.056
- [36]. Wang Y., Li Y., Yang S., Zhang G., An D. et al., "A convenient route to polyvinyl pyrrolidone/silver nanocomposite by electrospinning", *Nanotechnology*, 17 (13), (2006), 3304-3307. doi:10.1088/0957-4484/17/13/037
- [37]. Kamyshny A., Magdassi S., "Aqueous dispersions of metallic nanoparticles" in *Nanoscience: Colloidal and Interfacial Aspects*, V. M. Starov, Ed. Boca Raton: CRC Pres, (2010), 747-778.
- [38]. Tolaymat T.M., El Badawy A.M., Genaidy A., Scheckel K. G., Luxton T. P. et al., "An evidence based environmental perspective of manufactured silver nanoparticle in syntheses and applications: A systematic review and critical appraisal of peer-reviewed scientific papers", *Science of the Total Environment*, 408 (5), (2010), 999-1006. doi:10.1016/j.scitotenv.2009.11.003
- [39]. Elechiguerra J.L., Burt J.L., Morones J.R., Camacho-Bragado A., Gao X. et al., "Interaction of silver nanoparticles with HIV-1", *Journal of Nanobiotechnology*, 3, (2005), 6. doi:10.1186/1477-3155-3-6
- [40]. Chen D., Qiao X., Qiu X., Chen J., "Synthesis and electrical properties of uniform silver nanoparticles for electronic applications", *Journal of Materials Science*, 44, (2009), 1076-1081. doi: 10.1007/s10853-008-3204-y
- [41]. Kim J., "Reduction of silver nitrate in ethanol by poly(N-vinylpyrrolidone)", *Journal of Industrial and Engineering Chemistry*, 13 (4), (2007), 566-570.

- [42]. Shin H.S., Yang H.J., Kim S.B., Lee M.S., "Mechanism of growth of colloidal silver nanoparticles stabilized by polyvinyl pyrrolidone in γ - irradiated silver nitrate solution", *Journal of Colloid and Interface Science*, 274 (1), (2004), 89-94. doi:10.1016/j.jcis.2004.02.084
- [43]. Khondoker M.A.H., Mun S.C., Kim J., "Synthesis and characterization of conductive silver ink for electrode printing on cellulose film", *Applied Physics A: Materials Science and Processing*, 112 (2), (2013), 411-418. doi:10.1007/s00339-012-7419-z
- [44]. Li Z., Wang C., *One-Dimensional Nanostructures: Electrospinning Technique and Unique Nanofibers*. Berlin, Heidelberg: Springer, (2013).
- [45]. Ignatova M., Manolova N., Rashkov I., "Electrospinning of poly(vinyl pyrrolidone)-iodine complex and poly(ethylene oxide)/poly(vinyl pyrrolidone)-iodine complex—a prospective route to antimicrobial wound dressing materials", *European Polymer Journal*, 43 (5), (2007), 1609-1623. doi:10.1016/j.eurpolymj.2007.02.020
- [46]. Newsome T.E., Olesik S.V., "Electrospinning silica/polyvinylpyrrolidone composite nanofibers", *Journal of Applied Polymer Science*, 131 (21), (2014), 40966. doi:10.1002/app.40966
- [47]. Jin M., Zhang X., Nishimoto S., Liu Z., Tryk D. et al., "Large-scale fabrication of Ag nanoparticles in PVP nanofibres and net-like silver nanofibre films by electrospinning", *Nanotechnology*, 18 (7), (2007), 075605. doi:10.1088/0957-4484/18/7/075605
- [48]. Francis L., Giunco F., Balakrishnan A., Marsano E., "Synthesis, characterization and mechanical properties of nylon-silver composite nanofibers prepared by electrospinning", *Current Applied Physics*, 10 (4), (2010), 1005-1008. doi:10.1016/j.cap.2009.12.025
- [49]. Zhang H., Wu M., Sen A., "Silver nanoparticle antimicrobials and related materials" in *Nano-antimicrobials: Progress and Prospects*, N. Cioffi and M. Rai, Eds. Berlin, Heidelberg: Springer, (2012), 3-45.
- [50]. Rai M., Yadav A., Gade A., "Silver nanoparticles as a new generation of antimicrobials", *Biotechnology Advances*, 27 (1), (2009), 76-83. doi:10.1016/j.biotechadv.2008.09.002
- [51]. Konop M., Damps T., Misicka A., Rudnicka L., "Certain aspects of silver and silver nanoparticles in wound care: A minireview", *Journal of Nanomaterials*, 2016, (2016), 7614753. doi: 10.1155/2016/7614753
- [52]. García-Barrasa J., López-de-Luzuriaga J. M., Monge M., "Silver nanoparticles: synthesis through chemical methods in solution and biomedical applications", *Central European Journal of Chemistry*, 9 (1), (2011), 7-19. doi: 10.2478/s11532-010-0124

Investigation of fatty acid composition, thermal and rheological behavior of yak, cow and horse fats

Jamila Smanalieva^{1,*}, Zhyldyzai Ozbekova², Asylbek Kulmyrzaev³, Peter Fischer⁴

^{1,*}Department of Food Engineering, Kyrgyz-Turkish Manas University, 720038, Bishkek, Kyrgyz Republic, jamila.smanalieva@gmail.com, jamila.smanalieva@manas.edu.kg, ORCID: 0000-0002-3929-4291

² Department of Food Engineering, Kyrgyz-Turkish Manas University, 720038, Bishkek, Kyrgyz Republic, ORCID: 0000-0002-2471-5006

³ Department of Food Engineering, Kyrgyz-Turkish Manas University, 720038, Bishkek, Kyrgyz Republic

⁴ Institute of Food, Nutrition and Health, ETH Zurich, 8092, Zurich, Switzerland

ABSTRACT

The objective of this paper was to study the fatty acid composition, and thermal and rheological behavior of Kyrgyz yak (*Bos grunniens*) visceral fats compared to visceral fats of cow (*Bos taurus*) and horse (*Equus caballus*). The result of the study revealed that the content of saturated fatty acids (SFA) in yak fat was higher than those of unsaturated fatty acids (UFA) (about 58.3 and 38.0 %, respectively). The UFA content in yak fat was higher compared to cow fat (about 27.1 %) and lower than that of horse fat (about 60.0 %). The melting temperatures determined using DSC were found to be 55.18 ± 0.71 , 54.98 ± 3.01 , 37.60 ± 1.92 °C for yak, cow and horse fat, respectively. These results were close to the solid-liquid transition temperature determined by oscillation rheology (52.20 ± 0.89 °C for yak, 53.56 ± 3.53 °C for cow and 33.7 ± 1.84 °C for horse fat). Rotational rheological measurements at 35 °C have shown that yak fat had shear thinning flow behavior with high a viscosity of 226 mPa·s compared to horse fat, which has Newtonian flow behavior with a viscosity of about 36 mPa·s ($\gamma = 100$ s⁻¹). Results on properties obtained in this study will help to understand the contribution of yak fats to the structural properties of new products with these alternative fat sources.

ARTICLE INFO

Research article

Received: 07.05.2019

Accepted: 29.05.2019

Keywords:

Yak fat,
fatty acids,
rheology,
flow behavior,
melting,
phase transition.

*Corresponding author

1. Introduction

Fat is an important source of essential fatty acids since it facilitates the absorption of fat-soluble micronutrients such as vitamins and trace elements. In addition, fat is an important attribute for determining the consumers' acceptance of food products, that is, of their desirable appearance, flavor, aroma, texture, and mouth feel [1]. Fat tissue is the second most important anatomical and morphological component of eviscerated animals. Animal fat is a natural product with a low level of non-nutritional substances. Moreover, animal fats are mostly saturated, stable at elevated temperatures, and can be stored longer compared to plant-based fats. Reduced oxidation in animal fats ensures less susceptibility to toxins and carcinogens [2].

In recent times, the world's scientific literature pays more attention to the content of fatty acids in animal raw materials

of various origin. The majority of studies on the fatty acid compositions have been carried out concerning beef cattle, lamb, goat, pig and chicken fats [3-5]. The thermal behavior of animal fats has been also widely investigated to detect adulteration and identification and to study the oxidative stability and enzymatic interesterification [6-9]. Rheological properties, such as elastic modulus of fats, have been found to be a suitable indicator of the hardness of fats [10-11]. Moreover, these properties can provide information regarding spreadability and mouth feel [12]. Rheological methods were also used to understand the microstructure of fat crystal network [13-14] and to determine the melting and crystallization temperatures [15-16].

An increasing consumer demand for meat-based products, such as sausage, has encouraged research on alternative fat sources, including yak fat. Yak (*Bos grunniens*) is a multi-purpose animal. There are approximately 31,000 heads of

yak, and they are an important cattle species in the Tian-Shan mountain of Kyrgyzstan [17]. Yaks are adapted to extreme living conditions and high altitude (2,000 to 5,000 m above sea level). Living in the severe climatic conditions of high mountains, yaks survive by grazing on highland pastures with widely dispersed feed, mostly composed of grass and herbs. Along with milk, meat and wool, slaughtered yak gives up to 10 kg of visceral fat [18]. Due to the higher carotene content (19.1 mg/kg), yak fat is a typical reddish-yellowish color. For comparison, the cow fat has a carotene content of 7.2 mg/kg [19]. The cholesterol level of subcutaneous yak fat is low and varies from 13 to 17 mg/g [19], while this level in lard is 38 - 76 mg/g and in cow fat is 95 - 140 mg/g [20]. The results of the previous research [3, 21] reported that the main fatty acids in yak body and kidney fat were palmitic acid (C16:0), stearic acid (C18:0), and oleic acid (C18:1). The contents of monounsaturated fatty acids (MUFA) and polyunsaturated fatty acids (PUFA) in yak body fat were 42.7 and 7.95 %, respectively [3]. Consequently, yak fat can be considered as a potentially useful product and utilization of yak fat as an ingredient of new meat-based products could be of high interest. However, little information is available on the fatty acid profiles, rheological and thermal properties of visceral yak fat.

The aim of this study was to analyze the fatty acid composition of Kyrgyz yak fats. First, fatty acid profile of yak fat was measured using gas chromatography (GC) and the results were compared with fatty acid compositions of cow and horse fat. Cow and horse fat were chosen as reference systems due to their common bovine origin (cow fat) and similar nutritional values (horse fat). Secondly, thermal and rheological properties of yak, cow, and horse fats were studied to determine the processing conditions of yak fat in meat-based products. Finally, the correlation of the thermal and rheological properties of animal fat and its fatty acid composition was calculated.

2. Materials and methods

2.1. Materials and Sample Preparation

Fat samples were collected from animals of the autumn slaughtering season in 2012 (female animals, 2.5 - 3.5 years old, of medium nutritional state). The visceral fats of 6 yaks, 5 cows, and 6 horses were used for each fat sample. All animals were kept in the highland pastures of Issyk-Kul region (the northeastern part of Kyrgyzstan) at an average altitude of 3,800 m above sea level. The climate is continental and characterized by an extraordinary change of climatic conditions, i.e. high-temperature differences during the season and intense solar insolation.

Preparation of samples was done in accordance with the general guidelines on sampling CAC/GL 50-2004 (Codex Alimentarius, 2007) and ISO 3100-1-91, 1991 [22-23]. Primary fat samples of 200 g each were taken from three

different parts of each animal visceral fat. A composite sample was obtained by mixing the primary samples. The composite fat sample was minced and placed in steel cups and then kept at 110°C for 30 to 60 minutes in a heating chamber of Model FD 56 (Binder, Tuttlingen, Germany) until a clear melt appeared. The molten samples were filtered using 5.0 µm filters (Sartorius, CA Membran) and divided into three aliquots by types of analyses performed: for fatty acid analysis, rheological analysis, and DSC analysis. Each analysis was done at least in three times in order to avoid inaccuracy.

2.2. Measurement of Fatty Acid Profile

The sample preparation procedure was performed according to application note described by David et al. (2002) [24-25]. To do so, 100 mg of each melted fat sample was transferred into a test tube; 100 µL of 2 M KOH in methanol was added to each sample and the content of tubes was vortexed for 2 - 3 minutes. Upon cooling, 5 mL of hexane was added to the sample and the content of the test tube was thoroughly mixed; afterward, it was centrifuged. The clear supernatant was removed from the test tube and injected to a gas chromatography (Agilent 7890 A, USA), which was equipped with flame ionization detector (FID) and DB-Wax column (30 m × 0.25 mm × 0.25 µm, Agilent Technologies, USA). Nitrogen was used as a carrier gas with a flow rate of 6.4941 mL/min. The temperature of the detector was at 275 °C. An initial column temperature of 80°C was held for 3 min, then increased at 7°C/min to a final temperature of 240 °C, where it was held for 10 min. Identification of peaks was based on the comparison of their retention times with those of the standard fatty acids (Carl Roth GmbH, Karlsruhe, Germany). Fatty acids were identified by comparison of retention times to those of a standard FAME mixture (Carl Roth, Karlsruhe, Germany). The fatty acid contents were calculated based on a percentage of the peak area.

2.3. Differential Scanning Calorimetry (DSC)

DSC measurements were carried out by using a Simultaneous DSC/TG Thermal Analyzer STA409C (Netzsch Gerätebau GmbH, Selb, Germany). Indium (melting temperature 156.6°C, $\Delta H = 28.45$ J/g) was used for calibration of the instrument and an empty pan was used as a reference. At 80°C 15 min melted fat samples of 10 - 30 mg were weighed in aluminum pans and sealed with a pierced lid and cooled until - 20°C and kept overnight at this temperature in order to ensure solid crystallization. DSC analyses of the samples were done in a temperature range from - 10 to 80°C at a rate of 5°C/min. All data recordings were carried out using nitrogen as a purge gas (75 mL/min) to reach the desired temperatures and to prevent samples from oxidation. All samples were analyzed at least three times. The liquid fraction LF at T_i was determined from equation 1 [26]:

$$LF = \frac{\int_{T_0}^{T_f} A dT}{\int_{T_0}^{T_f} A dT} \cdot 100\% \quad (1)$$

where T_0 is the temperature where the melting process begins (T_{onset}) and T_f is the temperature of the end of the melting process (T_{offset}). The low melting (LM) and high melting (HM) peaks in the DSC curve were established according to their melting temperatures, i.e. -10 to 23°C for the low melting peak and 23 to 80°C for the high melting peak.

2.4. Rheological Measurements

Steady and dynamic rheological experiments were carried out using a rheometer MCR 302 (Anton Paar, Graz, Austria) equipped with concentric cylinder geometry CC27. All measurements were conducted after equilibration of temperature at 70, 60, 50, 40, and 35°C. Samples were placed into the measurement chamber in the molten state at 80 °C with the equilibration time 15 min, 0.1°C.

The individual flow curves were recorded by decreasing the shear rate from 100 to 5 s⁻¹ (20 data point in total) within 60 s. High shear stress was chosen as an initial value to ensure a homogenous sample distribution and movement. The power law equation (Eq. 2) was used for samples with non-Newtonian flow behavior (35°C), while the Newtonian law (Eq. 3) was applied to samples with linear flow behavior in the temperature range from 40 to 70°C:

$$\tau = K \cdot \dot{\gamma}^n \quad (2)$$

$$\tau = \eta \cdot \dot{\gamma} \quad (3)$$

where τ is the shear stress (Pa), $\dot{\gamma}$ is the shear rate (s⁻¹), K is the consistency coefficient (Pasⁿ), and n is the flow behavior index. The non-Newtonian case was treated as a shear-thinning fluid ($n < 1$) [27]. In the case of the Newtonian fluid ($n = 1$) Eq. 2 can be simplified to Eq. 3, in which η is the viscosity. In addition, the activation energy E_a was calculated at maximum shear stress ($\dot{\gamma}_{max} = 100$ s⁻¹) according to the Arrhenius-type relationship (Eq. 4, 5) at the temperature range 40 - 70°C:

$$\eta(T) = A \exp\left(-\frac{E_a}{R \cdot T}\right) \quad (4)$$

$$\ln \eta = \ln A + \left(\frac{E_a}{R}\right) \cdot \left(\frac{1}{T}\right) \quad (5)$$

where A is the pre-exponential factor, R is the ideal gas constant (8.31 J/mol·K), T is the absolute temperature (K), and E_a is the activation energy (J/mol) [28].

The viscoelasticity and phase transition temperatures of the fats were studied in an oscillatory temperature sweep experiment at constant strain γ of 10⁻³ % (Linear viscoelastic range) and the constant angular frequency of 1 Hz. The temperature profile of the cooling-heating-cycle was set from 60 to 0°C followed by 0°C to 60°C. The sample temperature was decreased and increased within the experiments by cooling and heating rates of 0.5 °C/min to ensure sufficient sample equilibration. The measured elastic G' and loss G'' moduli provide detailed information on the fat elasticity (stored energy in the form of deformation) and fat viscosity (energy dissipation as heat by internal friction), as well as on the melting and crystallization behavior of the fats. The crystallization and melting temperatures from oscillatory measurements were determined by the loss factor $\tan \delta = G''/G'$. The loss factor relates the viscous properties was denoted by G'' versus the elastic properties denoted by G' . Thus, values above 1 thus indicate more viscous flow behavior while any value below 1 is related to elastic network response [26]. The RHEOPLUS V 3.61 software (Anton Paar, Ostfildern, Germany) was used for the rheological data evaluation. Steady and dynamic rheological measurements were carried in triplicate.

2.5. Statistical Analysis

Analysis of variance (ANOVA) was used to test the differences between the fatty acid contents, thermal and rheological data (Group 1) and investigated animal fats (Group 2). Duncan test was applied to compare the difference between the means (SPSS software version 16 (SPSS Inc., Chicago, IL), with the 95% confidence interval.

3. Results and discussion

3.1. Fatty Acid Composition

The identified saturated fatty acids (capric, lauric, tridecylic, myristic, pentadecylic, palmitic, margaric, stearic, nonadecylic, arachidic, heneicosylic and behenic acids) and unsaturated fatty acids (myristoleic, ginkgolic, palmitoleic, heptadecenoic, oleic, linoleic, paullinic and conjugated linoleic acid) of yak, cow, and horse fat are listed in Table 1. A significant difference ($P < 0.05$) between the fatty acids content and animal types are obvious (Table 1). In general, the mean difference of the content of palmitic (C16:0, from 19.36 to 26.29 %), stearic (C18:0, from 3.61 to 34.33 %), and oleic acids (C18:1, from 22.34 to 52.2 %) were found to be significant in all fats ($P < 0.05$). The amount of these acids accounts for three-quarters of the total amount of fatty acids. When compared to lard fat, which is widely used in the meat product industry, the content of palmitic acid in yak fat was lower, 19.36 %, whereas lard contains 22.68 % [29].

Table 1. Fatty acid composition (% of total fatty acids) of visceral yak, cow and horse fats

Fatty acids	Yak fat	Cow fat	Horse fat
1 Capric acid (10:0)	0.08 ^{l,m,B} ± 0.00	0.09 ^{j,k,A} ± 0.02	ND
2 Lauric acid (12:0)	0.05 ^{m,o,C} ± 0.00	0.14 ^{h,i,j,A} ± 0.00	0.10 ^{e,B} ± 0.01
3 Tridecyl acid (13:0)	0.17 ^{k,C} ± 0.00	0.31 ^{g,h,B} ± 0.01	0.36 ^{e,A} ± 0.04
4 Myristic acid (14:0)	2.12 ^{f,C} ± 0.01	3.66 ^{d,A} ± 0.04	2.50 ^{d,B} ± 0.06
5 Pentadecyl acid (15:0)	0.30 ^{j,B} ± 0.00	0.44 ^{g,A} ± 0.01	0.24 ^{e,C} ± 0.02
6 Palmitic acid (16:0)	19.36 ^{c,B} ± 0.06	26.29 ^{b,A} ± 0.26	20.05 ^{b,B} ± 1.61
7 Margoric acid (17:0)	1.15 ^{g,B} ± 0.00	1.13 ^{f,B} ± 0.01	2.58 ^{d,A} ± 1.44
8 Stearic acid (18:0)	34.33 ^{a,A} ± 0.13	33.54 ^{a,B} ± 0.31	3.61 ^{d,C} ± 0.28
9 Nonadecyl acid (19:0)	0.17 ^{k,B} ± 0.00	0.12 ^{i,j,k,B} ± 0.00	2.38 ^{d,A} ± 0.03
10 Arachidic acid (20:0)	0.40 ^{i,A} ± 0.00	0.12 ^{i,j,k,B} ± 0.00	0.10 ^{e,C} ± 0.02
11 Heneicosyl acid (21:0)	0.13 ^{k,l,A} ± 0.00	0.07 ^{j,k,B} ± 0.02	0.08 ^{e,B} ± 0.00
12 Behenic acid (22:0)	0.08 ^{l,m,B} ± 0.00	0.10 ^{j,k,B} ± 0.01	0.42 ^{e,A} ± 0.03
13 Myristoleic acid (14:1)	0.13 ^{k,l,C} ± 0.01	0.21 ^{h,i,j,B} ± 0.01	0.35 ^{e,A} ± 0.11
14 Ginkgolic acid (15:1)	0.19 ^{k,B} ± 0.00	0.18 ^{h,i,j,B} ± 0.00	0.24 ^{e,A} ± 0.02
15 Palmitoleic acid (16:1)	2.33 ^{e,B} ± 0.01	2.60 ^{e,A} ± 0.02	0.82 ^{e,C} ± 0.04
16 Heptadecenoic acid (17:1)	ND	ND	0.07 ^{e,A} ± 0.10
17 Oleic acid (18:1)	32.06 ^{b,B} ± 0.12	22.34 ^{c,C} ± 0.20	52.20 ^{a,A} ± 4.01
18 Linoleic acid (18:2)	2.52 ^{d,B} ± 0.20	1.19 ^{f,C} ± 0.49	5.10 ^{e,A} ± 0.89
19 Conjugated linoleic acid	0.54 ^{h,B} ± 0.04	0.29 ^{g,h,i,C} ± 0.22	1.17 ^{e,A} ± 0.15
20 Paullinic acid (20:1)	0.27 ^{j,B} ± 0.00	0.29 ^{g,h,i,A} ± 0.00	0.09 ^{e,C} ± 0.00
Unidentified fatty acid	3.63	6.90	7.56
∑ (SFA) %	58.34	66.01	32.40
∑ (UFA) %	38.03	27.09	60.04
MUFA	34.97	25.62	53.77
PUFA	3.06	1.47	6.27
∑ (SFA + UFA) %	96.37	93.11	92.44
SFA / UFA	1.5	2.4	0.5
UFA / SFA	0.7	0.4	1.9
UFA : SFA	1 : 1.5	1 : 2.4	1 : 0.5

The fatty acids were reported as the mean ± standard deviation of three independent measurements.

ND not detected, SFA total saturated fatty acids, UFA total unsaturated fatty acids, MUFA total monounsaturated fatty acids, PUFA total polyunsaturated fatty acids.

^{a-o} Differences within the fatty acids content are statistically significant ($p < 0.05$)

^{A-C} Differences within the investigated fats are statistically significant ($p < 0.05$).

The content of oleic acid (18:1) in horse fat was significantly higher ($P < 0.05$), 52.20 %, whereas in cow and yak fats it was significantly lower ($P < 0.05$) 22.34 and 32.06 %, respectively. These results are in compliance with reports in the literature relating to distinct fatty acid compositions of horse fat [30-31]. The oleic acid content of yak fat was similar as in lard 29.94% [30] and 38.24% [29].

Linoleic acid (18:2) belongs to one of two families of essential fatty acids and its amount in horse fat was 5.10 %, while in yak and cow fats the content of linoleic acid was as low as 2.52 and 1.19 %, respectively. Similarly, the percentage of conjugated linoleic acid in horse fat (1.17 %) was also higher than yak and cow fat (0.54 % and 0.29 %, respectively). Cow fat contains the highest amount of SFA (66.01 %) and the lowest amount of UFA (27.09 %), which is similar to previous results [6]. Yak fat contains high amounts of SFA (58.34 %) and lower amounts of UFA (38.03 %). These findings go in line with the result obtained

by Liu et al. [31], where it was shown that yak hepatic lipids have a higher content in SFA (58.11 %) than in UFA (41.89 %). A relatively high content of UFA (60.04 %) was determined in horse fat, which is close to the results obtained by Tonial et al. (2009) [32]. The content of MUFA (53.77 %) and PUFA (6.27 %) in horse fat were higher than those of yak and cow fats. Calculation of the UFA/SFA ratio (Table 1) of yak fat is 0.7, which is higher than in cow fat (0.4). Finally, the highest UFA/SFA ratio was observed for horse fat (1.9). The data in Table 1 were analyzed using ANOVA test on SPSS software version 16 (SPSS Inc., Chicago, IL). Significant differences between fatty acid content and investigated fats were compared with Duncan's test at a significance level of $P \leq 0.05$.

3.2. Thermal Behavior

Differential scanning calorimetry (DSC) was used to characterize the fat thermal behavior by monitoring associated changes in enthalpy upon heating. Fig. 1 shows the melting thermograms from -10 to 80°C for the three animal fats studied (cow, yak, and horse). The fat melting profile of animal fats exhibited two endothermic DSC peaks. The minor peak for

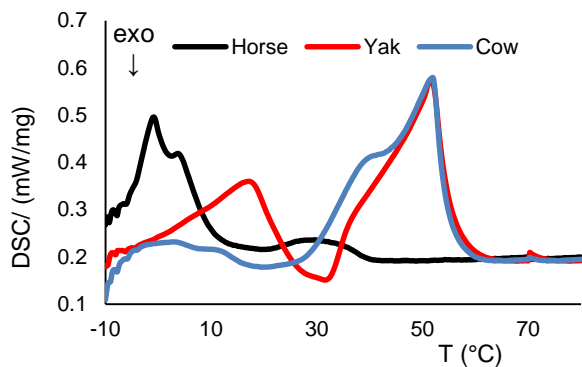


Figure 1. DSC melting curve of cow, yak and horse visceral fats in a temperature range of -10 to 80°C

yak fat was found in the low-temperature region ($15.98 \pm 0.62^\circ\text{C}$), while the major peak was observed in the high-temperature region ($51.31 \pm 0.46^\circ\text{C}$). On the contrary, for horse fat, the major endotherm peak was observed at $5.17 \pm 1.13^\circ\text{C}$ and a minor peak at $28.70 \pm 1.19^\circ\text{C}$, which is attributed to its large amount of unsaturated fatty acids. Thus, the wide range of melting temperatures of the animal fats can be explained by various melting temperature of individual fatty acids. As previously reported [20, 33], the low-temperature endotherm peak was assigned to olein fraction and the high-temperature endotherm peak to stearin fraction. For example, the melting point of stearic acid is 69.6°C , whereas that of oleic acid is 13.4°C . The melting points of polyunsaturated fatty acids of the C_{18} series are even lower (-5°C) [34]. Integral area ($\int A$) and enthalpy (H) of high melting (HM) and low melting (LM) peaks of yak, cow and horse visceral fats calculated from DSC curves (Eq. 4) are given in Table 2. The $\int A_{\text{HM}} / \int A_{\text{LM}}$ -ratio (1.01, 2.27 and 0.48 for yak, cow and horse fat, respectively) in Table 2 and SFA/UFA-ratio (1.5, 2.4 and 0.5 for yak, cow and horse fat, respectively) in Table 1 are almost similar. Therefore, the obtained low melting (LM) peak can be attributed to UFA and high melting (HM) peak to SFA. The specific heat parameter of the experimental fats was also determined by DSC. The peak area of both low and high-temperature regions was used to determine the melting enthalpies ΔH of the samples. The melting enthalpies ΔH in the high-temperature region were observed for yak fat = 67.93 J/g , cow fat = 71.86 J/g . These values are significantly higher than the melting enthalpy determined for horse fat = 3.93

J/g . The lard had the lower melting enthalpy of 44.36 J/g [9], which is comparable to yak and cow fats, but considerably higher than the melting enthalpy of horse fat.

Table 2. Integral area ($\int A$) and enthalpy (H) of high melting (HM) and low melting (LM) peaks of yak, cow and horse visceral fats calculated from DSC curves

DSC Parameters	Yak fat	Cow fat	Horse fat
$\int A_{\text{HM}} (\text{W}^2/\text{g}^2)$	$10.67^{\text{c},\text{B}} \pm 0.34$	$13.62^{\text{c},\text{A}} \pm 0.55$	$4.63^{\text{c},\text{C}} \pm 0.42$
$\int A_{\text{LM}} (\text{W}^2/\text{g}^2)$	$10.6^{\text{c},\text{A}} \pm 0.29$	$5.97^{\text{d},\text{C}} \pm 0.46$	$9.73^{\text{a},\text{B}} \pm 0.16$
$H_{\text{HM}} (\text{J/g})$	$67.93^{\text{a},\text{B}} \pm 0.34$	$71.86^{\text{a},\text{A}} \pm 0.21$	$3.93^{\text{d},\text{C}} \pm 0.62$
$H_{\text{LM}} (\text{J/g})$	$63.3^{\text{b},\text{A}} \pm 0.36$	$30.54^{\text{b},\text{B}} \pm 0.73$	$7.06^{\text{b},\text{C}} \pm 0.79$
$\int A_{\text{HM}} / \int A_{\text{LM}}$	1.01	2.27	0.48
$\int A_{\text{LM}} / \int A_{\text{HM}}$	0.99	0.44	2.10

DSC parameters were reported as the mean \pm standard deviation of three independent measurements

^{a-d} Differences within the thermal properties are statistically significant ($p < 0.05$)

^{A-C} Differences within the investigated fats are statistically significant ($p < 0.05$).

3.3. Viscosity

Shear rate dependence of apparent viscosity of yak fat shows the strong shear thinning behavior at 35°C , while horse fat showed a Newtonian behavior. No flow-curve data were obtained from cow fat samples at 35°C (Fig. 2). The flow behavior index (n) and consistency index (K) values of yak fat were obtained by fitting the shear rate versus apparent viscosity data to a power law model (Eq. 2). The values of the flow behavior index, n , of yak fat were

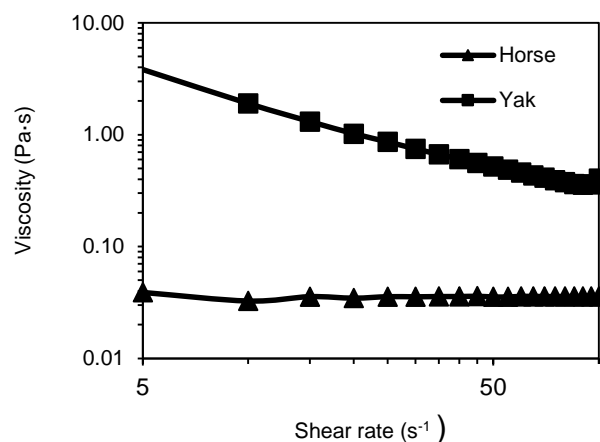


Figure 2. Viscosity as a function of shear rate for yak, cow (not measurable) and horse visceral fats at 35°C .

0.23 at 35°C . The consistency index, K , was $10.93 \text{ Pa}\cdot\text{s}^n$ for yak fat. The smaller n values the greater the departure from Newtonian behavior. As shown by DSC analysis, horse fat

melted already at 28.6°C, therefore it has the lowest viscosity of 35.7 ± 0.6 mPa·s compared to yak fat at 35°C. There is a negative correlation between UFA/SFA ratio and average melting temperature of the individual fat, i.e. the melting points decrease with an increase in unsaturation of fatty acids [2]. Therefore, at 35°C yak fat exhibits shear-thinning behavior with a high effective viscosity of 226.8 ± 1.4 mPa·s than horse fat due to the low ratio of UFA/SFA. The viscosity of the widely used lard fat at 35°C was reported to be 42.8 mPa·s [15]. Consequently, industrial application, e.g. replacing lard fat in sausages by the addition of yak fat becomes possible when mixed with horse fat, and, thus obtaining the melting and crystallization behavior of lard. As mentioned above, by the DSC analysis, increasing the temperature from 35 to 70°C caused the progressive phase transition from solid to the liquid-like state for cow and yak fats. Thus, at $T \geq 40^\circ\text{C}$ all fat samples exhibited distinct Newtonian flow behavior for shear rates obtain approximately greater 10 s^{-1} (Fig. 3). Comparison of the viscosity values at 70 °C of fats showed that yak fat has almost the same viscosity (15 ± 0.2 mPa·s) as cow (15 ± 0.5 mPa·s) and horse fats (12 ± 0.3 mPa·s).

An Arrhenius-type relationship (Eq.4) was employed to estimate the activation energy for fat samples. A least squares linear regression was used to estimate the activation energy from the slope of Eq. 5. The activation energy requirement for the cow fat $E_{a, \text{cow}} = 30.46 \pm 0.5$ kJ/mol with $R^2 = 0.996$ is higher and for horse fat $E_{a, \text{horse}} = 25.5 \pm 0.6$ kJ/mol with $R^2 = 0.999$ is lower, which indicate that the viscosity of cow fat was more sensitive to temperature changes compared to horse fat. The activation energy of yak fat was $E_{a, \text{yak}} = 29.5 \pm 0.7$ kJ/mol with $R^2 = 0.995$. Similar values of activation energy (26.5 kJ/mol) were reported of lard at 35 - 90°C [15], 26.3 kJ/mol of coconut fat containing 90% of saturated fatty acids at 30-90°C [16], 36.5 kJ/mol of rendered cow fat at 10 - 62 °C [35] and 20.1 kJ/mol at 58 - 94°C [36].

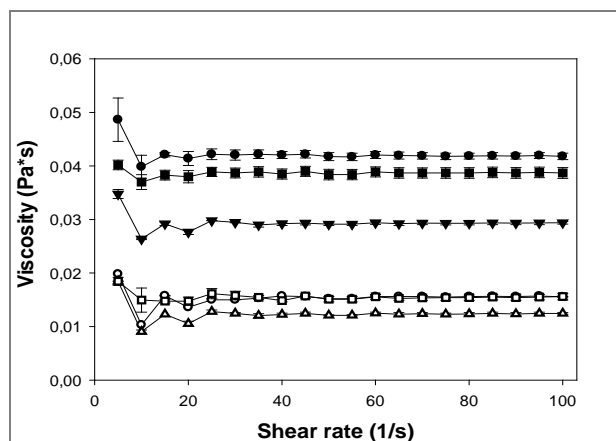


Figure 3. Viscosity as a function of shear rate for yak (○, ●), cow (□, ■) and horse visceral fats (△, ▼) at 40 and 70 °C, respectively.

3.4. Viscoelastic Behavior

Figure 4 shows elastic G' and loss G'' moduli obtained in temperature sweep experiments throughout the entire cooling (Fig. 4A) and heating processes (Fig. 4B), as well as the behavior of the loss factor $\tan \delta$ (Fig. 4C). Fully melted fats showed a weak viscoelastic liquid structure with the loss modulus (G'') higher than the elastic modulus (G') at a temperature range from 60 to 50°C. The shift in G' and G'' of cow and yak fat during heating and cooling were almost similar behavior (Fig. 4B) due to their similar fatty acid compositions. The significant difference ($P \leq 0.05$) between yak and horse fat is more obvious (Fig. 4A), which is explained by the different fatty acid composition. Yak fat samples continued to develop their microstructure during cooling at $37.43 \pm 0.94^\circ\text{C}$, for horse fat samples this temperature is at $10.34 \pm 2.94^\circ\text{C}$.

A standard procedure for determining the liquid-solid (l-s) or solid-liquid (s-l) transition temperatures is done by calculating loss factor $\tan \delta = G''/G'$, which provides a measurement of crystallization T_{l-s} and melting T_{s-l} temperatures. With decreasing loss factor $\tan \delta$ the sample progressively solidifies and the viscoelastic behavior changes from viscous to elastic, i.e. when loss factor $\tan \delta > 1$ sample obtains liquid and viscous properties, and when $\tan \delta < 1$ it becomes solid and elastic [28].

Fig. 4C also shows the changes in loss factors $\tan \delta$ during the process of heating and cooling. As shown in Fig. 4C, the loss factor $\tan \delta$ for horse fat upon heating at a temperature range from 0 to 40°C is higher than that of cow fat. At temperatures higher than 40°C, loss factor $\tan \delta$ of cow fat increases more than that of horse fat. Thus, the liquid-solid transition temperatures at $\tan \delta < 1$ for yak fat was $T_{l-s, \text{yak}} = 37.43 \pm 0.94^\circ\text{C}$, for cow fat $T_{l-s, \text{cow}} = 38.40 \pm 0.77^\circ\text{C}$, and for horse fat $T_{l-s, \text{horse}} = 10.34 \pm 2.94^\circ\text{C}$. The solid-liquid transition temperatures at $\tan \delta < 1$ of yak fat $T_{s-l, \text{yak}} = 52.2 \pm 0.89^\circ\text{C}$ found to be similar to that of cow fat $T_{s-l, \text{cow}} = 53.56 \pm 1.91^\circ\text{C}$. The temperature sweep method applied to lard fat showed the solid-liquid transition temperature was 47°C [15]. Horse fat has solid-liquid transition temperature at $T_{s-l, \text{horse}} = 33.7 \pm 1.84^\circ\text{C}$ (Table 3) and it is comparable with that of the goose fat ($T_{s-l, \text{goose}} = 38.5^\circ\text{C}$) [15].

Table 3. Temperature range of crystallization (T_{l-s} , °C) and melting (T_{s-l} , °C) of yak, cow and horse visceral fats, according to oscillatory temperature sweep and DSC melting curve

	Oscillatory temperature sweep		DSC (melting curve)			
	T_{l-s}	T_{s-l}	$T_{peak\ 1}$	$T_{peak\ 2}$	$T_{peak\ 3}$	$T_{peak\ end}$
Yak fat	37.43 ^{a,B} ± 0.94	52.20 ^{a,A} ± 0.89	15.98 ^{b,D} ± 0.62	30.01 ^{a,C} ± 2.28	51.31 ^{a,B} ± 0.46	55.18 ^{a,A} ± 0.71
Cow fat	38.40 ^{a,B} ± 0.77	53.56 ^{a,A} ± 3.53	18.55 ^{a,D} ± 1.91	27.33 ^{a,C} ± 4.72	50.77 ^{a,B} ± 2.86	54.98 ^{a,A} ± 3.01
Horse fat	10.34 ^{b,B} ± 2.94	33.70 ^{b,A} ± 1.84	5.17 ^{c,D} ± 1.13	19.70 ^{b,C} ± 1.07	28.70 ^{b,B} ± 1.19	37.60 ^{b,A} ± 1.92

The temperature ranges were reported as the mean ± standard deviation of three independent measurements.

^{a-d} Differences within the transition temperatures are statistically significant ($P \leq 0.05$)

^{A-C} Differences within the investigated fats are statistically significant ($P \leq 0.05$).

As previously mentioned Table 3 summarizes the melting temperatures obtained from the DSC measurements and the phase transition temperature range during the cooling and heating of cow, yak, and horse fat based on $\tan \delta$, G' , and G'' data. Comparison of the transition temperatures during heating, given in Table 3, shows the temperatures obtained from the DSC measurements ($T_{peak\ end}$ 55.18±2.5, 54.98±3.01, 37.6±1.92°C for yak, cow and horse fat, respectively) agreed with the transition temperatures obtained from oscillatory tests (for yak 52.2±0.89 °C, cow 53.56±3.53°C and horse fat 33.7±1.84°C), especially in case of $T_{peak\ end}$. This observation is in line with the results reported by López-Martínez et al. (2014), who concluded that the G' behavior of monoglycerides – oil systems are clearly associated with the thermal transition behavior observed by DSC [37].

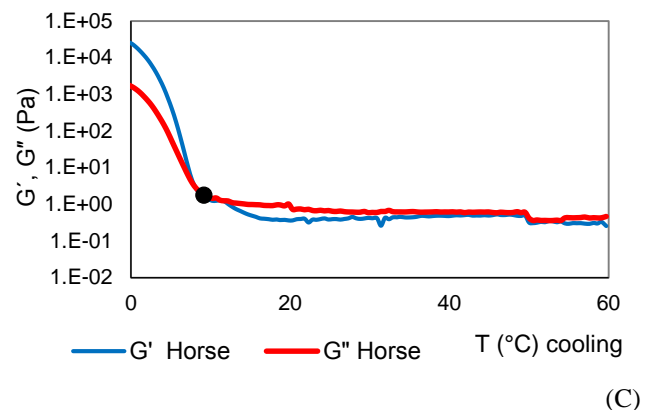
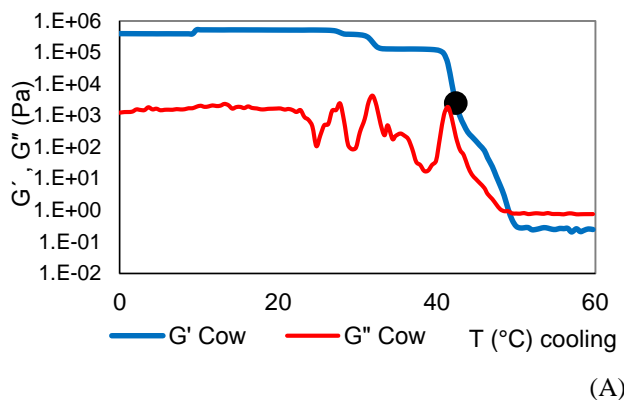
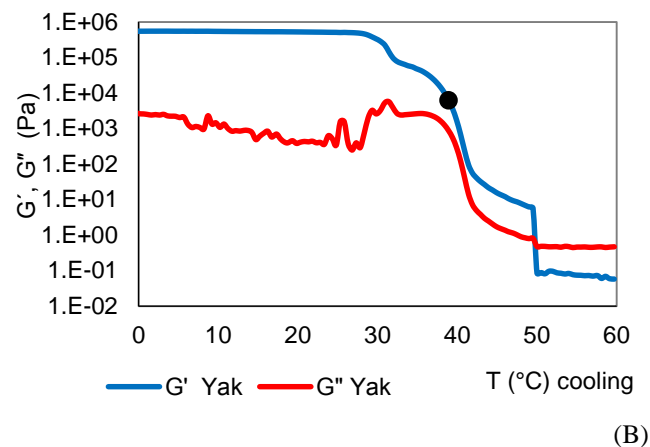


Figure 4A. Temperature sweep: Changes of moduli G' and G'' during the cooling /solidification process (A) cow fat; (B) yak fat; (C) horse fat.

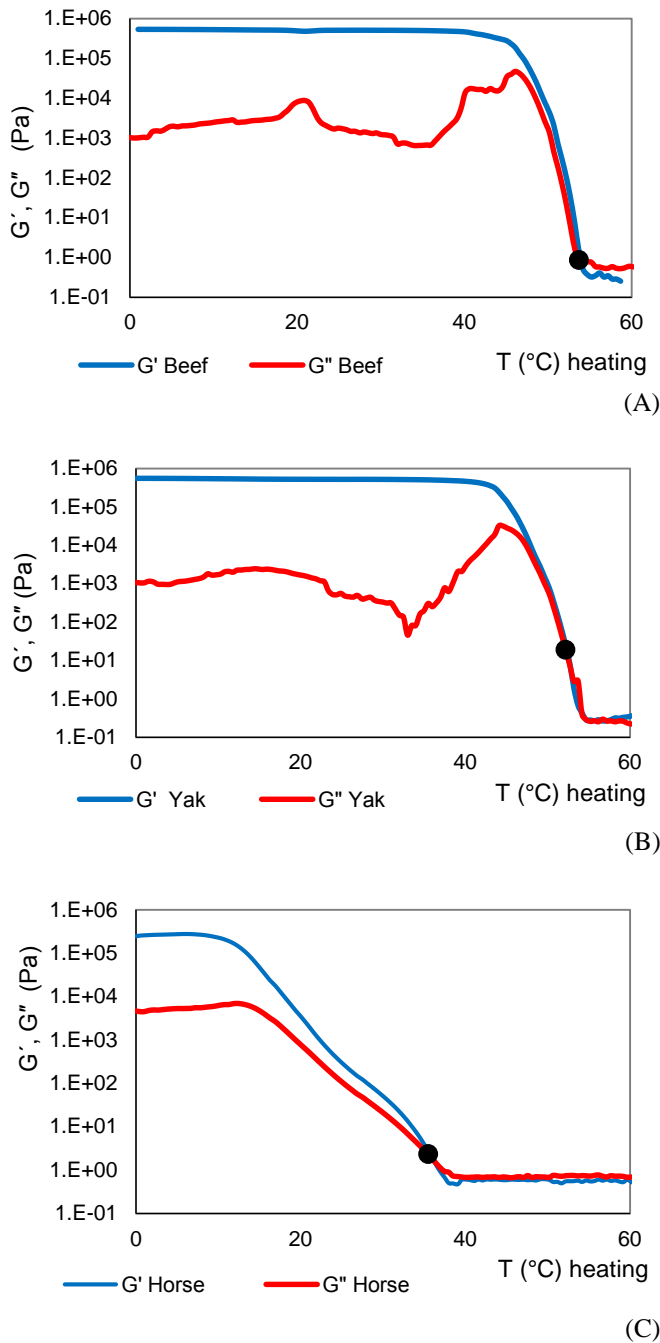


Figure 4B. Changes of moduli G' and G'' during the heating /melting process (A) cow fat; (B) yak fat; (D) horse fat

4. Conclusion

The fatty acid composition, rheological and thermal properties of yak visceral fat were investigated and compared with cow and horse fats. The fatty acid content of the fats varied considerably depending on the animal species. The yak fat may be considered to be more valuable than cow fat, due to its higher UFA content. Based on these results we can conclude that yak

and horse meat has higher nutritional values compared to a cow meat, due to the richer sources of polyunsaturated fatty acids. The difference in fatty acid composition directly influences the physical properties of animal fats such as the rheological and thermal behavior of the animal fat. Rheological measurements have shown that yak fat had more complex rheological behavior compared to horse fat at 35 °C, but at temperatures above 40 °C, all fat samples show Newtonian behavior for shear rates greater than approximately 10 s^{-1} . Calculations on the activation energy from 40 to 70 °C resulted in the following order: cow > yak > horse fat. Phase transition temperatures were measured using two different methods, DSC and rheological oscillatory measurements. The melting temperatures, obtained from the oscillatory tests, were close to the transition temperatures obtained from DSC measurements. Furthermore, oscillatory measurements were most suitable for the assessment of the structural changes as a function of temperature. DSC analysis showed that for yak fat: the melting process takes place within a broader temperature range compared to that of cow and horse fat. Thus, industrial application of yak fat is of practical interest. Obtained parameters provide useful information for the development of new products, optimization of industrial processes and control of quality and authenticity of yak fat.

Acknowledgments

The first author is grateful for the financial support of this project provided by the German Academic Exchange Service (DAAD). The authors also thank Dr. B. Blochwitz and Ms. A. Kliegel for their help with measurements and Prof. Dr. Coskan Ilicali for his comments on the revised manuscript.

References

- [1]. Rios R.V., Pessanha M.D.F., de Almeida P.F., Vienna, C.L., Lannes S.C., "Application of fats in some food products", *LWT- Food Science and Technology*, 34, (2014), 3-15.
- [2]. Casimir C.A., David B.M. *Food Lipids*. New York: Marcel Dekker, (2002).
- [3]. Wang Q., Zhao X., Ren Y., Fan E., Chang H., Wu H., "Effects of high-pressure treatment and temperature on lipid oxidation and fatty acid composition of yak (*Capra hircus*) body fat", *Meat Science*, 94, (2013), 489–494.
- [4]. Rule D.C., Smith S.B., Romans J.R., "Fatty acid composition of muscle and adipose tissue of meat animals", in *The biology of fat in meat animals-Current advances*, S.B. Smith D.R. Smith, Eds. Champaign: American Society of Animal Science, (1995), 144-165.
- [5]. Coltro W.K.T., Ferreira M.M.C., Macedo F.A.F., Oliveira C.C., Visentainer J.V., Souza N.E., Matsushita

- M., "Correlation of animal diet and fatty acid content in young goat meat by gas chromatography and chemometrics", *Meat Science*, 71, (2005), 358–363.
- [6]. Marikkar J.M.N., Ghazali H.M., Che Man Y.B., Lai O.M., "The use of cooling and heating thermograms for monitoring of tallow, lard and chicken fat adulterations in canola oil", *Food Research International*, 35, (2002), 1007-1014.
- [7]. Yılmaz M.T., Karakaya M., Aktaş N., "Composition and thermal properties of cattle fats", *European Journal of Lipid Science and Technology*, 112, (2010), 410–416.
- [8]. Yanty N.A., Marikkar J.M., Man Y.B., Long K. "Composition and thermal analysis of lard stearin and lard olein", *Journal of Oleo Science*, 60(7), (2011), 333-338.
- [9]. Budryn G., Nebesny E., Zyzelewicz D. "Oxidative stability of lard and sunflower oil supplemented with coffee extracts under elastic conditions", *Grasas Y Aceites*, 62(2), (2011), 155-161.
- [10]. Narine S.S., Marangoni A.G. "Microscopic and rheological studies of fat crystal networks", *Journal of Crystal Growth*, 198, (1999), 1315–1319.
- [11]. Narine S.S., Marangoni A.G. "Elastic modulus as an indicator of macroscopic hardness of fat crystal networks", *LWT - Food Science and Technology*, 34, (2001), 33–40.
- [12]. Rousseau D., Marangoni A.G. "The effects of interesterification on physical and sensory attributes of butterfat and butterfat- canola oil spreads", *Food Research International*, 31, (1999), 381–388.
- [13]. Tang D., Marangoni A.G., "Microstructure and fractal analysis of fat crystal networks", *Journal of the American Oil Chemists' Society*, 83(5), (2006), 377-388.
- [14]. Pe´rez-Martinez J.D., Reyes-Hernandez J., Dibildox-Alvarado E., Toro-Vazquez J.F. "Physical Properties of Cocoa Butter/Vegetable Oil Blends Crystallized in a Scraped Surface Heat Exchanger", *Journal of the American Oil Chemists' Society*, 89, (2012), 199–209.
- [15]. Hildebrandt N., Senge B. "Structure examinations of lard and goose dripping and spreadable fermented sausage", *Fleischwirtschaft*, 85(7), (2005), 91-96.
- [16]. Tipvarakarnkoon T., Blochwitz R., Senge B. "Rheological properties and phase change behaviors of coconut fats and oils", *Annual transactions of the Nordic rheology society*, 16, (2008), 1-7.
- [17]. Alymbekov K.A. "The meat of yak", Bishkek: Insanat, (2007).
- [18]. Wiener G., Jianlin H., Ruijin L. "The Yak", Bangkok: RAP Publication, (2003).
- [19]. Alymbekov K. ., "Production of yak meat of the competitive quality is the criteria of the economic development of mountainous Kyrgyzstan", *News of universities*, 2, (2002), 153-156.
- [20]. Thu T.N.D, Leslie D.T., Michael L.G., Brooks J.C., Kristine Y.P., Boylan L.M. "Cholesterol Content and Methods for Cholesterol Determination in Meat and Poultry", *Comprehensive Reviews in Food Science and Food Safety*, 10, (2011), 269-289.
- [21]. Wang Q., Wu J.P., Zhang S.G., Zhang Y.B., Zhang H.X., Fan E. "GC analysis of the fatty acid composition of yak kidney", *Chromatographia*, 69(1-2), (2009), 139-143.
- [22]. Methods of analysis and sampling. CAC / GL 50-2004. Methodical guidelines for sampling. Codex Alimentarius, (2007).
- [23]. Meat and meat products. Methods of sampling. ISO 3100-1-91. (1991).
- [24]. David F., Sandra P., Wylie P.L. "Improving the analysis of fatty acid methyl esters using retention time locked methods and retention time databases: Application (Agilent Technologies – 5988-5871EN)", (2003).
- [25]. David F., Sandra P., Vickers A.K. "Column Selection for the analysis of fatty acid methyl esters: Application (Agilent Technologies – 5989-3760EN)", 2005.
- [26]. Lecomte-Beckers J., Rassili A., Carton M., Robelet M., Koeune R. "Study of the Liquid Fraction and Thermophysical Properties of Semi-Solid Steels and Application to the Simulation of Inductive Heating for Thixoforming", in *Advanced Methods in Material Forming*, D. Banabic, Ed. Berlin: Springer, (2007), 321-347.
- [27]. Rosenthal A.J. "Food texture: measurement and perception". Gaithersburg: Aspen Publishers, Inc., (1999).
- [28]. Rao A.M. "Rheology of Fluid and Semisolid Foods. Principles and Applications". New York: Springer, (2007).

- [29]. Yanty N., Nazrim M., Shuhaimi M., Miskandar M.S. "Composition and thermal analysis of ternary mixtures of avocado fat: palm stearin: cocoa butter (Avo:PS:CB). *International Journal of Food Properties*", 20(2), (2017), 465-474.
- [30]. Lisitsyn A.B., Chernukha I.M., Ivankin A.N. "Comparative study of fatty acid composition of meat material from various animal species", *Scientific Journal of Animal Science*, 2(5), (2013), 124-131.
- [31]. Liu C., Jin G., Luo Z., Li S., Sun S., Li Y., Ma, M. "Chinese yak and yellow cow exhibit considerable differences in tissue content of squalene, tocopherol, and fatty acids", *European Journal of Lipid Science and Technology*, 117 (6), (2015), 899-902.
- [32]. Tonial I.B., Aguiar A.C., Oliveira C.C., Bonnafé E G., Visentainer J.V., de Souza N.E. "Fatty acid and cholesterol content, chemical composition and sensory evaluation of horse meat", *South African Journal of Animal Science*, 39, (2009), 328-332.
- [33]. Tan C.P., Che Man Y.B. "Differential Scanning Calorimetric Analysis of Edible Oils: Comparison of Thermal Properties and Chemical Composition", *Journal of the American Oil Chemists' Society*, 77(2), (2000), 144-157.
- [34]. Berg J.M., Tymoczko J.L., Stryer L., *Biochemistry*, New York: W. H. Freeman, (2002).
- [35]. Travnicek P., Krcalova E., Vitez T. "Rheopectic Behavior of Rendered Fat", *Polish Journal of Environmental Studies*, 22(5), (2013), 1499-1504.
- [36]. Capelli A., Martins P.J.R., Gabas A.L., Telis-Romero J. "Influence of Temperature in Rheological Properties of Bovine Fat – Alternative Source For Biodiesel Production", *Proceedings of the 2nd Brazilian Bioenergy Science and Technology (BBEST)*, (2014).
- [37]. López-Martínez A., Morales-Rueda J.A., Dibildox-Alvarado E., Charó-Alonso M.A., Marangoni A.G., Toro-Vazquez J.F. "Comparing the crystallization and rheological behavior of organogels developed by pure and commercial monoglycerides in vegetable oil", *Food Research International*, 64, (2014), 946–957.

Some quality qualifications of cooked meat sous vide in the storage process

Tarih Eren Babür ^{1,*}, Kemal Kaan Tekinşen ², Ümit Gürbüz ^{2,3}

^{1,*}Muğla Sıtkı Koçman University, Fethiye ASMK Vocational High School, Muğla, Turkey, ernbabur@gmail.com, ORCID: 0000-0003-3164-0783

² Selçuk University, Faculty of Veterinary Medicine, Department of Food Hygiene and Technology, Konya, Turkey, kktekinsen@selcuk.edu.tr, ORCID: 0000-0003-3287-3925

³ Kyrgyz Turkish Manas University, Faculty of Veterinary Medicine, Department of Food Hygiene and Technology, Bishkek, Kyrgyzstan, ugurbuz@selcuk.edu.tr, ORCID: 0000-0002-0980-0181

ABSTRACT

This study was carried out to determine the physicochemical and microbiological quality characteristics of some meat samples (*Longissimus dorsi*, LD; *Longissimus lumborum*, LL; *Longissimus thoracis*, LT) that were cooked in sous vide method at different time combinations (2 and 4 hours) at 70°C during the storage process. Meats used as materials in the study were obtained from 22-24 months old Simmental cattle. All experimental meat samples were cut in 2x15 cm size and salted. Salted meat samples were vacuum-packed and cooked by sous vide method. Cooked meat samples were stored at 2 ± 2°C for 7 days. Physicochemical and microbiological analyzes were performed on the 0., 3., 7th days of storage.

It was observed that the pH values of the samples remained within acceptable limits during storage and the pH values increased as the cooking time increased. It was observed that cooking loss rates increased in parallel with increasing cooking time, and this increase was more clear in LL samples. In addition, it was determined that as the cooking time of LT and LD samples gets longer the cooking loss increased and it affected the values of a* (redness) and L* (brightness). It was observed that no living microorganism produced in any samples taken into analysis during storage.

As a result; not finding microorganisms in the samples with sous vide technique for 7 days in the storage period, it is believed to strengthen the reliability of safe food production. It is concluded that sous vide method can provide advantages especially in terms of long shelf life and close to consumer preference.

ARTICLE INFO

Research article

Received: 30.05.2019

Accepted: 14.06.2019

Keywords:

Meat quality,
Cooking methods,
Microbiological quality

*Corresponding author

1. Introduction

Consumers now prefer products that are most similar to the fresh product in terms of their appearance and quality and that are treated very little. Therefore, in the last ten years, it has gained importance in the research and implementation of alternative technologies in food processing and preservation both in food industry and academic field [1]. The sous vide technique, also called vacuum cooking technique of alternative cooking methods, first appeared in France in the 1960s and started to be used in countries such as America, Canada, Belgium and Singapore. Sous vide technique is recognized by the vacuum packaging process that prevents the development of microorganisms and high organoleptic properties, especially in meat products, and is preferred as an

alternative method [2, 3, 4]. Today, only in France, there are 87 enterprises producing by sous vide method, and they produce about 10,000 tons of sous vide products per year. Due to its ease, the sous vide cooking method is widely preferred in catering sector providing services in transportation vehicles such as trains, airplanes, etc. as well as in food and beverage businesses such as hotels, restaurants [3].

The sous vide technique differs from the traditional cooking methods in two respects. The first is by vacuuming the raw product in a heat-resistant, plastic food bag; the second one is the application of the cooking process at fully controlled temperatures. Due to the sous vide technology, which is a kind of pasteurization process, the foods are cooked in vacuum

packaging. The temperature is distributed homogeneously throughout the cooking process and thus the heterogeneous temperature and color distribution in the traditional cooking method is not observed in the sous vide method. Therefore, in conventional cooking methods, processes such as turning or mixing applied to ensure homogeneous cooking of food are not required in this method [5].

Peiretti et al. [6] reported a decrease in the rate of carnosine formed by the incorporation of the alanine and histidine amino acids in the meat after heat treatment, a decrease in carnosine loss (50%), especially in the boiled meat due to its water soluble property. Because of the fact that the meat does not come into contact with water in the sous vide technique, the components with water-soluble properties remain in the food and the nutrient loss is minimal. In sous vide technique, food is put into heat-resistant plastic bags and vacuumed. The vacuumed bag is cooked according to the appropriate temperature-time parameter by placing the temperature in the cooking pot fully controllable and in the water circulation. At the end of cooking, the product removing from the water and is served directly by frying on a grill or pan [5, 7]. The process steps applied in the sous vide cooking method are shown in Fig. 1.

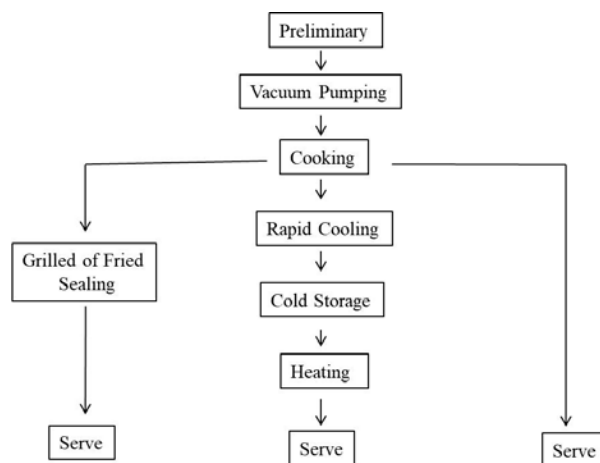


Figure 1. Processes used in sous vide cooking method [7]

2. Materials and methods

In the preparation of the experimental specimens added salted %0,2, 2 x 15 cm sliced tenderloin (*Longissimus dorsi*, LD), loin (*Longissimus lumborum*, LL) and entrecote (*Longissimus thoracis*, LT) preparations were used. The meats used as material in the study were obtained from 22-24 months old Simental cattle. Meat samples were vacuum packed using vacuum bags (Electrolux Sous Vide Vacuum Bags, Polyscience, USA) with certificate of conformity to food production. Then they were baked in the sous vide unit (Sous Vide Professional Crative Series, PolyScience, USA) for 2 and 4 hours at 70°C. They were stored at $2 \pm 2^\circ\text{C}$ for 7 days

following rapid cooling with the help of ice tanks. The samples were examined in terms of physicochemical and microbiological characteristics on the 0, 3 and 7th days of storage. Analyzes of the meat samples prepared 3 times were performed in parallel. The preparation and cooking steps of the samples are shown in Figure 2, respectively.



(I)



(II)



(III)



(IV)

Figure 2. Preparation steps of experimental meat samples (I: grouping, II: salting and vacuuming) and sous vide process (III: cooking, IV: rapid cooling)

2.1. Physicochemical Analysis

Four different analyzes including pH, cooking loss, reflectance color analysis and Warner Bratzler shear force analysis were performed within the scope of physicochemical analyzes. The pH values of the prepared meat samples were determined at $25 \pm 1^\circ\text{C}$ by electronic pH meter (Inolap-Series Wtw 7310) [8]. Cooking loss was weighed with precision scales at the end of the cooking process and were calculated with the help of the following formula [9].

$$\text{Cooking loss (\%)} = \frac{\text{Weight Before Cooking} - \text{Weight After Cooking}}{\text{Weight Before Cooking}} \times 100$$

Reflectance color analysis was performed with the help of a Minolta chrome meter (CR-400 model, Konica Minolta). For this purpose, the color measurements on the surface of each sample using a colorimeter with diffusion range of 8 mm in D Diffuse / O mode with D65 illumination, 2° observer, are expressed as brightness (L^*), redness (a^*) and yellowness (b^*) [10].

Samples for shear force analysis were removed from their packs on the specified days of storage and brought to room temperature. Samples with a diameter of 1.27 cm and a diameter of 2 cm were taken from the samples reaching room temperature with a special probe. The shear force values of the samples were determined with the help of the Warner Bratzler Share (WBS) V Slot Blade probe of the double sleeve texture device of TA.HDPlus (TA, Stable Microsystems Godalming, Surrey, UK) in Selcuk University Food Engineering laboratory [11].

2.2. General count of live microorganisms

he analysis was performed according to the Food and Drug Administration Bacteriological Analytical Manual (FDA BAM) [12]. 1 ml each of the dilution tubes was taken and plate count agar (Merck 1.12535) was applied to the medium by casting plate. Following incubation at 37°C for 48 hours, colonies between 30 and 300 were counted and evaluated by taking the dilution coefficient into account.

2.3. Statistical Analysis

SPSS 21.00 package program was used for statistical evaluation of the data obtained from the study. Variance analysis was applied to statistical data; differences between

significant variance sources were also determined by applying the Tukey test [13].

3. Results and discussion

Because of its quality characteristics and vacuum pack, sous vide cooking is more recognizable due to the advantages in terms of making the product more durable against storage conditions.

Especially in the last years, for food and tourism sectors, food prepared with sous vide technique - an alternative cooking method- is stored for a long time without breaking the cold chain food.. In order to detect changes in meat that may occur during the cold chain and which may affect consumer preference, pH, cooking loss, color, (Warner Bratzler Share Force WBSF) and microbial properties are important in the one week storage period.

In the study, the pH values were found to be acceptable level (5.74 - 6.01) on the 0, 3 and 7 days of storage. The pH values of the experimental samples increased during the storage period and the pH values of the LD were similar on the 0 and 3 days of storage and on the 7th day it was found to significantly increased ($p < 0.05$) (Table 1). Similar studies [14, 15] have reported that an increase in pH values during storage is observed, while the increase in pH observed during rest may be related to alkaline metabolic products resulting from protease activity [16].

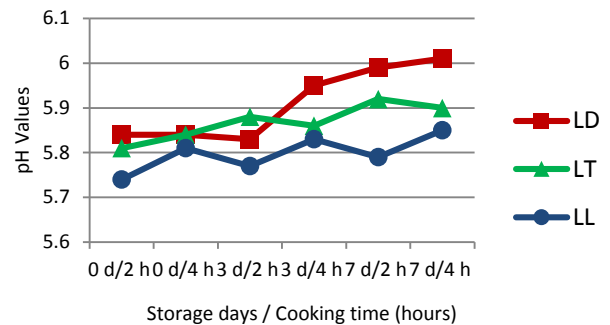


Figure 3. pH values of samples during storage

Table 1. pH, cooking loss, color and WBSF analysis findings of the samples prepared by sous vide method during storage.

Quality	Samples	Heat / Time (hour)	Storage Days			P
			0.	3.	7.	
pH	LD	70 °C/2	5.83±0.00 ^b	5.83±0.04 ^b	5.99±0.00 ^a	0.027*
		70 °C/4	5.84±0.03 ^b	5.94±0.02 ^b	6.00±0.02 ^a	0.049*
	LT	70 °C/2	5.81±0.05	5.87±0.07	5.91±0.03	0.494
		70 °C/4	5.84±0.10	5.86±0.01	5.90±0.03	0.827
	LL	70 °C/2	5.74±0.02	5.77±0.05	5.79±0.00	0.592
		70 °C/4	5.81±0.10	5.83±0.20	5.85±0.25	0.381
Cooking loss (%)	LD	70 °C/2	29.24±0.32	31.65±4.12	34.68±2.44	0.474
		70 °C/4	31.11±0.20	32.16±1.90	32.99±3.79	0.869
	LT	70 °C/2	24.32±0.66	28.70±2.10	23.22±0.86	0.148
		70 °C/4	30.70±0.07	31.70±2.12	26.43±2.68	0.279
	LL	70 °C/2	31.40±0.97	34.72±1.79	29.58±3.47	0.401
		70 °C/4	39.98±2.13	37.99±10.93	29.95±0.41	0.570
L*	LD	70 °C/2	33.45±1.19	37.02±1.91	33.71±1.70	0.143
		70 °C/4	36.00±3.47	39.75±4.87	30.59±3.49	0.310
	LT	70 °C/2	35.79±1.59	35.24±1.19	35.74±1.46	0.962
		70 °C/4	32.28±0.98 ^b	35.23±1.64 ^{ab}	39.44±1.26 ^a	0.003**
	LL	70 °C/2	37.97±0.71 ^b	42.16±0.78 ^a	40.19±1.54 ^{ab}	0.048*
		70 °C/4	37.74±1.05	39.83±1.89	38.85±0.92	0.518
a*	LD	70 °C/2	14.77±0.17 ^a	12.77±0.39 ^b	14.39±0.41 ^a	0.002**
		70 °C/4	13.60±0.36 ^a	9.93±1.21 ^b	14.12±0.52 ^a	0.002**
	LT	70 °C/2	12.92±0.38	11.77±0.54	12.28±0.81	0.429
		70 °C/4	13.13±0.62	13.43±1.68	10.57±0.57	0.051
	LL	70 °C/2	12.08±1.69 ^a	10.00±1.14 ^b	10.66±1.06 ^{ab}	0.046*
		70 °C/4	12.73±0.39 ^a	10.11±0.50 ^b	11.19±0.62 ^{ab}	0.024*
b*	LD	70 °C/2	18.68±0.31	17.44±0.38	16.66±0.81	0.059
		70 °C/4	17.98±0.66	16.64±0.69	16.50±0.19	0.085
	LT	70 °C/2	15.73±0.26	16.78±0.45	16.33±0.79	0.425
		70 °C/4	15.90±0.58	17.94±0.84	17.74±0.64	0.093
	LL	70 °C/2	15.83±0.50	15.98±0.31	16.98±0.24	0.090
		70 °C/4	17.54±0.40	18.16±0.65	18.16±0.82	0.602
WBSF	LD	70 °C/2	29.14±0.41 ^a	25.02±0.37 ^b	30.63±0.99 ^a	0.019*
		70 °C/4	29.84±2.44	24.13±0.00	25.82±2.61	0.279
	LT	70 °C/2	27.08±2.04	33.77±3.08	30.79±1.11	0.255
		70 °C/4	25.20±2.32	29.97±3.21	36.11±0.84	0.100
	LL	70 °C/2	36.54±2.09	33.68±2.58	36.18±0.13	0.582
		70 °C/4	30.36±0.61	36.84±2.21	34.33±3.00	0.254

(Longissimus dorsi, LD; Longissimus lumborum, LL; Longissimus thoracis, LT)

a, b, c: Differences between days with different letters in the same line are important.

(*: p<0,05, **: p<0,01, ***: p<0,001)

During the storage period, it was observed that the cooking loss values in the samples varied between 23.20 - 39.98%. A parallel increase was observed in the loss of cooking values during the storage period in LD (Table 1). Çiçek et al. [17] showed that the cooking loss rates of the meat samples kept in the vacuum package increased during the storage period; they emphasize that the rate of 21.32% on the first day of storage

increased to 27.44% on the last day of storage. Belibağlı and Ersan [18] stated that there was an increase in cooking losses in parallel with the storage time that samples with sous vide method. Most of the cooking loss in the meat occurs as a loss of water in the meat. As many researchers [19, 20, 21, 22] have stated, when the temperature of the meat reaches to 45 - 60 ° C, the fibers begin to shorten, and in 60 - 90°C, the

shortening takes place parallel to the axis of the muscle fibers and water between the muscle fibers leaks out. In this context, it is seen in Figure 4 that the cooking losses increase depending on the cooking time. The fact that the meat samples cooked for longer periods of time had higher cooking loss values than the samples cooked for 2 hours supports this view. There are similar studies [23, 24, 25, 26, 27] indicating that cooking losses are directly related to cooking time and cooking temperature. Zikirov [28] suggested that the cooking loss increased as the cooking time increased, and the cooking loss rates of samples cooked with sous vide method at 2°C and 4 hours at 75°C were 39.15% and 41.98%, respectively. Christensen et al. [24], who stated that the rate of cooking loss increased when they prolong the cooking time by keeping the temperature constant, supports the findings we obtained.

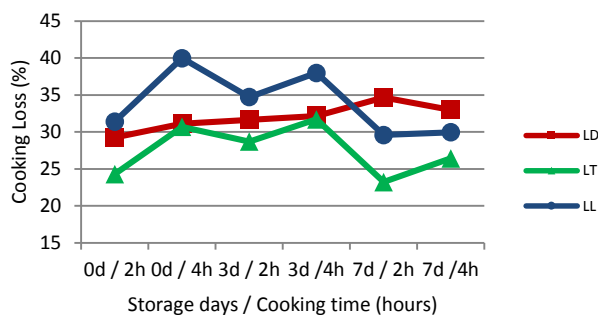


Figure 4. Cooking loss values of samples during storage

One of the important quality criteria for the consumer. Myoglobin, which gives the color of the meat, consists of the protein containing globin and the non-protein part to which the iron element is attached. The color of the meat is due to the oxidation state of iron and the fact that this pigment absorbs and reflects the light of a particular wavelength [29]. In particular, it is known that the surface color of the meat in the storage process varies according to the reaction of myoglobin [30]. However, in this technique, cooking meat in a vacuum bag and stored in the same bag until consumption limits the contact with oxygen. Figure 5 shows that the L * levels of the samples vary between 32, 28 and 42,16 during storage and these values are limited. On the other hand, in respect of statistical, it was found that the differences in the 0, 3 and 7 days of storage of 2 hours of heat treated LL with 4 hours of cooked LT were significant ($p < 0.05$, $p < 0.01$) (Table 1). It is seen that L * values decrease as the cooking time increases in the samples (Figure 5). This may be related to the denaturation levels of meat proteins. Similar results were found by Zikirov [28]. The researcher stated that the L * values (47,18 and 43,09) decreased as the cooking time increased with the sous vide technique for 2 and 4 hours.

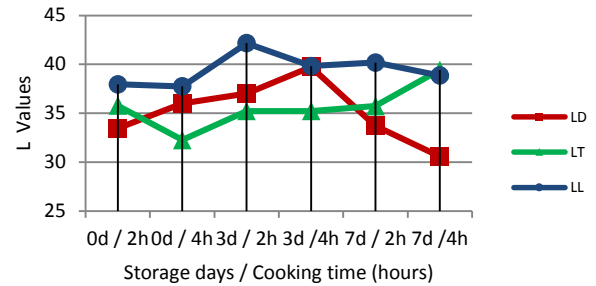


Figure 5. L values of samples during storage

a* values of the samples were determined between 9.93 and 14.77. While the values in days 0 and 7 were similar in LD during the storage period, on the 3rd day, a * values were lower than the other days and this difference was significant ($p < 0.01$). Furthermore, it was found that there was a significant difference ($p < 0,05$) on the 0 and 3 days of storage at the a * values of the LL samples; a * value obtained on the 7th day of storage was similar with the other days (Figure 6, Table 1). The decrease observed in the a * values of the samples during the storage process was also determined by many researchers [25, 31, 32].

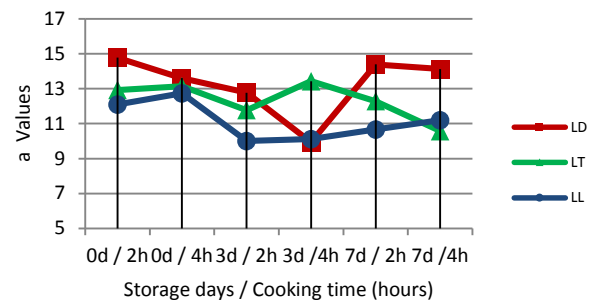


Figure 6. A values of samples during storage

It has been stated that the different heat time parameter is most affected by combinations applied in meat samples cooked with sous vide method [27]. While in our study, the cooking time of LT and LL samples cooked in sous vide method can be correlated with the increase in a * values and loss of cooking values, it may be associated with an increase in light absorbing properties with less water and a darker red color meat[33].

b* values, which were reported to be less effective on meat sensory characteristics and consumers' preference for meat [34], were determined between 15.73 and 18.68. While the b * value in other samples except LD was in an increase trend during storage, it was observed that this situation developed in the opposite direction in LD (Table 1). Çiçek et al. [31] also stated that they observed a decrease in the b * values of the meat samples (13,26 to 6,39) they kept in the vacuum package for a week during their studies. The b* increase

observed in LT and LL samples can be explained by the different amount of oil acting on the chemical composition of these preparations and the chemical and enzymatic changes in the oil [35].

The WBSF values of the samples ranged from 24.13 to 36.84 N, the lowest was LD, and the highest WBSF values were determined as LL samples (Figure 7). It is seen that the firmness ratios in the meat samples during storage are higher in LL and lower in LD. It is thought that the fat content they contain in determining the WBSF values of meat is effective. Thus, LD is softer than other meat because of its minimum meat content. It was determined that the storage time did not have a very determining effect on the WBSF values of meat samples (Figure 7).

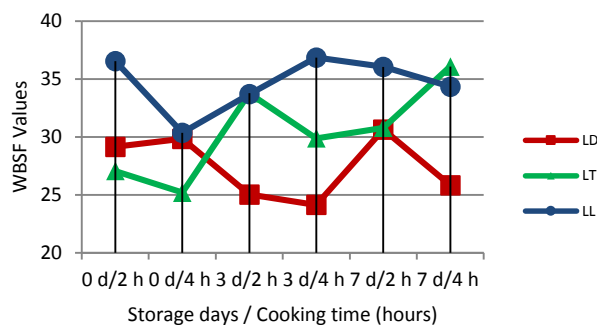


Figure 7. WBSF values of samples during storage

As a result of the analysis carried out during the storage, no live organisms were detected in any sample. This situation can be explained by cooking the meat samples prepared according to the hygienic conditions in accordance with the technique and then with rapid cooling and in suitable storage conditions (2 ± 2 °C). Some researchers [5, 30] reported that 70 °C heat treatment for microbiological safety in sous vide products is effective in the destruction of microorganisms, and rapid cooling after cooking provides protection of microbiological quality. It is further emphasized that the heat time combination applied to the meat and the failure of the cold chain after it are important for the microbiological quality of the product [4, 37]. However, it is also stated by many researchers [4, 15, 38, 39, 40, 41] that the use of vacuum packaging in the sous vide method further restricts the growth of microorganisms in the product and thus longer shelf life is obtained.

In fact, Özdemir and Şireli [42] emphasize that while vacuum packaging decreases the microbiological burden of the products, while *Brochothrix thermosphacta* is detected in only 28% of the vacuumed raw meat products, in majority of the non-vacuumed meat products participated in the study (48%) *B. thermosphacta* bacterium was found.

4. Conclusion

In the samples prepared with sous vide technique and stored for 7 days in the absence of general living microorganisms, sous vide technique is believed to strengthen the reliability of safe food production. However, the heat time combination to be applied should be determined according to the type of meat and hygienic production initial cost of microorganism need to be taken in to account.

During the storage period, the general live microorganism was not detected in the samples, and there was no significant difference between the cooking loss rates and the L* values between 0 and day 7th days of the storage is related to their remaining in the vacuum package during storage. It is thought that the more widespread use of this technique will provide food enterprises with advantages in terms of food safety and fast serviceability.

Note:

This paper is produced from “Comparative Implementation Of Traditional Cooking Methods and Sous Vide Cooking Methods In Different Beef Preparates” PhD thesis titled 16202044, which is supported by SU BAP

References

- [1]. Hecer C. “Et teknolojisinde ambalajlama yöntemleri”. Uludağ Univ. J. Fac. Vet. Med. 1, (2012), 57-61.
- [2]. Balpetek D., Gürbüz Ü. “Use of ohmic heating system in meat thawing and its effects on microbiological quality”. MANAS Journal of Engineering, 6, 2 (2018), 129 – 142.
- [3]. Meyer R.A. “Sous vide technology: American foodservice markets discovering the benefits”. Journal of Restaurant and Foodservice Marketing, 2, (2008), 51-62.
- [4]. Yılmaz H. “Sous vide üretim tekniği kullanılarak hazırlanan macar gulaş yemeğinde mikrobiyolojik kalitenin değerlendirilmesi”. Master Thesis, Gazi Üniv. Ankara, Türkiye, (2014).
- [5]. Haskaraca G., Kolsarıcı N. “Sous vide teknolojisi ve et teknolojisinde uygulama olanakları”. Akademik Gıda Dergisi, 11, 2, (2013), 94-101.
- [6]. Peiretti G.P., Medana C., Visentin S., Dal Bello F., Meineri G., “Effect cooking on carnosine and homologues, pentosidine and thiobarbituric acid-reactive substance content in beef and turkey meat”. Food Chem, 132, (2012), 80-85.
- [7]. Mol Ş., Özturan S. “Sous vide teknolojisi ve su ürünlerindeki uygulamalar”. Journal of Fisheries Sci, 3(1), (2009), 68-75.

- [8]. Lambooji E., Potgieter C.M., Britz C.M., Nortje G.L., Pieterse C. "Effect of electrical and mechanical stunning methods on meat quality in ostriches". *Meat Sci*, 52(3), (1999), 331-337.
- [9]. Li X., Babol J., Wallby A., Lundström K. "Meat quality, microbiological status and consumer preference of beef *gluteus melius* aged in a dry ageing bag or vacuum". *Meat Sci*, 95, (2013), 229-234.
- [10]. Röhrle F.T., Moloney A.P., Osorio M.T., Laciano G., Priolo A., Caplan P., Monahan F.J. "Carotenoid colour and reflectance measurements in bovine adipose tissue to discriminate between beef from different feeding system". *Meat Sci*, 88, (2011), 347-353.
- [11]. Huidobro F.B., Micguel E., Blasquez B., Onega E. "Acomparision between two methods (Warner Bratzler-texture profile analysis) for testing either raw or cooked meat". *Meat Sci*, 69, (2005) 527-536.
- [12]. Food and Drug Administration (FDA) BAM, Bacteriological analytical manual, Aerobic plate count, Chapter 3, January (2001) edition.
- [13]. Özdamar K. Paket programlar ile istatistiksel veri analizi I. Anadolu Üniv. Eskişehir. (1997).
- [14]. Diaz P., Nieto G., Garrido M.D., Banon S. "Microbial, physical-chemical and sensoryspoilage during the refrigerated storage of cooked pork loin processed by the sous vide method". *Meat Sci*, 80(2), (2008) 287-292.
- [15]. Harun F. "Tavuk köftelerinin sous vide yöntemi ile muhafazası". Cumhuriyet Üniv. Fen Bilimleri Ens. Master Thesis. Sivas, Turkey (2012).
- [16]. Feiner G. "Meat products handbook practical science and technology". Cambridge: WoodheadPublishing Limited, (2006) 27-50.
- [17]. Çiçek Ü., Karabıyıklı Ş., Çabuk D., İyiekmekçi B., Cevahiroğlu H. "Vakum ambalajlı olarak soğukta muhafaza edilen dana, kuzu ve tavuk etlerinin bazı fizikokimyasal ve mikrobiyolojik özellikleri." *Gaziosmanpaşa Üniv. Ziraat Fak. Derg.*, 31(1), (2014) 54-62.
- [18]. Belibağlı K.B., Ersan E., "Effects of storage on the quality of sous vide processed lamb liver." *Harran Gıda ve Tarım Bilimleri Dergisi*, 22, (1), (2018) 1-11.
- [19]. Genççelep H., "Et proteinlerinin fonksiyonel özellikleri." *Gıda Teknolojileri Elektronik Dergisi*, 2, (2008) 9-18.
- [20]. Palka K., Daum H. "Change in texture, cooking losses and myofibrillar structure of bovine *M. semitendinosus* during heating". *Meat Sci*, 51, (1999) 237 – 243.
- [21]. Rodriguez-Estralla M.T., Lercker G. "Effecet of different cooking methods on some lipid and protein components of hamburgers". *Meat Sci*, 45(3), (1997) 365-375.
- [22]. Sanchez Del Pulgar J, Gazquez A, Rulz-Carrascal J, "Physico-chemical, textural and structural characteristics of sous-vide cooked pork cheeks as affected by vacuum, cooking temperature and cooking time". *Meat Sci*, 90(3), (2012) 828-835.
- [23]. Becker A., Boulaaba A., Pinggen S., Krischek C., Klein G. "Low temperature cooking of pork meat – physicochemical sensory aspects". *Meat Sci*, 118, (2016) 82-88.
- [24]. Christensen L., Gunvig A., Torngren M.A., Aaslyng M.D., Knochel S., Christensen M. "Sensory characteristics of meat cooked for prolonged times at low temperature". *Meat Sci*, 90, (2012) 485-489.
- [25]. Garcia-Segovia P., Andres-Bello A. Martinez-Monzo J. "Effect of cooking method on mechanical properties, color and structure of beef muscle". *Journal of Food Engineering*, 80, (2007) 813-821.
- [26]. Roldan M., Antequera T., Martin A., Mayoral A.I., Ruiz J. "Effect of different temperature– time combinations on physicochemical, microbiological, textural and structural features of sous-vide cooked lamb loins". *Meat Sci*, 93, (2013) 572-578.
- [27]. Vaudagna S.R., Sanchez G., Neira M.S., Insani E.M., Picallo A.B., Gallinger M.M., Lasta J.A. "Sous vide cooked beef muscles: effects of low temperature-long time (LT-LT) treatments on their quality characteristics and storage stability". *Int. J. of Food and Technology*, 37, (2002) 425-441.
- [28]. Zikirov E, "Sous vide pişirme yönteminin sığır etinde heterosiklik aromatik amin oluşumunu ve bazı kalitatif kriterler üzerine etkileri". Master Thesis. Atatürk Üniv. Erzurum, Türkiye (2014).
- [29]. Taşçı F. "Etlerde meydana gelen renk değişikliği". *Ayrıntı Dergisi*, 4, 47. (2017)
- [30]. Girolami A., Napolitano F., Faraone D., Braghieri A. "Measurement of meat color using a computer system". *Meat Sci*, 93, (2007) 111-118.

- [31]. Çiçek Ü., Karabıyıklı Ş., Kılınçer F.N., Yıldırım A.T., Kurbandurdiyev H., Cevahiroğlu H. "Dana etinin bazı fizikokimyasal ve mikrobiyolojik özellikleri üzerine farklı ambalajlama yöntemleri ve depolama süresinin etkisi". Gaziosmanpaşa Ün. Ziraat Fak. Derg, 30(2), (2013) 62-70.
- [32]. Kahraman H.A. "Kemikli ve kemiksiz sığır kontrfilelerine farklı dinlendirme yöntemlerinin uygulanması ve kalite niteliklerinin belirlenmesi". Selçuk Ün. Sağlık Bilimler Ens. Doktora Tezi. Konya. (2016).
- [33]. Kim Y.H.B., Hunt M.C. "Advance technology to improve meat color". Ed. Joo ST: Control of Meat Quality Kerala, India: Research Signpost. (2011) p. 31-60.
- [34]. O'Sullivan M.G., Byrne D.V., Martens H., Gidskehang G.H., Andersen H.J., Martens M. "Evaluation of pork colour prediction of visual sensory quality of meat from instrumental and computer vision methods of colour analysis". Meat Sci. 65(2), (2003) 909-918.
- [35]. Renerre M. "Factors involved in the discoloration of beef meat". International Journal of Food Sci, and Tech, 25(6), (1990) 613-630.
- [36]. Sebastia C., Soriano J.M., Iranzo M., Rico H. "Microbiological quality of sous vide cook-chill preserved food at different shelf life". Journal of Food Processing and Preservation, 34, (2009) 964-74.
- [37]. Wang H., Badoni M., Zawadski S., McLeod B., Uttaro B., Yang X. "Effects on beef microflora of a three-step sous vide method". Nurturing Locally, Growing Globally, (2017) 484.
- [38]. Jang J.D., Lee D.S. "Development of a sous vide packaging process dor korean seasoned beef". Food Control, 16(3), (2005) 285-91.
- [39]. Özturan S., "Vakum ambalajda pişirilmiş (sous vide) balıkta kalite ve raf ömrünün belirlenmesi". Yüksek Lisans Tezi. İstanbul Ün. Fen Bilimleri Ens. İstanbul, Türkiye (2009).
- [40]. Shakila R.J., Jeyasekaran G. Vijeyakumar A., Sukumar D. "Microbiological quality of sous vide cook chill fish cakes during chilled storage". International Journal of Food Sci. And Tech, 44 11, (2009) 2120-26.
- [41]. Topal Ş., Pala M., Saygı B. "Sous vide teknolojisinin geleneksel yemeklerimize uygulanması". Gıda/The Journal of Food, 2(2), (1996), 131-144.
- [42]. Özdemir H., Şireli T. "Et ve et ürünlerinde Brochotrix Thermosphacta'nın bulunuşu". Gıda Derg. 26 (2), (2001), 115-120.



Determination of soil pollution derived from polychlorinated biphenyls (PCBs) in Bursa: spatial and temporal variations

Gizem Eker Sanlı^{1,*}, Busra Tandogan²

^{1,*} Department of Environmental Engineering, Faculty of Engineering, Bursa Uludag University, 16059, Nilüfer, Bursa, Turkey, geker@uludag.edu.kg, ORCID: 0000-0002-7175-2942

² Department of Environmental Engineering, Faculty of Engineering, Bursa Uludag University, 16059, Nilüfer, Bursa, Turkey, ORCID: 0000-0003-1629-7796

ABSTRACT

The soil is a natural reservoir and a transporter component of the terrestrial ecosystem for polychlorinated biphenyls (PCBs). The determination of PCBs is important to identify the necessary precautions to be taken. The objective of this study is to determine seasonal and regional PCB variations in the soil in Bursa-Turkey. In this context, soil samples were collected from 19 different points during summer and winter seasons and analyzed by gas chromatography-electron capture detector (GC-ECD) for Σ_{82} PCB. The regional variation of Σ_{82} PCB concentrations was 0.03-85 ng/g dry matter (DM). The highest Σ_{82} PCB concentration was measured at sampling points near the iron-steel plant in both seasons. At all sampling points, Σ_{82} PCB concentrations were higher in winter than those in summer. In general, high-chlorinated homolog groups (>6-CBs) in summer and low-chlorinated homolog groups (<5-CBs) dominated in winter. Also, a significant correlation was found between the heavy species (>5-CBs) and TOC, while no significant correlation was observed between the light species (<5-CBs) and TOC. The Σ_7 PCB range of winter and summer seasons were 0.043-3.87 ng/g DM and 0.02-1.97 ng/g DM, respectively. The average Dutch Σ_7 PCB concentration in winter was 0.735 ± 1.05 ng/g DM, while in summer it was 0.462 ± 0.72 ng/g DM.

ARTICLE INFO

Research article

Received: 03.04.2019

Accepted: 25.04.2019

Keywords:

Bursa soil areas of usage,
PCB homolog groups,
total organic carbon.

*Corresponding author

1. Introduction

Polychlorinated biphenyls (PCBs) are anthropogenic persistent organic pollutants (POPs) that are widespread, toxic, and persistent in the environment and could be transported to large distances [1]. PCBs are aromatic compounds that come into play by bonding of different numbers (1 to 10) of chlorine ions on the biphenyl structure with different configurations (ortho, meta and para). PCBs were widely used for industrial and commercial applications before their production was gradually banned or restricted starting in 1970s [2]. PCBs are among the compounds that have been investigated carefully by researchers due to the threat of living organisms and carcinogenic property [3-7]. Therefore, these pollutants must be removed from any environmental media such as air, water, and soil.

The soil is a natural reservoir for PCBs and a carrier of the terrestrial ecosystem. PCBs are the compounds that

accumulate in the soil and are absorbed by organic materials [8]. The concentration of PCBs in the soil varies depending on some factors such as the structure of the soil (organic matter content etc.), plant species, plant surface areas, environmental conditions (wind direction and intensity, temperature, humidity) [9]. It is known that concentrations of these compounds are generally higher in urban and industrial district soils [3],[5]. PCBs are usually arisen from burning of PCB-containing materials, contaminated water/air, mass transfer in soil/air interactions, waste storage areas, sludge drying beds, evaporation from the trash storage areas [1,10]. The PCB homolog group distribution in soil is affected by area properties, industrial characteristics, emission source and distance from this source. On the other hand, PCB distributions in soil might ensure information about pollution sources and the transport of PCBs at this distance. However, if there are various PCB sources in the sampling

area, it is difficult to establish a clear relationship between homolog groups and sources.

Various restrictions were introduced to control the PCB levels around the world [11-14]. Several studies have been carried out to determine the PCB pollution level in soils in different countries. These countries include Norway [15], Spain [16], Sweden [9], France [17], Czech Republic [18], the United Kingdom [19] and Russia [20]. In our country, studies about PCB levels in soils are limited [3, 21, 22].

Bursa (40° 10' N, 29° 4' E), is an agricultural and industrial center which is one of Turkey's major metropolitan cities with a population of 2,901,396 in Turkey [23]. Intense industrial activities and population growth have led to increased environmental pollution. Bursa is the center of the Turkish automotive industry. Factories of motor vehicle producers, as well as automotive parts producers have been active in the city for decades. Textile and food industries are also strong, as well as fresh and canned food industries being present in the city's organized industrial zones. In the present study, it was aimed to determine concentrations, profiles and homolog distributions of PCB in Bursa at 19 sites over two seasons.

Limited studies have been carried out to find out the effects of PCBs on soil and to determine the PCB pollution in the soil in Bursa-Turkey. Determining the PCB pollution in the industrial soil in Bursa is important because PCB has a mutagenic, carcinogenic effect by reaching to people through the food chain. The study is of scientific importance for evaluating an alternative application for the removal of PCB from soil.

2. Material and methods

2.1. Soil Sampling

The selected 19 sampling points for determining soil pollution were shown in Fig. 1. PCB pollution levels were determined in 5 different land use areas (traffic, industrial, urban, rural, traffic+barbecue+urban). Surface soil samples were collected in winter and summer seasons in 2015. All experiments were made with two repetitions. The composite soil was obtained by mixing samples taken from 4 different points in the surface soil (0-5 cm) within an area of approximately 10 m². Stones and plants were removed from 100-150 g soil, which was then wrapped in aluminum foil and stored in air-tight plastic bags.



Figure 1. Sampling points.

The soil temperature was measured during the sampling. Also, pH, dry matter and total organic carbon (TOC) measurements were performed in the laboratory. The pH of the soil was measured with a Metler Toledo brand pH meter after mixing for 5 minutes and adding 30 mL of purified water to 15 g of soil. Samples were stored at 105 °C for 24 hours to determine dry matter (DM) values. SDM-5000 Shimadzu TOC Analyzer (TOC-V CPN) was used for TOC measurements. The soil was sieved through 2 mm. After a preliminary analysis, PCB concentrations were measured using gas chromatograph-electron capture detector (GC-ECD). Soil temperature (ST), pH, DM and TOC values of the soils were given in Table 1.

Table 1. Seasonal characterization of soil samples.

Sampling Points	ST (°C)		pH		DM (%)		TOC (%)	
	Winter	Summer	Winter	Summer	Winter	Summer	Winter	Summer
1.Traffic	17	33	9.1	8.5	88	88	1.3	4.2
2.Industrial	15	32	8.9	8.4	83	91	2.9	3.9
3.Traffic	6	34	9.5	8.7	93	98	0.6	0.8
4.Urban	6	19	8.6	8.2	78	87	2.7	2.4
5.Urban	8	24	8.2	8.5	85	88	2.6	2.4
6.Urban	12	33	8.4	8.1	86	94	2.5	2.1
7.Urban	12	27	8.5	6.5	87	91	1.0	1.3
8.Traffic	12	34	9.3	8.5	92	90	6.0	1.8
9.T+B+U	16	32	9.4	6.4	94	98	4.8	5.8
10.Industrial	7	30	9.4	8.1	88	93	3.1	4.1
11.Industrial	15	24	8.9	8.6	87	91	2.1	2.8
12.Urban	17	25	8.7	9.0	91	93	1.1	0.8
13.Industrial	16	27	10.1	9.7	88	92	2.7	3.8
14.Industrial	14	29	8.6	9.1	87	93	2.4	1.7
15.Rural	14	35	8.5	8.2	84	97	1.1	0.8
16.Rural	9	28	8.9	9.0	89	92	0.1	0.9
17.Rural	2	21	8.9	8.0	81	93	1.2	1.9
18.Rural	16	23	8.8	7.5	81	95	1.6	1.9
19.Rural	18	27	8.5	8.3	75	93	6.0	5.5

2.2. Extraction and Other Pretreatments

A 30 mL solvent mixture consisting of dichloromethane / petroleum ether (DCM / PE) in volume (1/1: v / v) was added to 10 g soil sample. The samples were shaken at 200 rpm in an orbital shaker for 5 hours and afterward were extracted for 30 minutes in a 35 kHz Bandelin Sonorex brand ultrasonic bath. Then the sample was filtered with a glass fiber filter. Twenty-five mL of a DCM / PE (1/1: v / v) mixture was added to the soil remaining in the bottle and again subjected to extraction (30 minutes), the filtration process was repeated, and the filtrates were combined. Following this, the solvent exchange was performed with a rotary evaporator. The sample was concentrated to 5 mL (30 rpm, 25 °C). Then, 15 mL of hexane (HEX) was added to the sample for solvent exchange, and the volume was again decreased to 5 mL. Then, the volume was reduced to 2 mL under a gentle nitrogen stream. Samples were cleaned and fractionated (PAH, PCB) by passing through a glass column with 3 g deactive silicic acid, 2 g deactive alumina, 1 g active sodium sulfate (Na_2SO_4). The fractionation column was first cleaned to remove possible pollutions by washing with 20 mL DCM and 20 mL PE. 2 mL of sample filtered through the cleaned column and PCBs were collected by adding 25 mL PE. Then, the volume was reduced to 1 mL with a slow stream of nitrogen gas. The samples were stored at -16 °C until analyzed with GC-ECD.

2.3. Quality Assurance / Quality Control

Ten percent of the soil samples were used as field blanks to test any contamination during sample handling and analysis. Then, 5 g Na_2SO_4 was weighed and placed in amber colored bottles to prepare field blanks. All the steps applied to the soil samples have been applied to the blank samples. A PAH surrogate standard was added to each sample (both soil samples and field blanks) to determine recovery efficiencies of the targeted PCB compounds. Average recovery values ranged between 30%-100%. All glass materials used in the laboratory were washed with HEX to prevent contamination after each operation. Limit of detection (LOD) for each PCB type was calculated. The LOD value was calculated as the mean blank mass plus three standard deviations [24]. PCB concentrations less than LOD were not reported in this study.

In this study, it was targeted to identify 82 PCB compounds, which can be listed as follows: PCB #4/10, #9/7, #6, #8/5, #19, #12/13, #18, #15/17, #16/32, #26, #31, #28, #21/53, #22, #45, #52, #47, #49/48, #44, #37/42, #41/64/71, #100, #74, #61/70, #66/95, #91, #56/60, #92, #84, #89/101, #99, #119, #83, #81/87, #86, #85, #135/144, #118, #114/149, #123, #131, #153, #132/105, #138/163, #126, #128, #167, #174, #156/171/202, #172, #180, #200, #170/190, #169, #199, #207, #194, #205, #206. Gas chromatograph analyzes for PCB measurements on the

GC-ECD were performed with the HP 7890A GC- μ ECD (Micro-Electron Capture Detector) (Hewlett-Packard, USA). Temperature program used during the analysis: oven temperature is raised to 70°C (2 min), ramp speed is 25°C / min to 150°C, 3°C / min to 200°C, 8°C / min to 280°C and kept at 280°C for 8 min. The ramp rate is increased from 10°C / min to 300°C and held for 2 min at 300°C. The injector inlet temperature is 250°C and the detector temperature is 320°C. Helium gas as carrier gas and nitrogen gas in high purity were used as a basic gas together with helium. The flow rate of this gas was 1.9 mL / min. DB5-MS (30 m x 0.250 mm x 0.25 μ m) was used as a column [25].

3. Results and discussion

3.1. Comparison of PCB Concentrations in Bursa Soils with Concentrations in Other Countries

Several studies around the world have been carried out to determine the PCB concentrations in soils and results were given below in Table 2. The highest PCB pollution was measured in Washington, USA [26] whereas the lowest one was obtained in Turkey-Hatay (Σ_{41} PCB: 0.18 ng/g) [27]. In the present study, it was determined that the regional Σ_{82} PCB concentrations in Bursa soil were ranged between 0.03-85 ng/g DM. So, the results in this study were comparable with the PCB concentrations obtained in other studies.

Table 2. PCB concentrations in soils around the world.

City, country	Sample number	PCB congener	Total PCB concent. (ng/g DM)	Ref.
Stockholm, Sweden	11	44	2.3-332	[9]
Izmir Turkey	48	41	0.2-805	[21]
Stockholm, Sweden	6	13	0.5-55	[28]
Washington, USA	34	65	260-23000	[26]
Trondheim, Norway	41	31	0.05-22	[29]
Shanghai, China	55	74	0.2-11	[30]
South England	4	30	10-670	[31]
Birmingham, UK	10	9	0.3-81	[32]
Britain	39	209	14-670	[8]
Catalonia, Spain	191	27	0.03-97	[33]
Gdansk, Poland	12	7	2.5-12	[7]
Hong Kong, China	66	7	0.1-9.87	[34]
Toronto, Canada	52	51	0.1-1	[35]
Nepal, South Asia	39	12	0.4-44	[36]
Taiyuan, China	15	144	0.1-4.7	[6]
France	22	7	0.1-150	[17]
Britain	46	37	1.1-1600	[15]
Norway	12	37	5.3-30	[15]
United Kingdom	200	33	0.3-80.6	[19]
Lithuanian	5	7	0.6-24	[37]
Hatay, Turkey	20	41	0.003-0.18	[27]
Izmir Turkey	6	36	4.9-66	[38]
Bursa, Turkey	43	83	0.8-3	[3]
Bursa, Turkey	19	82	0.03-85	This study

PCB concentration in Bursa-Turkey (this study) was found to be similar to those measured in Birmingham-England [32], United Kingdom [19] and Catalonia-Spain [33]. However, these levels were lower than the results in the United Kingdom, USA, France, South England, and Sweden [9,15,17,26,31]. The Σ_{82} PCB concentration in Bursa reached 85 ng/g DM. However, it was the case only at the sampling point 11 (industrial area), and concentrations at the other sampling points were found to be below 20 ng/g DM. Taşdemir et al. [3] investigated 82 PCB compounds in Bursa soil in 2008, and the maximum Σ_{82} PCB amount was five ng/g DM. In the present study and the study by Taşdemir et al. [3] PCB number and some

sampling points were similar (17 points) whereas two sampling points were different. Comparing the results of the two studies, PCB concentrations in Bursa soil have increased in the last seven years. Rapid growth in industrial activities and increasing population in the city might have caused to obtain high PCB concentration in the present study.

There are two limit values for PCBs on the list of pollutant limit values in the Soil Pollution Control and Regulation on Point Source Polluted Land in Turkey [12]. The present results did not exceed the limit values of 0.2 and 6 mg/kg, which are the limits for the "ingestion of soil-skin-based transport route" in the regulation. However, the limit value of 0.003 mg/kg given in "transport route to groundwater" (for dilution factor = 1 and mixtures outside Arochlor 1016) was exceeded. Therefore, there was a risk for sites where the dilution was expected to be low, and the groundwater was close to the earth.

3.2. Spatial and Temporal Variation of PCB Concentrations

The spatial and temporal variation of Σ_{82} PCB concentrations measured during summer and winter seasons were given in Fig. 2. As expected, PCB concentrations at different sampling points varied temporally. Concentration values for Σ_{82} PCB ranged between 0.03-17 ng/g DM (min.-max.) and 1.13-85 ng/g DM (min.-max.) for the summer and winter seasons, respectively. The highest Σ_{82} PCB concentration was measured at the sampling point 11 in both seasons. It was thought that combustion activities in the iron-steel plant were effective in increasing the PCB pollution and the emissions generated during the recycling stages of the dielectric fluids, part metals, condensers, softeners in the casting plant might have transferred to the soil by atmospheric deposition. During winter the number 13 (Kestel) region and during summer the number 14 (Çemtaş) region were the other regions where PCB concentrations were high. It was thought that the industrial activities carried out at these sampling points were effective in increasing PCB concentrations. Previous researchers showed that the risk of PCB pollution and exposure to PCBs in soils close to industrial areas were high especially near iron-steel plants [17,21,22]. Likewise, high PCB concentrations were also measured in the studies conducted around thermal power plants [39, 40].

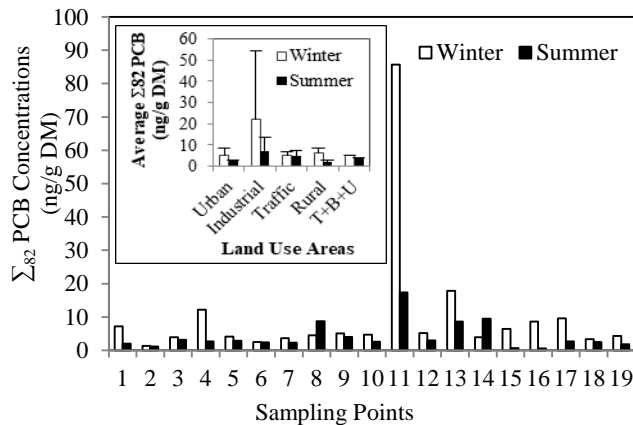


Figure 2. Spatial and temporal variations of PCB concentrations.

The sampling points were divided into five different categories regarding land use areas. Average Σ_{82} PCB concentrations and standard deviation values were provided in the small chart in Fig. 2. PCB concentrations in summer were lower than in winter in all land use areas. Semi-volatile PCB compounds with high vapor pressure were expected to evaporate with increasing temperature. Also, PCB compounds in surface might have photodegraded with sunlight [41]. Similarly, Kurokawa et al. [42] found that PCB concentrations in winter were higher than in the summer. However, in the study conducted by Tasdemir et al. [3] seasonal PCB concentrations in soils did not differ very clearly.

The lowest concentrations were measured in rural areas (1.8 ng/g DM) in summer and traffic + barbecue + urban (T+B+U) area (5.1 ng/g DM) in winter while the maximum PCB pollution was observed in industrial areas in both seasons. In the industrial area, average Σ_{82} PCB concentrations were calculated as 22 ng/g DM in winter and 7.3 ng/g DM in summer. As discussed previously, it was seen that the facilities in the industrial regions were significant PCB sources. In rural areas, the source of PCB pollution was considered to be the transportation an atmospheric deposition from industrial and urban areas located near rural regions [3, 42]. Additionally, in winter possible PCB sources in the direction of the dominant wind may have resulted in higher concentrations than expected in rural areas. In these regions, decreased PCB levels was obtained probably due to evaporation and photolysis in summer [43, 44]. Similar to our study, several researchers found that PCB concentrations in urban areas were higher than those in rural areas [34, 45, 46]. Another source of PCB was found to be exhaust emissions by several researchers [47-51].

3.3. Relationship between PCB Concentrations and TOC

Seasonal TOC values of soil samples were given in Table 1. In the winter season, TOC values ranged from 0.1% (sampling point 16) to 6% (sampling points 8 and 19) with an average value of 2.41%. These values ranged between 0.8% (sampling points 3, 12 and 15) and 5.8% (sampling point 9) during the summer. It was commonly observed that PCB concentrations in environmental media are effected by TOC content, with higher concentrations accompanied by high TOC [33]. In the present study, a relationship between PCB concentrations and TOC was examined by correlation analysis and no significant correlation was found ($r = 0.04$, $p > 0.05$) whereas there was a significant correlation in summer ($r = 0.20$, $p < 0.05$). In addition, the correlation between the Dutch 7 and the TOC content was found to be significant for both seasons (winter: $r = 0.23$, $p < 0.05$, summer: $r = 0.25$, $p < 0.05$). There was no significant correlation between light species (<penta-CB) in winter and summer. However, significant correlations between heavy species (> penta-CB) and TOC were found in summer ($r = 0.26$, $p < 0.05$) and winter ($r = 0.12$, $p < 0.05$). This result showed that TOC content might have affected the accumulation of the heavy PCB congeners in the soils of Bursa. This indicates that the PCB concentrations in the soils can partly be explained by the adsorption of the PCB burden by soil organic fractions as it was observed by [3]. Similar to our results in a previous study [19] a significant relationship was found between soil organic content and 5-, 6-, 7-, 8- and 9-CB except for light PCB groups. Heywood et al. [19] attributed this to the potential for high-chlorinated PCBs to have more relevance to organic carbon than to less chlorinated PCBs. Likewise, [35] found a statistically significant correlation between total PCB and soil organic content. On the other hand, [20] and [52] found no relationship between organic carbon and PCB levels. They partially explained this by the extremely low levels of organic carbon in the soil samples, varying between 0.09 and 0.34% [52].

3.4. Homolog Distributions of PCBs in Soil

PCB compounds with medium molecular weight were detected at high ratios among the PCB types obtained in the soil samples, and these data were comparable with the results of the previous study in the Bursa soil [3]. Fig. 3 showed the temporal variation of the homogeneous distributions of PCBs concentrations measured in soil samples from 19 different points. According to Fig. 3, 5-CB species in winter and 6-CB species in summer were predominant with the concentrations as 22 ± 20 ng/g DM and 17 ± 16 ng/g DM, respectively.

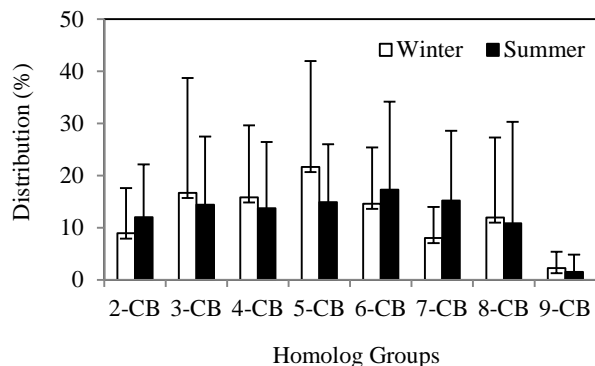


Figure 3. Seasonal variation of PCB homolog groups in Bursa soils.

3-,4-,5-CB species were predominant in winter, while 6-, 7-CB species predominated in summer as seen in Fig. 3. The least homolog group in both seasons was 9-CBs. At 19 sampling points, there were found only four species of the 9-CB in winter and three species of 9-CB in summer. Similar results were obtained in 2008 and 9-CBs were observed in 8 of 43 sampling points [3]. Several researchers found that the homolog distributions of PCBs in the soil can vary. For example, Breivik et al. [2] showed that the 3-,4- and 5-CB species formed 70% of the Σ_{22} PCB concentrations. 3-,4-CB in Harbin-China [53] and 5-, 6-CB were predominant in England soil [15]. Similarly, examinations in Izmir-Turkey [38] and Spain [33] resulted that the 5-, 6-CB PCBs were predominant in the soil. In another study conducted in Taiyuan-China [6], the concentrations of 2-,3-,4-CB were found to be higher.

The percentage of 3-,4-,5-CB light PCB species in summer were lower than in winter. It was estimated that these species were removed from the soil by evaporation and photolysis with increasing temperature [43, 44]. It was emphasized by several researchers that the concentrations of PAHs in the group of semi-volatile organic compounds (SVOCs) such as PCBs were partially removed by photodegradation in the presence of sunlight [54, 55]. It was thought that some of the organic compounds and the PCBs other than targeted PCB species in the soil structure might have been converted to targeted 2-CBs species by photodegradation.

When the homolog distributions according to land use areas were examined 3-,4-,5-,6-,8-,9-CB species predominated in industrial regions in winter while 2-, 7-CB species predominated in the traffic area. Broz et al. [49] showed that there might be more contributions to the level 3- and 4-CB of traffic than other groups. In summer, 3-,4-,6-,8-,9-CB species were dominant in industrial areas, 2-,5-,7-CB species were dominant in the traffic area. In industrial areas, it was seen that the heavier species PCBs deposited to the soil. Similarly, Ren et al. [35] found that

heavy chlorinated PCBs were deposited near sources, while light PCBs were transported over long distances.

3.5. Total Dutch 7 Concentrations in Land Use Areas

Dutch Σ_7 PCBs concentrations in winter and summer seasons in different land use areas were given in Table 3. The molecular weights of the Dutch 7 PCBs (PCB-28, 52, 101, 118, 138, 153 and 180) are 257.54, 291.99, 326.43, 326.43, 360.88, 360.88, 395.32 g/mol (Analytical standard-Sigma Aldrich). The average Dutch Σ_7 PCB concentration in winter was 0.735 ± 1.05 ng/g DM, while it was calculated as 0.462 ± 0.72 ng/g DM in summer. Dutch 7 amounts accounted for 7% of Σ_{82} PCBs in winter and 11% in summer. As mentioned above, the amount of Σ_{82} PCB in winter was higher than those in the summer. However, it was noticed that the percentage of 7 Dutch in winter (%) was less than the amount in summer. This data showed that the evaporation of Dutch 7 group was relatively low in summer.

Table 3. Dutch Σ_7 PCB concentrations in different land use areas.

7 Dutch Species	PCB Concentration (ng/g DM) (Winter)				
	Industrial	Rural	Urban	Traffic	T+U+B
PCB 28	<LOD	<LOD	<LOD	<LOD	<LOD
PCB 52	0.02 ± 0.04	0.4 ± 0.6	0.12 ± 0.21	0.2 ± 0.21	<LOD
PCB 101	<LOD	0.1 ± 0.25	<LOD	<LOD	<LOD
PCB 118	<LOD	<LOD	<LOD	<LOD	<LOD
PCB 138	0.4 ± 0.8	0.09 ± 0.16	0.15 ± 0.33	0.26 ± 0.29	<LOD
PCB 153	<LOD	0.27 ± 0.45	0.07 ± 0.16	0.61 ± 0.55	<LOD
PCB 180	0.6 ± 1.06	0.07 ± 0.14	0.11 ± 0.06	0.24 ± 0.22	0.04 ± 0
7 Dutch Species	PCB Concentration (ng/g DM) (Summer)				
	Industrial	Rural	Urban	Traffic	T+U+B
PCB 28	0.01 ± 0.02	<LOD	<LOD	<LOD	<LOD
PCB 52	0.19 ± 0.34	0.004 ± 0.006	<LOD	0.02 ± 0.016	<LOD
PCB 101	<LOD	<LOD	<LOD	<LOD	<LOD
PCB 118	<LOD	<LOD	<LOD	<LOD	<LOD
PCB 138	0.20 ± 0.24	<LOD	0.06 ± 0.13	0.34 ± 0.41	<LOD
PCB 153	0.16 ± 0.19	0.02 ± 0.05	0.16 ± 0.26	0.12 ± 0.11	<LOD
PCB 180	0.63 ± 0.54	0.02 ± 0.04	0.14 ± 0.27	0.50 ± 0.49	<LOD

Σ_7 PCB range in winter and summer seasons were 0.043-3.87 ng/g DM and 0.02-1.97 ng/g DM, respectively. In previous years, the amount of Σ_7 PCB (0.2-1 ng/g DM) in Bursa soil was at similar levels [3]. Bozlaker et al. [21] measured Σ_7 PCB in an industrial area in Izmir as 0.23-805 ng/g DM. Wang et al. [46] reported that the Σ_7 PCB ranged between 0.14 and 1.00 ng/g DM and the average concentration was 0.57 ng/g DM in Chinese soil. For a total of 6 PCBs (28, 52, 101, 138, 153, 180) measured in Central Germany, the concentration ranged between 0.9-3 ng/g DM and was higher than in Bursa for both seasons [56]. The total average concentration value of 5 PCBs in Glasgow and Torino in European cities was measured between 43-86 ng/g DM [57] and PCB pollution was found to be much higher than in Bursa soil.

4. Conclusions

The present study was conducted to examine seasonal and regional concentrations and homolog of PCBs in Bursa where population and industrial activities are intense. The major results can be listed as follows:

- PCB concentrations in soil ranged between 0.03 and 85 ng/g DM. The highest Σ_{82} PCB concentration in summer and winter season was measured near the iron-steel plant. PCB concentrations in other industrial areas were also high.
- At all sampling points, Σ_{82} PCB concentrations in summer were lower than those in winter.
- In summer, 6-,7-,8- CB species were dominant, while 3-,4-,5- chlorinated species dominated in winter. It was observed that the less chlorinated species evaporated in summer and the lower concentrations measured in the soil.
- At the sampling point 11, Dutch Σ_7 PCB compounds accounted for constituted approximately 20% of the PCBs. In winter, max. Dutch Σ_7 PCBs was 24% at the sampling point 13. In summer, max. Dutch Σ_7 PCB was measured (19%) at sampling point 11.
- There was no significant correlation between TOC and lighter PCB species (<5-CBs) for both seasons. Furthermore, it was found that there was a correlation between heavy PCB species (> 5-CBs) and TOC.
- The results showed that PCB levels did not exceed the legal limit values of 0.2 and 6.0 mg/kg, which are the specified figures for the "ingestion of soil-skin-based transport route" but the limit value of 0.003 mg/kg given for "transport route to groundwater" was exceeded. Therefore, there was a risk for sites where the dilution is expected to be low, and the groundwater is close to the earth considering the highest measured value.

Hazardous/toxic pollutants in the solid and liquid phase as a result of increasing industrial activities cause environmental pollution. The time and amount of soil exposure to these contaminants should be investigated. Suggestions about control of PCB pollution in the environment can be written as follow:

- If wastes from industries are discharged to the soil, they should be identified and checked at regular intervals. Inappropriate discharges should be monitored and prohibited.

- Due to the fact that PCBs are found in the environment for a long time, PCB levels should be measured in equipment such as transformers, capacitors, computers, etc., and these and these devices which are contaminated with PCBs should be stored or disposed of in proper conditions.
- The materials used in the market such as paint and waste oil should be checked regularly and their PCB levels should be minimized.
- Studies should be made to reduce PCB pollution at the source (at home, at work, etc.).

Acknowledgment

We would like to thank Gamze Dindar and Kubra Unal for their selfless laboratory work. Furthermore, we would like to thank Egemen Sakın for performing the PCB measurements with GC-ECD.

References

- [1]. Biterna M., Voutsas, D. "Polychlorinated Biphenyls in Ambient Air of Nw Greece and in Particulate Emissions", *Environment International*, 31, (2005), 671-77.
- [2]. Breivik K., Sweetman A., Pacyna J.M., Jones K.C. "Towards a Global Historical Emission Inventory for Selected PCB Congeners-a Mass Balance Approach. 1. Global Production and Consumption", *Science of the Total Environment*, (2002), 181-98.
- [3]. Taşdemir Y., Aksoy E., Salihoğlu G., Salihoğlu K. "Regional and Seasonal Determination of PCB Distributions and Air / Soil Intersection in the Bursa Soils", *Dept. Environ. Eng., Uludag Univ., Turkey*, (2012).
- [4]. Dönmez B.G. "Investigation of polychlorinated biphenyl (PCB) pollution in soil samples and evaluation of the applicability of legal limit values", *Dept. Environ. Eng., Istanbul Technical Univ., Turkey*, (2012).
- [5]. Batterman S., Chernyak S., Gouden Y., Hayes J., Robins T., Chetty S. "PCBs in Air, Soil and Milk in Industrialized and Urban Areas of Kwazulu-Natal, South Africa", *Environmental Pollution*, 157, (2009), 654-63.
- [6]. Fu S., Cheng H., Liu Y., Yang Z., Xu X. "Spatial Character of Polychlorinated Biphenyls from Soil and Respirable Particulate Matter in Taiyuan, China", *Chemosphere*, 74, (2009), 1477-84.
- [7]. Melnyk A., Dettlaff A., Kuklinska K. "Concentration and Sources of PAHs and PCBs in Surface Soil near a

- Municipal Soil Waste Landfill”, *Science of the Total Environment*, 18-27, (2015), 530-31.
- [8]. Alcock .R.E., Johnston A.E., McGrath S.P., Berrow M.L., Jones K.C. “Long-Term Changes in the Polychlorinated Biphenyl Content of United Kingdom Soils”, *Environmental Science & Technology*, 27, (1993), 1918-23.
- [9]. Backe C., Cousins I.T., Larsson P. “PCB in Soil and Estimated Soil-Air Exchange Fluxes of Selected Pcb Congeners in the South of Sweden”, *Environmental Pollution*, 128, (2004), 59-72.
- [10]. Tasdemir Y., Odabaşı M., Holsen T.M. “Measurement of Vapor Phase Deposition of Polychlorinated Biphenyls (Pcbs) Using a Water Surface Sampler”, *Atmospheric Environment*, 39, (2005), 885-97.
- [11]. Delegation of the European Union to the United States, NW, Washington, DC 20037.
- [12]. Ministry of Environment and Urbanization, General Directorate of Environmental Management "Regulation on the Control of Soil Pollution (SPCR) and the Polluted Site with Point Source", 2012.
- [13]. Ministry of Environment and Urbanization, General Directorate of Environmental Management. "Regulation on Control of Polychlorobiphenyl and Polychlorinated Terphenyls (PCB / PCT)", 2007.
- [14]. United States Environmental Protection Agency (EPA), Washington, DC, 1970.
- [15]. Lead W.A., Steinnes E., Bacon J.R., Jones K.C. "Polychlorinated Biphenyls in UK and Norwegian Soils: Spatial and Temporal Trends", *Science of the Total Environment*, 193, 3, (1997), 229-36.
- [16]. Alonso S. G., Perez-Pastor R.M. "Occurrence of PCBs in ambient air and surface soil in an urban site of Madrid", *Water Air Soil Pollution*, 146, (2003), 283-295.
- [17]. Motelay-Massei A., Ollivon D., Garban B., Teil M.J., Blanchard M., Chevreuil M. "Distribution and Spatial Trends of Pahs and Pcbs in Soils in the Seine River Basin, France", *Chemosphere*, 55, (2004), 555-65.
- [18]. Koblizkova M., Ruzickova P., Cupr P., Komprda J., Holoubek I., Klanova J. "Soil burdens of persistent organic pollutants: their levels, fate, and risks. Part iv. Quantification of volatilization fluxes of organochlorine pesticides and polychlorinated biphenyls from contaminated soil surfaces", *Environmental Science & Technology*, 43, 10, (2009), 3588-95.
- [19]. Heywood E., Wright J., Wienburg C.L., Black H.I.J., Long S.M., Osborn D., Spurgeon D.J. "Factors Influencing the National Distribution of PAH and PCB in British Soils", *Environmental Science and Technology*, 40, 24, (2006), 7629-35.
- [20]. Wilcke W., Krauss M., Safronov G., Fokin A.D., Kaupenjohann M. "Polychlorinated Biphenyls (Pcbs) in Soils of the Moskow Region: Concentrations and Dsmall-Scale Distribution Along an Urban-Rural Transect", *Environmental Pollution*, 141, (2006), 327-35.
- [21]. Bozlaker A., Odabasi M., Muezzinoğlu A. "Dry Deposition and Soil-Air Gas Exchange of Polychlorinated Biphenyls (PCBs) in an Industrial Area", *Environmental Pollution*, 156, (2008), 784-93.
- [22]. Kaya E., Dumanoglu Y., Kara M., Altioğ H., Bayram A., Elbir T., Odabasi M., "Spatial and Temporal Variation and Air-Soil Exchange of Atmospheric Pahs and Pcbs in an Industrial Region", *Atmospheric Pollution Research*, 3, (2012), 435-49.
- [23]. Turkish Statistical Institute, 2016. [Online]. Available: <http://www.tuik.gov.tr>. [Accessed: June, 2017].
- [24]. Eker G. "Spatial Distribution of Polycyclic Aromatic Hydrocarbon (PAH) Concentration in Soils from Bursa, Turkey", *Archives of Environmental Contamination and Toxicology*, 70, (2016), 406-17.
- [25]. Sakin E., Taşdemir Y., "Determination of Atmospheric Pcb Level Variations in Continuously Collected Samples." *Archives of Environmental Contamination and Toxicology*, 71, (2016), 235-45.
- [26]. Vorhees D., Cullen A., Altshul L. "Polychlorinated Biphenyls in House Dust and Yard Soil near a Superfund Site", *Environmental Science & Technology*, 33, (1999), 2151-56.
- [27]. Odabasi M., Bayram A., Elbir T., Seyfioglu M., Dumanoglu Y., Ornektekin S. "Investigation of Soil Concentrations of Persistent Organic Pollutants, Trace Elements and Anions Due to Iron-Steel Plant Emissions in an Industrial Region in Turkey", *Water, Air & Soil Pollution*, 213, 1-4, (2010), 375-88.
- [28]. Armitage J., Hanson M., Axelman J., Cousins I. "Levels and Vertical Distribution of Pcbs in Agricultural and Natural Soils from Sweden", *Science of the total environment*, 371, (2006), 344-52.
- [29]. Meijer N. S., Steinnes E., Ockender A., Jones K. "Influence of Environmental Variables on the Spatial Distribution of PCBs in Norwegian and U.K. Soils: Implications for Global Cycling." *Environmental Science & Technology*, 36, (2002), 2146-53.
- [30]. Jiang Y., Wang X., Zhu K., Wu M., Sheng G., Fu J. "Polychlorinated biphenyls contamination in urban

- soil of Shanghai: Level, compositional profiles and source identification", *Chemosphere*, 83, (2011), 767-773.
- [31]. Harner T., Mackay D. "Model of the Long-Term Exchange of Pcb's between Soil and the Atmosphere in the Southern U.K.", *Environmental Science & Technology*, 29, (1995), 1200-09.
- [32]. Jamshidi A., Hunter S., Hazrati S., Harrad S. "Concentrations and Chiral Signatures of Polychlorinated Biphenyls in Outdoor and indoor Air and Soil in a Major U.K. Conurbation", *Environmental Science & Technology*, 41, (2007), 2153-58.
- [33]. Meijer S.N., Ockenden W.A., Sweetman A., Breivik K., Grimalt J.O., Jones K.C. "Global Distribution and Budget of PCBs and HCB in Background Surface Soils: Implications for Sources and Environmental Processes", *Environmental Science & Technology*, 37, (2003), 667-72.
- [34]. Zhang H.B., Luo Y.M., Wong M.H., Zhao Q.G., Zhang G.L. "Concentrations and Possible Sources of Polychlorinated Biphenyls in the Soils of Hong Kong", *Geoderma*, 138, (2007), 244-51.
- [35]. Ren N., Que M., Li Y., Liu Y., Wan X., Xu D., Sverko E., Ma J. "Polychlorinated Biphenyl in Chinese Surface Soils", *Environmental Science & Technology*, 41, 11, (2007), 3871-76.
- [36]. Aichner B., Glaser B., Zech W. "Polycyclic Aromatic Hydrocarbons and Polychlorinated Biphenyls in Urban Soils from Kathmandu, Nepal", *Organic Geochemistry*, 38, (2007), 700-15.
- [37]. Milukaite A. "Persistent Organic Pollutants in Lithuania: Assessment of Air and Soil Contamination", *Lithuanian Journal of Physics*, 48, 4, (2008), 357-66.
- [38]. Cetin B., Yatkin S., Bayram A., Odabasi M. "Ambient Concentrations and Source Apportionment of PCBs and Trace Elements around an Industrial Area in Izmir, Turkey", *Chemosphere*, 69, (2007), 1267-77.
- [39]. Dumanoglu Y., Gaga E.O., Gungormus E., Sofuoglu S.C., Odabasi M. "Spatial and Seasonal Variations, Sources, Air-Soil Exchange, and Carcinogenic Risk Assessment for PAHs and PCBs in Air and Soil of Kutahya Turkey, the Province of Thermal Power Plants", *Science of the Total Environment*, 580, (2017), 920-35.
- [40]. Zhao X., Zhu W., Huang J., Li M., Gong M. "Emission Characteristics of PCDD/Fs, PAHs and PCBs During the Combustion of Sludge-Coal Water Slurry", *Journal of the Energy Institute* 88, 2, (2015), 105-11.
- [41]. Lin Y., Teng L. S., Lee A., Chen Y.L. "Effect of Photosensitizer Diethylamine on the Photodegradation of PCBs", *Chemosphere*, 55, 6, (2004), 879-84.
- [42]. Kurokawa Y., Matsueda T., Nakamura M., Takada S., Fukamachi K. "Characterization of Non-Ortho Coplanar PCBs, Polychlorinated Dibenzo-P-Dioxins and Dibenzofurans in the Atmosphere", *Chemosphere*, 32, (1996), 491-500.
- [43]. Salihoglu G., Tasdemir Y. "Prediction of the Pcb Pollution in the Soils of Bursa, an Industrial City in Turkey." *Journal of Hazardous Materials*, 164, (2009), 1523-31.
- [44]. Halsall C.J., Gevao B., Howsam M., Lee R.G.M., Ockenden W.A., Jones K.C. "Temperature Dependence of PCBs in the UK Atmosphere", *Atmospheric Environment*, 33, (1999), 541-52.
- [45]. Creaser C.S., Fernandes A.R., Harrad S.J., Hurst T., Cox E.A. "Background Levels of Polychlorinated Biphenyls in British Soils-II", *Chemosphere*, 19, (1989), 1457-66.
- [46]. Wang D., Yang M., Jia H., Zhou L. "Levels, Distributions and Profiles of Polychlorinated Biphenyls in Surface Soils of Dalian, China", *Chemosphere*, 73, 1, (2008), 38-42.
- [47]. Granier L., Chevreuil M. "Automobile Traffic: A Source of PCBs to the Atmosphere", *Chemosphere*, 23, (1991), 785-88.
- [48]. Benfenati E., Valzacchi S., Mariani G., Airoldi L., Fanelli R. "PCDD, PCDF, PCB, PAH, Cadmium and Lead in Roadside Soil: Relationship between Road Distance and Concentration", *Chemosphere*, 24, (1992), 1077-83.
- [49]. Broz J., Grabic R., Kilian J., Lojkasek M., Marklund S., Ocelka T., Pekarek V., Pribyl J., Tydlit V., Vyska J. "The Effects of Oils on PAH, PCDD, PCDF, and PCB Emissions from a Spark Engine Fueled with Leaded Gasoline", *Chemosphere*, 41, (2000), 1905-11.
- [50]. Capuano F., Cavalchi B., Martinelli G., Pecchini G., Renna E., Scaroni I., Bertacchi M., Bigliardi G. "Environmental Prospection for PCDD/PCDF, PAH, PCB and Heavy Metals around the Incinerator Power Plant of Reggio Emilia Town (Northern Italy) and Surrounding Main Roads", *Chemosphere*, 58, (2005), 1563-69.
- [51]. Tian F., Chen J., Oiao X., Cai X., Yang P., Wang Z., Wang D. "Source Identification of Pcd/f's and Pcb's

- in Pine (*Cedrus Deodara*) Needles: A Case Study in Dalian, China", *Atmospheric Environment*, 42, (2008), 4769-77.
- [52]. Klanova J., Matykiewiczova N., Macka Z., Prosek P., Laska K., Klan P. "Persistent Organic Pollutants in Soils and Sediments from James Ross Island, Antarctica", *Environmental Pollution*, 152, (2008), 416-23.
- [53]. Zhang Z., Liu L., Li Y., Wang D., Jia H., Harner T., Sverko E., Wan X., Xu D., Ren N., Ma J., Pozo K. "Analysis of Polychlorinated Biphenyls in Concurrently Sampled Chinese Air and Surface Soil", *Environmental Science and Technology*, 42, (2008), 6514-18.
- [54]. Karaca G., Taşdemir Y. "Removal of Polycyclic Aromatic Hydrocarbons (PAHs) from Industrial Sludges in the Ambient Air Conditions: Automotive Industry", *Journal of Environmental Science and Health: Part A* 48, (2013), 855-61.
- [55]. Oleszczuk P., Baran S. "Optimization of Ultrasonic Extraction of Polycyclic Aromatic Hydrocarbons from Sewage Sludge Samples", *Chemia analityczna*, 48, 2, (2003), 211-21.
- [56]. Manz M., Wenzel K.D., Dietze U., Schüürmann G. "Persistent Organic Pollutants in Agricultural Soils of Central Germany", *Science of the Total Environment*, 277, (2001), 187-98.
- [57]. Cachada A., Lopes L.V., Hursthouse A.S., Biasioli M., Grcman H., Otabbong E., Davidson, C.M., Duarte A.C. "The Variability of Polychlorinated Biphenyls Levels in Urban Soils from Five European Cities", *Environmental Pollution*, 157, (2009), 511-18.

Two-dimensional parabolic problem with a rapidly oscillating free term

Asan Omuraliev¹, Ella Abylaeva^{2,*}

¹ Kyrgyz – Turkish Manas University, Faculty of Science, Department of Applied Mathematics and Informatics, Bishkek, Kyrgyzstan, asan.omuraliev@manas.edu.kg, ORCID:0000-0002-9356-6841

^{2,*} Kyrgyz – Turkish Manas University, Faculty of Science, Department of Applied Mathematics and Informatics, Bishkek, Kyrgyzstan, ella.abylaeva@manas.edu.kg, ORCID: 0000-0002-8680-6675

ABSTRACT

In this paper, it is aimed to construct regularized asymptotics of the solution of a two-dimensional partial differential equation of parabolic type with a small parameter for all spatial derivatives and a rapidly oscillating free term.

The case when the first derivative of the phase of the free term at the initial point vanishes is considered. The two-dimensionality of the equation leads to the existence of a two-dimensional boundary layer. The presence in the free term as a rapidly oscillating factor leads to the inclusion in the asymptotic of the boundary layer with a rapidly oscillating nature of change. Vanishing of the derived phase of the free term leads to the asymptotic of a new type of boundary layer function. A complete asymptotic solution of the problem is constructed by the method of regularization of singularly perturbed problems developed by S.A. Lomov and adapted the authors for singularly perturbed parabolic equations.

ARTICLE INFO

Research article

Received: 13.02.2019

Accepted: 25.04.2019

Keywords:

Asymptotics,
singularly perturbed,
parabolic problem,
oscillating free term.

*Corresponding author

1. Introduction

Singularly perturbed problems with rapidly oscillating free terms were studied in [1-3]. In [5], the solution was found using the regularization method for singularly perturbed problems. The method used in [5] was also exploited for differential equations of parabolic type with a small parameter, where fast-oscillating functions are free members, were studied in [2-3]. The one-dimensional parabolic equation, when the scalar equation contains a free term consisting of a finite sum of rapidly oscillating functions is studied in [4]. In the current paper, a two-dimensional parabolic equation are studied.

The asymptotic of the scalar equation contains a rapidly oscillating, power, parabolic boundary layer function and their product [5], while the asymptotic solution of a multidimensional equation additionally contains a multidimensional boundary layer function.

2. Asymptotic construction

2.1. Statement of the Problem

In this paper, the following problem is studied:

$$L_\varepsilon u(x, t, \varepsilon) \equiv \partial_t u - \varepsilon^2 \Delta_a u - b(x, t)u = f(x, t) \exp\left(\frac{i\theta(t)}{\varepsilon}\right), (x, t) \in E, \quad (1)$$

$$u|_{t=0} = 0, u|_{\partial\Omega} = 0,$$

where $\varepsilon > 0$ – is a small parameter, $x = (x_1, x_2)$, $\Omega = (0 < x_1 < 1) \times (0 < x_2 < 1)$, $E = (0 < t \leq T) \times \Omega$, $\Delta_a \equiv \sum_{l=1}^2 a_l(x_l) \partial_{x_l}^2$.

The problem is solved under the following assumptions:

1. $\forall x_l \in [0, 1]$ the function $a_l(x_l) \in C^\infty[0, 1], l = 1, 2;$
2. $b(x, t), f(x, t) \in C^\infty[E];$
3. $\theta'(0) = 0.$

2.2. Regularization of the Problem

Following the method of regularization of singularly perturbed problems [5-6], along with the independent variables (x, t) we introduce regularizing variables:

$$\begin{aligned} \mu &= \frac{t}{\varepsilon}, \xi_l = \frac{(-1)^{l-1}}{\sqrt{\varepsilon^3}} \int_{l-1}^{x_1} \frac{ds}{\sqrt{a_1(s)}}, \eta_l = \frac{\varphi_l(x_1)}{\varepsilon^2}, \xi_{l+2} = \frac{(-1)^{l-1}}{\sqrt{\varepsilon^3}} \int_{l-1}^{x_2} \frac{ds}{\sqrt{a_2(s)}}, \eta_{l+2} = \frac{\varphi_{l+2}(x_2)}{\varepsilon^3} \\ \sigma &= \int_0^t e^{\frac{i[\theta(s)-\theta(0)]}{\varepsilon}} ds, \tau_2 = \frac{i[\theta(t)-\theta(0)]}{\varepsilon}, \tau_1 = \frac{t}{\varepsilon^2}, \varphi_l(x_r) = (-1)^{l-1} \int_{l-1}^{x_r} \frac{ds}{\sqrt{a_r(s)}} \end{aligned} \tag{2}$$

Instead of the desired function $u(x, t, \varepsilon)$ we study the extended function:

$$\begin{aligned} \tilde{u}(M, \varepsilon), \quad M &= (x, t, \tau, \xi, \eta), \quad \chi = (\tau, \xi, \eta), \quad \tau = (\tau_1, \tau_2), \quad \xi = (\xi_1, \xi_2, \xi_3, \xi_4), \\ \eta &= (\eta_1, \eta_2, \eta_3, \eta_4), \quad \psi(x, t, \varepsilon) = \left(\frac{t}{\varepsilon^2}, \frac{t}{\varepsilon}, \frac{i[\theta(t)-\theta(0)]}{\varepsilon}, \frac{\varphi(x)}{\varepsilon}, \frac{\varphi(x)}{\varepsilon^2} \right), \\ \varphi(x) &= (\varphi_1(x_1), \varphi_2(x_1), \varphi_3(x_2), \varphi_4(x_2)) \end{aligned}$$

such that its restriction by regularizing variables coincides with the desired solution:

$$\tilde{u}(M, \varepsilon)|_{\mu=\psi(x,t,\varepsilon)} \equiv u(x, t, \varepsilon), \tag{3}$$

Taking into account (2) and (3), we find the derivatives:

$$\begin{aligned} \partial_t u &\equiv \left(\partial_t \tilde{u} + \frac{1}{\varepsilon} \partial_\mu \tilde{u} + \frac{1}{\varepsilon^2} \partial_{\tau_1} \tilde{u} + \frac{i\theta'(t)}{\varepsilon} \partial_{\tau_2} \tilde{u} + \exp(\tau_2) \partial_\sigma \tilde{u} \right) |_{\chi=\psi(x,t,\varepsilon)}, \\ \partial_{x_r} u &\equiv \left(\partial_{x_r} \tilde{u} + \sum_{l=2r-1}^{2r} \left[\frac{\varphi_l'(x_r)}{\sqrt{\varepsilon^3}} \partial_{\xi_l} \tilde{u} + \frac{\varphi_l'(x_r)}{\varepsilon^2} \partial_{\eta_l} \tilde{u} \right] \right) |_{\chi=\psi(x,t,\varepsilon)}, \\ \partial_{x_r}^2 u &\equiv \left(\partial_{x_r}^2 \tilde{u} + \sum_{l=2r-1}^{2r} \left[\frac{\varphi_l'^2(x_r)}{\varepsilon^3} \partial_{\xi_l}^2 \tilde{u} + \frac{\varphi_l'^2(x_r)}{\varepsilon^4} \partial_{\eta_l}^2 \tilde{u} \right] \right. \\ &\quad + \sum_{l=2r-1}^{2r} \left[\frac{2\varphi_l'(x_r)}{\sqrt{\varepsilon^3}} \partial_{x_r \xi_l}^2 \tilde{u} + \frac{\varphi_l''(x_r)}{\sqrt{\varepsilon^3}} \partial_{\xi_l} \tilde{u} \right. \\ &\quad \left. \left. + \frac{1}{\varepsilon^2} (\varphi_l'(x_r) \partial_{x_r \eta_l}^2 \tilde{u} + \varphi_l''(x_r) \partial_{\eta_l} \tilde{u}) \right] \right) |_{\chi=\psi(x,t,\varepsilon)}, \end{aligned} \tag{4}$$

Below it is shown that the solution of the iterative problems does not contain terms depending on $(\xi_1, \xi_2), (\xi_3, \xi_4), (\zeta_1, \zeta_2), (\zeta_3, \zeta_4), (\xi_1, \xi_k), l, k = 1, 2.$ Therefore, to simplify the expression, the mixed derivatives of these variables are omitted. Based on (1), (3), (4), for extended function $\tilde{u}(M, \varepsilon)$ set the problem:

$$\tilde{L}_\varepsilon \tilde{u} \equiv \frac{1}{\varepsilon^2} T_0 \tilde{u} + \frac{1}{\varepsilon} i\theta'(t) \partial_{\tau_2} \tilde{u} + \frac{1}{\varepsilon} T_1 \tilde{u} + D_\sigma \tilde{u} - L_\eta \tilde{u} - \sqrt{\varepsilon} L_\xi \tilde{u} - \varepsilon^2 \Delta_a \tilde{u} = f(x, t) \exp\left(\tau_2 + \frac{i\theta(0)}{\varepsilon}\right), \tag{5}$$

$$\tilde{u}|_{t=\tau_1=\tau_2=0} = 0, \quad \tilde{u}|_{x_l=r-1, \xi_k=\eta_k=0} = 0, \quad r = 1, 2, \quad l = 1, 2, \quad k = \overline{1, 4}.$$

$$T_0 \equiv \partial_{\tau_1} - \Delta_\eta, \quad T_1 \equiv \partial_t - \Delta_\xi, \quad D_\sigma \equiv D_t + \exp(\tau_2) \partial_\sigma, \quad D_t \equiv \partial_\mu - b(x, t), \quad L_\eta \equiv \sum_{r=1}^2 \sum_{l=2r-1}^{2r} a_r(x_r) D_{x_r, \eta}^{r, l},$$

$$D_{x,\xi}^{r,l} \equiv [2\varphi'_l(x_r)\partial_{x_r\xi_l}^2 + \varphi''_l(x_r)\partial_{\eta_l}], \Delta_\eta \equiv \sum_{k=1}^4 \partial_{\eta_k}^2, E_1 = E \times (0, \infty)^{10}.$$

The problem (5) is regular in ε as $\varepsilon \rightarrow 0$.

$$(\tilde{L}_\varepsilon \tilde{u})|_{\chi=\psi(x,t,\varepsilon)} \equiv L_\varepsilon u(x, t, \varepsilon). \tag{6}$$

2.3. Solution of Iterative Problems

The solution of problem (5) is determined in the form of a series:

$$\tilde{u}(M, \varepsilon) = \sum_{i=0}^{\infty} \varepsilon^i u_i(M), \tag{7}$$

For the coefficients of this series, the following iterative problems are obtained:

$$\begin{aligned} T_0 u_v(M) &= 0, v = 0, 1, T_0 u_q = -i\theta'(t)\partial_{\tau_2} u_{q-2} - T_1 u_{q-2}, q = 2, 3. \\ T_0 u_4 &= f(x, t) \exp\left(\tau_2 + \frac{i\theta(0)}{\varepsilon}\right) - T_1 u_2 - D_\sigma u_0 + L_\eta u_0, \\ T_0 u_i &= -i\theta'(t)\partial_{\tau_2} u_{i-2} - T_1 u_{i-2} - D_\sigma u_{i-4} + L_\eta u_{i-4} + L_\xi u_{i-5} + \Delta_a u_{i-8}, \\ u_i|_{t=\tau=0} &= 0, u_i|_{x_l=r-1, \xi_k=\eta_k=0} = 0, l, r = 1, 2. k = \overline{1, 4}, \end{aligned} \tag{8}$$

We introduce a class of functions in which the iterative problems are solved:

$$\begin{aligned} U_0 &= \{V_0(N) = [c(x, t) + F_1(N) + F_2(N)] \exp(\tau_2), F_1(N) \in U_4, F_2(N) \in U_5, c(x, t) \in C^\infty(\bar{E})\}, \\ U_1 &= \{V_1(M) : V_1(M) = v(x, t) + F_1(M) + F_2(M), F_1(M) \in U_4, F_2(M) \in U_5, v(x, t) \in C^\infty(\bar{E})\}, \\ U_2 &= \{V_2(M) : V_2(M) = [z(x, t) + F_1(M) + F_2(M)]\sigma, F_1(M) \in U_4, F_2(M) \in U_5, z(x, t) \in C^\infty(\bar{E})\}, \\ U_4 &= \left\{ V_4(M) : V_4(M) = \sum_{l=1}^4 Y^l(N_l), \quad |Y^l(N_l)| < c \exp\left(-\frac{\eta_l^2}{8\tau_1}\right) \right\}, \\ U_5 &= \left\{ V_5(M) : V_5(M) = \sum_{r,l=1}^4 Y^{r+2,l}(N_{r+2,l}), \quad |Y^{r+2,l}(N_{r+2,l})| < c \exp\left(-\frac{|\eta^{r,l}|^2}{8\tau_1}\right), |\eta^{r,l}| = \sqrt{\eta_r^2 + \eta_l^2} \right\}, \end{aligned}$$

From these spaces, a new space is constructed:

$$U = U_0 \oplus U_1 \oplus U_2.$$

The element $u(M) \in U$ has the form:

$$\begin{aligned} u(M) &= v(x, t) + c(x, t) \exp(\tau_2) + z(x, t) \sigma \\ &+ \left[\sum_{l=1}^4 Y^l(N_l) + \sum_{r,l=1}^2 Y^{r+2,l}(N_{r+2,l}) \right] \exp(\tau_2) + \sum_{l=1}^4 w^l(x, t) \operatorname{erfc}\left(\frac{\xi_l}{2\sqrt{\mu}}\right) \\ &+ \sum_{l,r=1}^2 w^{r+2,l}(M_{r+2,l}) + \left[\sum_{l=1}^4 q^l(x, t) \operatorname{erfc}\left(\frac{\xi_l}{2\sqrt{\mu}}\right) + \sum_{l,r=1}^2 z^{r+2,l}(M_{r+2,l}) \right] \sigma, \\ N_l &= (x, t, \tau_1, \eta_l), N_{r+2,l} = (x, t, \tau_1, \eta_l, \eta_{r+2}), M_l = (x, t, \mu, \xi_l), M_{r+2,l} = (x, t, \mu, \xi_l, \xi_{r+2}). \end{aligned} \tag{9}$$

To satisfy this function to the boundary conditions:

$$\begin{aligned}
 v(x, 0) &= -c(x, 0), Y^l(N_l)|_{t=\tau_1=0} = 0, Y^{r+2,l}(N_{r+2,l})|_{t=\tau_1=0} = 0, w^l|_{t=0} = \bar{w}^l(x), \\
 q^l|_{t=0} &= \bar{q}^l(x), w^{r+2,l}(M_{r+2,l})|_{t=\mu=0} = 0, z^{r+2,l}(M_{r+2,l})|_{t=\mu=0} = 0, \\
 w^l(x, t)|_{x_1=l-1} &= -v(l-1, x_2, t), q^l(x, t)|_{x_1=l-1} = -z(l-1, x_2, t), \\
 Y^l|_{x_1=l-1, \eta_l=0} &= -c(l-1, x_2, t), Y^{r+2,l}|_{x_1=l-1, \eta_l=0} = -Y^{r+2,l}(N_{r+2,l})|_{x_1=l-1}, \\
 w^{r+2,l}|_{x_1=l-1, \xi_l=0} &= -w^{r+2}(l-1, x_2, t) \operatorname{erfc}\left(\frac{\xi_{r+2}}{2\sqrt{t}}\right), z^{r+2,l}|_{x_1=l-1, \xi_l=0} \\
 &= -q^{r+2}(l-1, x_2, t) \operatorname{erfc}\left(\frac{\xi_{r+2}}{2\sqrt{t}}\right), \\
 w^l(x, t)|_{x_r=l-1} &= -v(x, t)|_{x_r=l-1}, q^l(x, t)|_{x_r=l-1} = -z(x, t)|_{x_r=l-1}, \\
 Y^{r+2}|_{x_2=l-1, \eta_{r+2}=0} &= -c(x_1, l-1, t), Y^{r+2,l}|_{x_2=l-1, \eta_{r+2}=0} = -Y^l|_{x_2=l-1}, \\
 w^{r+2,l}|_{x_2=l-1, \xi_{r+2}=0} &= -w^l|_{x_2=l-1} \operatorname{erfc}\left(\frac{\xi_l}{2\sqrt{t}}\right), \\
 z^{r+2,l}|_{x_2=l-1, \xi_{r+2}=0} &= -q^l|_{x_2=l-1} \operatorname{erfc}\left(\frac{\xi_l}{2\sqrt{t}}\right), l, r = 1, 2.
 \end{aligned} \tag{10}$$

The action of the operators T_0, T_1, L_η, L_ξ on function $u(M) \in U$ is computed

$$\begin{aligned}
 T_1 u(M) &= \sum_{r,l=1}^2 \{ \partial_\mu w^{r+2,l} - \Delta_\xi w^{r+2,l} + \sigma [\partial_\mu z^{r+2,l} - \Delta_\xi z^{r+2,l}] \}, \\
 L_\eta u &= \sum_{r=1}^2 \sum_{l=2r-1}^{2r} D_{x,\eta}^{r,l} Y^l(N_l) + \sum_{v=1}^2 \sum_{r,l=1}^2 D_{x,\eta}^{v,l} Y^{r+2,l}(N_{r+2,l}), \\
 L_\xi u &= \sum_{r=1}^2 \sum_{l=2r-1}^{2r} D_{x,\xi}^{r,l} w^l(x, t) \operatorname{erfc}\left(\frac{\xi_l}{2\sqrt{\mu}}\right) + \sum_{v=1}^2 \sum_{r,l=1}^2 D_{x,\xi}^{v,l} w^{r+2,l}(M_{r+2,l}) \\
 &\quad + \sigma \left[\sum_{r=1}^2 \sum_{l=2r-1}^{2r} D_{x,\xi}^{r,l} q^l(x, t) \operatorname{erfc}\left(\frac{\xi_l}{2\sqrt{\mu}}\right) + \sum_{v=1}^2 \sum_{r,l=1}^2 D_{x,\xi}^{v,l} z^{r+2,l}(M_{r+2,l}) \right], \\
 D_\sigma u(M) &= D_t v(x, t) + \sum_{l=1}^4 D_t w^l(x, t) \operatorname{erfc}\left(\frac{\xi_l}{2\sqrt{\mu}}\right) \\
 &\quad + \sum_{r,l=1}^2 D_t w^{r+2,l}(M_{r+2,l}) + \left[D_t c(x, t) + \sum_{l=1}^4 D_t Y^l(N_l) + \sum_{r,l=1}^2 D_t Y^{r+2,l}(N_{r+2,l}) \right] \exp(\tau_2) \\
 &\quad + \sigma \left[D_t z(x, t) + \sum_{l=1}^4 D_t q^l(x, t) \operatorname{erfc}\left(\frac{\xi_l}{2\sqrt{\mu}}\right) + \sum_{r,l=1}^2 D_t z^{r+2,l}(M_{r+2,l}) \right] \\
 &\quad + \left[z(x, t) + \sum_{l=1}^4 q^l(x, t) \operatorname{erfc}\left(\frac{\xi_l}{2\sqrt{\mu}}\right) + \sum_{r,l=1}^2 z^{r+2,l}(M_{r+2,l}) \right] \exp(\tau_2).
 \end{aligned}$$

The iterative equations (8) are written in the form:

$$T_0 u(M) = H(M) \tag{11}$$

Theorem 1. Let $H(M) \in U_4 \oplus U_5$ and condition 1) is satisfied. Then the equation (11) is solvable in U , if the equations are solvable:

$$T_0 Y^l(N_l) = H_1(N_l), l = \overline{1,4}, T_0 Y^{r+2,l}(N_{r+2,l}) = H_2(N_{r+2,l}), r, l = 1,2.$$

Theorem 2. Let $H_1(N_l) \in U_4$. Then the problem:

$$\partial_{\tau_1} Y^l(N_l) = \Delta_\eta Y^l(N_l) + H_1(N_l), Y^l(N_l)|_{\tau_1=0} = 0, Y^l(N_l)|_{\eta_l=0} = d^l(x, t), l = \overline{1,4} \tag{12}$$

has a solution $Y^l(N_l) \in U_4$.

Theorem 3. Let be $H_2(N_{r+2,l}) \in U_5, Y^l(N_l) \in U_4$, then the problem $\partial_{\tau_1} Y^{r+2,l}(N_{r+2,l}) = \Delta_\eta Y^{r+2,l}(N_{r+2,l}) + H_2(N_{r+2,l}), Y^{r+2,l}(N_{r+2,l})|_{\eta_l=0} = -Y^{r+2,l}(N_{r+2,l}), Y^{r+2,l}(N_{r+2,l})|_{\eta_{r+2}=0} = -Y^l(N_l), r, l = 1,2$ has a solution $Y^{r+2,l}(N_{r+2,l}) \in U_5$.

The proof of these theorems is given in [7].

The equation (8) is homogeneous under $v = 0, 1$. By Theorem 1, it has a solution representable in the form $u_0(M) \in U$ if functions $Y^l(N_l)$ and $Y^{r+2,l}(N_{r+2,l})$ are solutions of the following equations:

$$T_0 Y_v^l(N_l) = 0, T_0 Y_v^{r+2,l}(N_{r+2,l}) = 0.$$

Based on the boundary conditions from (10), the solution is written as:

$$\begin{aligned} Y_v^l(N_l) &= d_v^l(x, t) \operatorname{erfc}\left(\frac{\eta_l}{2\sqrt{\tau_1}}\right), l = 1, 2, 3, 4, \\ Y_v^{r+2,l}(N_{r+2,l}) &= -\int_0^{\tau_1} \int_0^\infty Y_v^l(*) \left[\frac{\partial}{\partial \xi} G(N_l, \xi, \eta, \tau_1 - \tau) \right] |_{\xi=0} d\eta d\tau - \\ &\int_0^t \int_0^\infty Y_v^{r+2,l}(*) \left[\frac{\partial}{\partial \eta} G(N_{r+2,l}, \xi, \eta, \tau_1 - \tau) \right] |_{\eta=0} d\xi d\tau, \end{aligned}$$

where $d^l(x, t)$ is an arbitrary function such as:

$$\begin{aligned} d_v^p(x, t)|_{t=0} &= -\bar{d}_v^p(x), d_v^l(x, t)|_{x_1=l-1} = -c_v(l-1, x_2, t), \\ G(\eta_l, \eta_{r+2,l}, \xi, \eta, \tau_1) &= \frac{1}{4\pi\tau_1} \left\{ \exp\left(-\frac{(\eta_l - \xi)^2}{4\tau_1}\right) - \exp\left(-\frac{(\eta_l + \xi)^2}{4\tau_1}\right) \right\} \left\{ \exp\left(-\frac{(\eta_{r+2} - \eta)^2}{4\tau_1}\right) - \exp\left(-\frac{(\eta_{r+2} + \eta)^2}{4\tau_1}\right) \right\}, \end{aligned} \tag{13}$$

The function $d_v^l(x, t)$ is equal to zero under $t = \tau_1 = 0$, that is, $d_0^l(x, t)|_{t=0} = -\bar{d}_0^l(x)$. Thus, $-\bar{d}_0^l(x)$ can be taken as an arbitrary function and its values under $x_1 = l - 1$ is determined from the second relation.

According to Theorem 2 and Theorem 3, the functions found by the equation (13) satisfy the estimates:

$$|Y_v^l(N_l)| < c \exp\left(-\frac{\eta_l^2}{8\tau_1}\right), |Y_v^{r+2,l}(N_{r+2,l})| < c \exp\left(-\frac{\eta_{r+2}^2 + \eta_l^2}{8\tau_1}\right), r, l = 1,2. \tag{14}$$

Free member of equations (8) under $v = 2,3$ has a form:

$$\begin{aligned}
 F_{v-2}(M) &\equiv T_1 u_{v-2}(M) + i\theta'(t)\partial_\sigma u_{v-2}(M) \\
 &= i\theta'(t) \left[c_{v-2}(x, t) + \sum_{l=1}^4 Y_{v-2}^l(N_l) + \sum_{r,l=1}^2 Y_{v-2}^{r+2,l}(N_{r+2,l}) \right] \exp(\tau_2) \\
 &\quad + \sum_{l,r=1}^2 \{ \partial_\mu w_{v-2}^{r+2,l} - \Delta_\xi w_{v-2}^{r+2,l} + \sigma [\partial_\mu z_{v-2}^{r+2,l} - \Delta_\xi z_{v-2}^{r+2,l}] \}
 \end{aligned}$$

So, that the equation (8), under $v = 2,3$ has a solution in U , we set:

$$c_{v-2}(x, t) = 0, T_1 w_{v-2}^{r+2,l} = 0, T_1 z_{v-2}^{r+2,l} = 0.$$

Solutions of last equations under the boundary conditions from (10) has a form (12) for which estimates of the form (15) is satisfied. For $i=4$, the equation (8) has a free term:

$$\begin{aligned}
 F_4(M) &= -i\theta'(t)\partial_{\tau_2} - T_1 u_2 + f(x, t) \exp\left(\frac{i\theta(0)}{\varepsilon}\right) - D_\sigma u_0 + L_\eta u_0 \\
 &= -i\theta'(t) \left[c_2(x, t) + \sum_{l=1}^4 Y_2^l(N_l) + \sum_{r,l=1}^2 Y_2^{r+2,l}(N_{r+2,l}) \right] \exp(\tau_2) \\
 &\quad - \sum_{l,r=1}^2 [T_0 w_2^{r+2,l}(M_{r+2,l}) + \sigma T_0 z_2^{r+2,l}] - D_t v_0(x, t) \\
 &\quad - \sum_{l=1}^4 D_t w_0^l(x, t) \operatorname{erfc}\left(\frac{\xi_l}{2\sqrt{\mu}}\right) \\
 &\quad - \sum_{l,r=1}^2 D_t w_0^{r+2,l}(x, t) - \exp(\tau_2) \left[\partial_t c_0(x, t) + \sum_{l=1}^4 \partial_t Y_0^l + \sum_{l,r=1}^2 D_t Y_0^{r+2,l} \right] \\
 &\quad - \sigma \left[D_t z_0(x, t) + \sum_{l=1}^4 D_t q_0^l(x, t) \operatorname{erfc}\left(\frac{\xi_l}{2\sqrt{\mu}}\right) + \sum_{r,l=1}^2 D_t z_0^{r+2,l}(M_{r+2,l}) \right] \\
 &\quad - \left[z_0(x, t) + \sum_{l=1}^4 q_0^l(x, t) \operatorname{erfc}\left(\frac{\xi_l}{2\sqrt{\mu}}\right) + \sum_{r,l=1}^2 z_0^{r+2,l}(M_{r+2,l}) \right] \exp(\tau_2) \\
 &\quad + \sum_{r=1}^2 \sum_{l=2r-1}^{2r} D_{x,\xi}^{r,l} w_0^p(x, t) \operatorname{erfc}\left(\frac{\xi_l}{2\sqrt{\mu}}\right) + \sum_{v=1}^2 \sum_{r,l=1}^2 D_{x,\eta}^{v,l} Y_0^{r+2,l}(N_{r+2,l}).
 \end{aligned}$$

Provided that $F_4(M) \in U_4 \oplus U_5$ with regard to $c_v(x, t) = 0, v = 0,1$ we set:

$$\begin{aligned}
 -i\theta'(t)c_2(x, t) + f(x, t) \exp\left(\frac{i\theta(0)}{\varepsilon}\right) - z_0(x, t) &= 0, \\
 D_t v_0(x, t) = 0, D_t z_0(x, t) = 0, D_t Y_0^l(N_l), T_0 w_2^{r+2,l} = 0, T_0 z_2^{r+2,l} = 0, \\
 D_t w_0^l = 0, D_t w_0^{r+2,l} = 0, D_t Y_0^{r+2,l} = 0, D_t q_0^l(x, t) = 0, D_t z_0^{r+2,l}(x, t) = 0, D_{x,\xi}^{r,l} w_0^l(x, t), \\
 = 0, D_{x,\eta}^{v,l} Y_0^{r+2,l} = 0, D_{x,\eta}^{r,l} Y_0^l = 0,
 \end{aligned} \tag{15}$$

then

$$\begin{aligned}
 F_4(M) &= -i\theta'(t) \left[\sum_{l=1}^4 Y_2^l(N_l) + \sum_{r,l=1}^2 Y_2^{r+2,l}(N_{r+2,l}) \right] \exp(\tau_2) \\
 &\quad - \left[\sum_{l=1}^4 q_0^l(x, t) \operatorname{erfc}\left(\frac{\eta_l}{2\sqrt{\tau_2}}\right) + \sum_{r,l=1}^2 z_0^{r+2,l}(N_{r+2,l}) \right] \exp(\tau_2).
 \end{aligned}$$

In the last equation, the transition from the variables $\frac{\xi_l}{2\sqrt{\mu}}$ to the variables $\frac{\eta_l}{2\sqrt{\tau_2}}$ is occurred.

Substitute the value $Y_0^l(N_l) = d_0^l(x, t) \operatorname{erfc}\left(\frac{\eta_l}{2\sqrt{\tau_1}}\right)$ into the equation $D_t Y_0^l(N_l) = 0$, with respect to $d_0^l(x, t)$ we get the equation $D_t d_0^l(x, t) = 0$, which is solved under an arbitrary initial condition $d_0^l(x, t)|_{t=0} = \bar{d}_0^l(x)$. This arbitrary function provides the condition $L_\eta Y_0^l = 0$, therefore $D_{x,\eta} Y_0^l = 0$. Initial condition for this equation is determined from the relation:

$$d_0^l(x, t)|_{x_1=l-1} = -c_0(l-1, x_2, t), d_0^{l+2}(x, t)|_{x_2=l-1} = -c_0(x_1, l-1, t),$$

which is due to (10) and (13). The function $Y_0^{r+2,l}(N_{r+2,l})$ expresses through $Y_0^l(N_l)$ therefore provided that

$$D_t Y_0^{r+2,l} = 0, D_{x,\eta}^{v,l} Y_0^{r+2,l} = 0.$$

The same is true for functions: $w_0^{r+2,l}(M_{r+2,l}), z_0^{r+2,l}(M_{r+2,l})$. In other words, the following relations hold: $D_t w_0^{r+2,l} = 0, D_t z_0^{r+2,l} = 0, D_{x,\xi}^{v,l} w_0^{r+2,l} = 0, D_{x,\xi}^{v,l} z_0^{r+2,l} = 0$.

Solutions of equations with respect to $w_0^{r+2,l}, z_0^{r+2,l}$ under appropriate boundary conditions from (10) are representable as (13) and they are expressed through $w_2^l(x, t), q_2^l(x, t)$. The first equation (16) is solvable if $z_0(x, t)|_{t=0} = f(x, 0) \exp\left(\frac{i\theta(0)}{\varepsilon}\right)$. This ratio is used by the initial condition for the equation $D_t z_0(x, t) = 0$. The remaining equations from (16) are solvable under the initial conditions from (10).

Thus, the main term of the asymptotics is uniquely determined. As can be seen from the representation (9) and the estimates (15), we note that the asymptotics of the solution has a complex structure. In addition to regular members, it contains various boundary layer functions. The boundary layer functions have rapidly oscillating exponential and power type of change of:

$$c(x, t) \exp(\tau_2), \sigma = \int_0^t e^{\frac{i[\theta(s)-\theta(0)]}{\varepsilon}} ds.$$

Parabolic boundary layer functions have an estimate:

$$|Y^l(N_l)| < c \exp\left(-\frac{\eta_l^2}{8\tau_1}\right), \left|w^l(x, t) \operatorname{erfc}\left(\frac{\xi_l}{2\sqrt{\mu}}\right)\right| < c \exp\left(-\frac{\xi_l^2}{8\mu}\right).$$

Multidimensional and angular parabolic boundary layer functions have an estimate:

$$\begin{aligned} |Y^{r+2,l}(N_{r+2,l})| &< c \exp\left(-\frac{\eta_{r+2}^2 + \eta_l^2}{8\tau_1}\right), \\ |w^{r+2,l}(M_{r+2,l})| &< c \exp\left(-\frac{\xi_{r+2}^2 + \xi_l^2}{8\mu}\right). \end{aligned}$$

In addition, the asymptotic contains the product of the above-mentioned boundary layer functions. Repeating the above process, the partial sum is constructed:

$$\tilde{u}_{\varepsilon n}(M) = \sum_{i=0}^n \varepsilon^{\frac{i}{2}} u_i(M) \tag{16}$$

3. Assessment of remainder

Substituting the function $\tilde{u}(M, \varepsilon) = u_{\varepsilon n}(M) + \varepsilon^{n+\frac{1}{2}} R_{\varepsilon n}(M)$ into problem (5), and taking into account the iterative problems of (8), (10), the following problem is obtained for the remainder term:

$$\begin{aligned} R_{\varepsilon n}(M): \tilde{L}_{\varepsilon} R_{\varepsilon n}(M) &= g_n(M, \varepsilon), \\ R_{\varepsilon n}(M)|_{t=0} &= R_{\varepsilon n}(M)|_{x_l=r-1, \xi_r=0, \eta_k} = 0, \\ r &= 1, 2; k = \overline{1, 4}, \end{aligned} \quad (17)$$

where

$$\begin{aligned} g_n(M, \varepsilon) &= -i\theta'(t)\partial_{\tau_2} u_{n-1} - \varepsilon^{\frac{1}{2}} i\theta'(t)\partial_{\tau_2} u_n(M) \\ &- T_1 u_{n-1}(M) - \varepsilon^{\frac{1}{2}} T_1 u_n(M) (D_{\sigma} - L_{\eta}) \sum_{k=0}^3 \varepsilon^{\frac{k}{2}} u_{n-3+k}(M) + L_{\eta} \sum_{k=0}^5 \varepsilon^{\frac{k}{2}} u_{n-5+k}(M) + \Delta_a \sum_{k=0}^7 \varepsilon^{\frac{k}{2}} u_{n-7+k}(M). \end{aligned}$$

We put in both parts (18) $\chi = \psi(x, t, \varepsilon)$ considering (6), with respect to:

$$L_{\varepsilon} R_{\varepsilon n}(x, t, \varepsilon) = g_{\varepsilon n}(x, t, \varepsilon), R_{\varepsilon n}|_{t=0} = 0, R_{\varepsilon n}|_{\partial\Omega=0}.$$

By virtue of the above constructions, the function is $|g_{\varepsilon n}(x, t, \varepsilon)| < c, \forall (x, t) \in \bar{E}$,
Therefore, applying the maximum principle, an estimate is established:

$$|R_{\varepsilon n}(x, t, \varepsilon)| < c.$$

Thus, the following has been proved:

Theorem 5. Suppose that the conditions 1) -3) are satisfied. Then, using the method, presented above, for solving $u(x, t, \varepsilon)$ of the problem (1) a regularized series (7) can be constructed such that $\forall n = 0, 1, 2, \dots$ and for small enough $\varepsilon > 0$ inequality holds.

$$|u(x, t, \varepsilon) - u_{\varepsilon n}(x, t, \varepsilon)| = |R_{\varepsilon n}(x, t, \varepsilon)| < c\varepsilon^{n+\frac{1}{2}},$$

where c is independent of ε .

4. Conclusion

It is shown that the asymptotic solution of the problem has a complex structure. In addition to regular members, it contains various boundary layer functions. The boundary layer functions have rapidly oscillating exponential and power type of change of:

$$c(x, t) \exp(\sigma \tau_2), \sigma = \int_0^t e^{\frac{i[\theta(s)-\theta(0)]}{\varepsilon}} ds.$$

References

- [1]. Feschenko S., Shkil N., Nikolaenko L. "Asymptotic methods in the theory of linear differential equations," Kiev, Naukova Dumka, 1966.
- [2]. Omuraliev A.S., Sadykova D.A. "Regularization of a singularly perturbed parabolic problem with a fast-oscillating right-hand side", Khabarshy –Vestnik of the Kazak National Pedagogical University, 20, (2007), 202-207.
- [3]. Omuraliev A.S., Sheishenova Sh. K. "Asymptotics of the solution of a parabolic problem in the absence of the spectrum of the limit operator and with a rapidly oscillating right-hand side", Investigated on the Integral-Differential Equations, 42, (2010), 122-128.
- [4]. Omuraliev A., Abylaeva E. "Asymptotics of the solution of the parabolic problem with a stationary phase and an additive free member", Manas Journal of Engineering, 6, 2, (2018), 193-202.
- [5]. Lomov S., "Introduction to the general theory of singular perturbations", Moscow, Nauka, 1981.
- [6]. Omuraliev A., "Regularization of a two-dimensional singularly perturbed parabolic problem", Journal of Computational Mathematics and Mathematical Physics, 8, 46, (2006), 1423-1432.
- [7]. Omuraliev A., Imash kyzy M. "Singularly perturbed parabolic problems with multidimensional boundary layers", Differential Equations, 53, 12, (2017), 1616–1630.



Solutions of the system of maximum difference equations

$$x_{n+1} = \max \left\{ \frac{1}{x_{n-3}}, \frac{y_n}{x_n} \right\}; y_{n+1} = \max \left\{ \frac{1}{y_{n-3}}, \frac{x_n}{y_n} \right\}$$

Dağıstan Şimşek^{1,2}, Burak Oğul^{3,*}

¹ Konya Technical University, Faculty of Engineering and Natural Sciences, Department of Industrial Engineering, Konya, Turkey, dsimsek@ktun.edu.tr

² Kyrgyz Turkish Manas University, Faculty of Science, Department of Applied Mathematics and Informatics, Bishkek, Kyrgyzstan, dagistan.simsek@manas.edu.kg

^{3,*} Kyrgyz Turkish Manas University, Graduate School, Bishkek, Kyrgyzstan, burak_1745@hotmail.com, ORCID: 0000-0002-3264-4340

ABSTRACT

The behaviour of the solutions of the following system of difference equations is examined,

$$x_{n+1} = \max \left\{ \frac{1}{x_{n-3}}, \frac{y_n}{x_n} \right\}; y_{n+1} = \max \left\{ \frac{1}{y_{n-3}}, \frac{x_n}{y_n} \right\},$$

where the initial conditions are positive real numbers.

ARTICLE INFO

Research article

Received: 09.02.2019

Accepted: 25.04.2019

Keywords:

Difference equation,
maximum operators,
semicycle.

*Corresponding author

1. Introduction

Latterly, there has been a great concern in studying the periodic nature of nonlinear difference equations. Although difference equations are relatively simple in form, it is, unfortunately, extremely difficult to understand thoroughly the periodic behavior of their solutions. The periodic nature of nonlinear difference equations of the max type has been investigated by many authors. See for example [1-34].

In this paper, we investigated of the solutions of the following system of difference equations

$$x_{n+1} = \max \left\{ \frac{1}{x_{n-3}}, \frac{y_n}{x_n} \right\}; y_{n+1} = \max \left\{ \frac{1}{y_{n-3}}, \frac{x_n}{y_n} \right\} \quad (1)$$

where the initial conditions are positive real numbers.

Definition 1: Let I be an interval of real numbers and let $f : I^{s+1} = I$ be a continuously differentiable function where s is a non-negative integer. Consider the difference equation

$$x_{n+1} = f(x_n, x_{n-1}, \dots, x_{n-s}) \quad (2)$$

with the initial values $x_{-s}, \dots, x_0 \in I$. A point \bar{x} called an equilibrium point of equation.(2) if $\bar{x} = f(\bar{x}, \dots, \bar{x})$.

Definition 2: A positive semicycle of a solutions $\{x_n\}_n^\infty = -s$ of equation (2) consist of a string of terms $\{x_l, x_{l+1}, \dots, x_m\}$ all greater than or equal to equilibrium \bar{x} with $l \geq -s$ and $m \leq \infty$ such that either $l = -s$ or $l > -s$ and $x_{l-1} < \bar{x}$ and either $m = \infty$ or $m < \infty$ and $x_{m+1} < \bar{x}$.

Definition 3: A negative semicycle of a solutions $\{x_n\}_n^\infty = -s$ of equation (2) consist of a string of terms $\{x_l, x_{l+1}, \dots, x_m\}$ all less than or equal to equilibrium \bar{x} with $l \geq -s$ and $m \leq \infty$ such that either $l = -s$ or $l > -s$ and $x_{l-1} \geq \bar{x}$ and either $m = \infty$ or $m \leq \infty$ and $x_{m+1} \geq \bar{x}$.

2. Main results

Let \bar{x} and \bar{y} be the unique positive equilibrium of equation. (1), then clearly,

$$\bar{x} = \max \left\{ \frac{1}{\bar{x}}, \frac{\bar{y}}{\bar{x}} \right\}; \bar{y} = \max \left\{ \frac{1}{\bar{y}}, \frac{\bar{x}}{\bar{y}} \right\}$$

$$\bar{x} = \frac{1}{\bar{x}} \Rightarrow \bar{x}^2 = 1 \Rightarrow \bar{x} = 1,$$

$$\bar{y} = \frac{1}{\bar{y}} \Rightarrow \bar{y}^2 = 1 \Rightarrow \bar{y} = 1,$$

and, we can obtain $\bar{x} = 1$ and $\bar{y} = 1$.

Lemma 1: Assume that,

$$1 < x_{-3} < x_{-2} < x_{-1} < x_0 < y_0 < y_{-3} < y_{-2} < y_{-1}, 1 < x_{-3} < x_{-2} < x_{-1} < x_0 < y_0 < y_{-3} < y_{-1} < y_{-2},$$

$$1 < x_{-3} < x_{-2} < x_{-1} < x_0 < y_0 < y_{-2} < y_{-3} < y_{-1}, 1 < x_{-3} < x_{-2} < x_{-1} < x_0 < y_0 < y_{-2} < y_{-1} < y_{-3},$$

$$1 < x_{-3} < x_{-2} < x_{-1} < x_0 < y_0 < y_{-1} < y_{-2} < y_{-3}, 1 < x_{-3} < x_{-2} < x_{-1} < x_0 < y_0 < y_{-1} < y_{-3} < y_{-2}.$$

Then the following statements are true for the solutions of equation (1):

- a) Every positive semicycle of length one is followed by a negative semicycle of length one for the first four terms.
- b) Every negative semicycle of length one is followed by a positive semicycle of length one for the first four terms.
- c) The last four terms of the solutions are positive.

Proof: Let consider the following initial conditions.

$$1 < x_{-3} < x_{-2} < x_{-1} < x_0 < y_0 < y_{-3} < y_{-2} < y_{-1}, 1 < x_{-3} < x_{-2} < x_{-1} < x_0 < y_0 < y_{-3} < y_{-1} < y_{-2},$$

$$1 < x_{-3} < x_{-2} < x_{-1} < x_0 < y_0 < y_{-2} < y_{-3} < y_{-1}, 1 < x_{-3} < x_{-2} < x_{-1} < x_0 < y_0 < y_{-2} < y_{-1} < y_{-3},$$

$$1 < x_{-3} < x_{-2} < x_{-1} < x_0 < y_0 < y_{-1} < y_{-2} < y_{-3}, 1 < x_{-3} < x_{-2} < x_{-1} < x_0 < y_0 < y_{-1} < y_{-3} < y_{-2}.$$

The solution x_n and y_n can be obtained as follows:

$$x_1 = \max \left\{ \frac{1}{x_{-3}}, \frac{y_0}{x_0} \right\} = \frac{y_0}{x_0} > \bar{x}; \quad y_1 = \max \left\{ \frac{1}{y_{-3}}, \frac{x_0}{y_0} \right\} = \frac{x_0}{y_0} < \bar{y};$$

$$x_2 = \max \left\{ \frac{1}{x_{-2}}, \frac{y_1}{x_1} \right\} = \max \left\{ \frac{1}{x_{-2}}, \frac{x_0^2}{y_0^2} \right\} = \frac{x_0^2}{y_0^2} < \bar{x}; \quad y_2 = \max \left\{ \frac{1}{y_{-2}}, \frac{x_1}{y_1} \right\} = \max \left\{ \frac{1}{y_{-2}}, \frac{y_0^2}{x_0^2} \right\} = \frac{y_0^2}{x_0^2} > \bar{y};$$

$$\begin{aligned}
 x_3 &= \max \left\{ \frac{1}{x_{-1}}, \frac{y_2}{x_2} \right\} = \max \left\{ \frac{1}{x_{-1}}, \frac{y_0^4}{x_0^4} \right\} = \frac{y_0^4}{x_0^4} > \bar{x}; \quad y_3 = \max \left\{ \frac{1}{y_{-1}}, \frac{x_2}{y_2} \right\} = \max \left\{ \frac{1}{y_{-1}}, \frac{x_0^4}{y_0^4} \right\} = \frac{x_0^4}{y_0^4} < \bar{y}; \\
 x_4 &= \max \left\{ \frac{1}{x_0}, \frac{y_3}{x_3} \right\} = \max \left\{ \frac{1}{x_0}, \frac{x_0^8}{y_0^8} \right\} = \frac{x_0^8}{y_0^8} < \bar{x}; \quad y_4 = \max \left\{ \frac{1}{y_0}, \frac{x_3}{y_3} \right\} = \max \left\{ \frac{1}{y_0}, \frac{y_0^8}{x_0^8} \right\} = \frac{y_0^8}{x_0^8} > \bar{y}; \\
 x_5 &= \max \left\{ \frac{1}{x_1}, \frac{y_4}{x_4} \right\} = \max \left\{ \frac{x_0}{y_0}, \frac{y_0^4}{x_0^4} \right\} = \frac{y_0^4}{x_0^4} > \bar{x}; \quad y_5 = \max \left\{ \frac{1}{y_{-1}}, \frac{x_2}{y_2} \right\} = \max \left\{ \frac{y_0}{x_0}, \frac{x_0^7}{y_0^7} \right\} = \frac{y_0}{x_0} > \bar{y}; \\
 x_6 &= \max \left\{ \frac{1}{x_2}, \frac{y_5}{x_5} \right\} = \max \left\{ \frac{y_0^2}{x_0^2}, \frac{x_0^6}{y_0^6} \right\} = \frac{y_0^2}{x_0^2} > \bar{x}; \quad y_6 = \max \left\{ \frac{1}{y_2}, \frac{x_5}{y_5} \right\} = \max \left\{ \frac{x_0^2}{y_0^2}, \frac{y_0^{15}}{x_0^{15}} \right\} = \frac{y_0^{15}}{x_0^{15}} > \bar{y}; \\
 x_7 &= \max \left\{ \frac{1}{x_3}, \frac{y_6}{x_6} \right\} = \max \left\{ \frac{x_0^4}{y_0^4}, \frac{y_0^{13}}{x_0^{13}} \right\} = \frac{y_0^{13}}{x_0^{13}} > \bar{x}; \quad y_7 = \max \left\{ \frac{1}{y_3}, \frac{x_6}{y_6} \right\} = \max \left\{ \frac{y_0^4}{x_0^4}, \frac{x_0^{13}}{y_0^{13}} \right\} = \frac{y_0^4}{x_0^4} > \bar{y}; \\
 x_8 &= \max \left\{ \frac{1}{x_4}, \frac{y_7}{x_7} \right\} = \max \left\{ \frac{y_0^8}{x_0^8}, \frac{x_0^9}{y_0^9} \right\} = \frac{y_0^8}{x_0^8} > \bar{x}; \quad y_8 = \max \left\{ \frac{1}{y_4}, \frac{x_7}{y_7} \right\} = \max \left\{ \frac{x_0^8}{y_0^8}, \frac{y_0^9}{x_0^9} \right\} = \frac{y_0^9}{x_0^9} > \bar{y}; \\
 &\vdots \\
 &\vdots \\
 &\vdots
 \end{aligned}$$

Hence, we obtained:

$$\begin{aligned}
 x_1 &> \bar{x}, x_2 < \bar{x}, x_3 > \bar{x}, x_4 < \bar{x}, x_5 > \bar{x}, x_6 > \bar{x}, x_7 > \bar{x}, x_8 > \bar{x}, x_9 > \bar{x}, \dots \\
 y_1 &< \bar{y}, y_2 > \bar{y}, y_3 < \bar{y}, y_4 > \bar{y}, y_5 > \bar{y}, y_6 > \bar{y}, y_7 > \bar{y}, y_8 > \bar{y}, y_9 < \bar{y}, \dots
 \end{aligned}$$

Hence, the solution x_n, y_n for $n \geq 0$, every positive semicycle consists of one terms for first four terms, every negative semicycle consists of one terms for first four terms. Hence, last four terms of the solutions are positive. The following Lemmas 2, 3 and 4 can be obtained similarly to Lemma 1.

Lemma 2: Assume that,

$$\begin{aligned}
 1 &< x_{-3} < x_{-2} < x_{-1} < x_0 < y_{-3} < y_{-2} < y_{-1} < y_0, \quad 1 < x_{-3} < x_{-2} < x_{-1} < x_0 < y_{-3} < y_{-1} < y_{-2} < y_0, \\
 1 &< x_{-3} < x_{-2} < x_{-1} < x_0 < y_{-2} < y_{-3} < y_{-1} < y_0, \quad 1 < x_{-3} < x_{-2} < x_{-1} < x_0 < y_{-2} < y_{-1} < y_{-3} < y_0, \\
 1 &< x_{-3} < x_{-2} < x_{-1} < x_0 < y_{-1} < y_{-3} < y_{-2} < y_0, \quad 1 < x_{-3} < x_{-2} < x_{-1} < x_0 < y_{-1} < y_{-2} < y_{-3} < y_0, \\
 1 &< x_{-3} < x_{-2} < x_{-1} < x_0 < y_{-3} < y_{-2} < y_0 < y_{-1}, \quad 1 < x_{-3} < x_{-2} < x_{-1} < x_0 < y_{-3} < y_{-1} < y_0 < y_{-2}, \\
 1 &< x_{-3} < x_{-2} < x_{-1} < x_0 < y_{-2} < y_{-3} < y_0 < y_{-1}, \quad 1 < x_{-3} < x_{-2} < x_{-1} < x_0 < y_{-2} < y_{-1} < y_0 < y_{-3}.
 \end{aligned}$$

Then the following statements are true for the solutions of equation (1):

- a) Every positive semicycle of length one is followed by a negative semicycle of length one for the first four terms.
- b) Every negative semicycle of length one is followed by a positive semicycle of length one for the first four terms.
- c) The last four terms of the solutions are positive.

Lemma 3: Assume that,

$$\begin{aligned}
 1 &< x_{-3} < x_{-2} < x_{-1} < x_0 < y_{-3} < y_0 < y_{-1} < y_{-2}, \quad 1 < x_{-3} < x_{-2} < x_{-1} < x_0 < y_{-3} < y_0 < y_{-2} < y_{-1}, \\
 1 &< x_{-3} < x_{-2} < x_{-1} < x_0 < y_{-2} < y_0 < y_{-1} < y_{-3}, \quad 1 < x_{-3} < x_{-2} < x_{-1} < x_0 < y_{-2} < y_0 < y_{-3} < y_{-1}, \\
 1 &< x_{-3} < x_{-2} < x_{-1} < x_0 < y_{-1} < y_0 < y_{-2} < y_{-3}, \quad 1 < x_{-3} < x_{-2} < x_{-1} < x_0 < y_{-1} < y_0 < y_{-3} < y_{-2}.
 \end{aligned}$$

Then the following statements are true for the solutions of equation (1) :

- a) Every positive semicycle of length one is followed by a negative semicycle of length one for the first four terms.
- b) Every negative semicycle of length one is followed by a positive semicycle of length one for the first four terms.
- c) The last four terms of the solutions are positive.

Lemma 4: Assume that,

$$1 < x_{-3} < x_{-2} < x_{-1} < x_0 < y_{-1} < y_{-2} < y_0 < y_{-3}, \quad 1 < x_{-3} < x_{-2} < x_{-1} < x_0 < y_{-1} < y_{-3} < y_0 < y_{-2}.$$

Then the following statements are true for the solutions of equation (1):

- a) Every positive semicycle of length one is followed by a negative semicycle of length one for the first four terms.
- b) Every negative semicycle of length one is followed by a positive semicycle of length one for the first four terms.
- c) The last four terms of the solutions are positive.

Theorem 1: Let (x_n, y_n) be a solution of equation (1) for

$$1 < x_{-3} < x_{-2} < x_{-1} < x_0 < y_0 < y_{-3} < y_{-2} < y_{-1}, \quad 1 < x_{-3} < x_{-2} < x_{-1} < x_0 < y_0 < y_{-3} < y_{-1} < y_{-2}, \\ 1 < x_{-3} < x_{-2} < x_{-1} < x_0 < y_0 < y_{-2} < y_{-3} < y_{-1}, \quad 1 < x_{-3} < x_{-2} < x_{-1} < x_0 < y_0 < y_{-2} < y_{-1} < y_{-3}, \\ 1 < x_{-3} < x_{-2} < x_{-1} < x_0 < y_0 < y_{-1} < y_{-2} < y_{-3}, \quad 1 < x_{-3} < x_{-2} < x_{-1} < x_0 < y_0 < y_{-1} < y_{-3} < y_{-2}.$$

Then for $n = 0, 1, \dots$ we have:

$$x(n) = \left\{ \frac{y_0}{x_0}, \frac{x_0^2}{y_0^2}, \frac{y_0^4}{x_0^4}, \frac{x_0^8}{y_0^8}, \frac{y_0^{16}}{x_0^{16}}, \frac{x_0^2}{y_0^2}, \frac{y_0^{13}}{x_0^8}, \frac{y_0^8}{x_0^8}, \frac{y_0}{x_0}, \frac{x_0^2}{y_0^2}, \frac{y_0^4}{x_0^4}, \frac{x_0^8}{y_0^8}, \frac{y_0^{16}}{x_0^{16}}, \frac{y_0^2}{x_0^2}, \frac{y_0^{13}}{x_0^8}, \frac{y_0^8}{x_0^8}, \dots \right\}, \\ y(n) = \left\{ \frac{x_0}{y_0}, \frac{y_0^2}{x_0^2}, \frac{x_0^4}{y_0^4}, \frac{y_0^8}{x_0^8}, \frac{y_0}{x_0}, \frac{y_0^{15}}{x_0^{15}}, \frac{y_0^4}{x_0^4}, \frac{y_0^9}{x_0^9}, \frac{x_0}{y_0}, \frac{y_0^2}{x_0^2}, \frac{x_0^4}{y_0^4}, \frac{y_0^8}{x_0^8}, \frac{y_0}{x_0}, \frac{y_0^{15}}{x_0^{15}}, \frac{y_0^4}{x_0^4}, \frac{y_0^9}{x_0^9}, \dots \right\}.$$

Proof: We obtain:

$$x_1 = \max \left\{ \frac{1}{x_{-3}}, \frac{y_0}{x_0} \right\} = \frac{y_0}{x_0}; \quad y_1 = \max \left\{ \frac{1}{y_{-3}}, \frac{x_0}{y_0} \right\} = \frac{x_0}{y_0}; \\ x_2 = \max \left\{ \frac{1}{x_{-2}}, \frac{y_1}{x_1} \right\} = \max \left\{ \frac{1}{x_{-2}}, \frac{x_0^2}{y_0^2} \right\} = \frac{x_0^2}{y_0^2}; \quad y_2 = \max \left\{ \frac{1}{y_{-2}}, \frac{x_1}{y_1} \right\} = \max \left\{ \frac{1}{y_{-2}}, \frac{y_0^2}{x_0^2} \right\} = \frac{y_0^2}{x_0^2}; \\ x_3 = \max \left\{ \frac{1}{x_{-1}}, \frac{y_2}{x_2} \right\} = \max \left\{ \frac{1}{x_{-1}}, \frac{y_0^4}{x_0^4} \right\} = \frac{y_0^4}{x_0^4}; \quad y_3 = \max \left\{ \frac{1}{y_{-1}}, \frac{x_2}{y_2} \right\} = \max \left\{ \frac{1}{y_{-1}}, \frac{x_0^4}{y_0^4} \right\} = \frac{x_0^4}{y_0^4}; \\ x_4 = \max \left\{ \frac{1}{x_0}, \frac{y_3}{x_3} \right\} = \max \left\{ \frac{1}{x_0}, \frac{x_0^8}{y_0^8} \right\} = \frac{x_0^8}{y_0^8}; \quad y_4 = \max \left\{ \frac{1}{y_0}, \frac{x_3}{y_3} \right\} = \max \left\{ \frac{1}{y_0}, \frac{y_0^8}{x_0^8} \right\} = \frac{y_0^8}{x_0^8}; \\ x_5 = \max \left\{ \frac{1}{x_1}, \frac{y_4}{x_4} \right\} = \max \left\{ \frac{x_0}{y_0}, \frac{y_0^4}{x_0^4} \right\} = \frac{y_0^{16}}{x_0^{16}}; \quad y_5 = \max \left\{ \frac{1}{y_{-1}}, \frac{x_2}{y_2} \right\} = \max \left\{ \frac{y_0}{x_0}, \frac{x_0^7}{y_0^8} \right\} = \frac{y_0}{x_0}; \\ x_6 = \max \left\{ \frac{1}{x_2}, \frac{y_5}{x_5} \right\} = \max \left\{ \frac{y_0^2}{x_0^2}, \frac{x_0^6}{y_0^7} \right\} = \frac{y_0^2}{x_0^2}; \quad y_6 = \max \left\{ \frac{1}{y_2}, \frac{x_3}{y_3} \right\} = \max \left\{ \frac{x_0^2}{y_0^2}, \frac{y_0^{15}}{x_0^{15}} \right\} = \frac{y_0^{15}}{x_0^{15}};$$

$$\begin{aligned}
 x_7 &= \max \left\{ \frac{1}{x_3}, \frac{y_6}{x_6} \right\} = \max \left\{ \frac{x_0^4}{y_0^4}, \frac{y_0^{13}}{x_0^{13}} \right\} = \frac{y_0^{13}}{x_0^{13}}; & y_7 &= \max \left\{ \frac{1}{y_3}, \frac{x_6}{y_6} \right\} = \max \left\{ \frac{y_0^4}{x_0^4}, \frac{x_0^{13}}{y_0^{13}} \right\} = \frac{y_0^4}{x_0^4}; \\
 x_8 &= \max \left\{ \frac{1}{x_4}, \frac{y_7}{x_7} \right\} = \max \left\{ \frac{y_0^8}{x_0^8}, \frac{x_0^9}{y_0^9} \right\} = \frac{y_0^8}{x_0^8}; & y_8 &= \max \left\{ \frac{1}{y_4}, \frac{x_7}{y_7} \right\} = \max \left\{ \frac{x_0^8}{y_0^8}, \frac{y_0^9}{x_0^9} \right\} = \frac{y_0^9}{x_0^9}; \\
 & & & \vdots \\
 & & & \vdots \\
 & & & \vdots
 \end{aligned}$$

Thus,

$$\begin{aligned}
 x(n) &= \left\{ \frac{y_0}{x_0}, \frac{x_0^2}{y_0^2}, \frac{y_0^4}{x_0^4}, \frac{x_0^8}{y_0^8}, \frac{y_0^{16}}{x_0^{16}}, \frac{y_0^2}{x_0^2}, \frac{y_0^{13}}{x_0^{13}}, \frac{y_0^8}{x_0^8}, \frac{y_0}{x_0}, \frac{x_0^2}{y_0^2}, \frac{y_0^4}{x_0^4}, \frac{x_0^8}{y_0^8}, \frac{y_0^{16}}{x_0^{16}}, \frac{y_0^2}{x_0^2}, \frac{y_0^{13}}{x_0^{13}}, \frac{y_0^8}{x_0^8}, \dots \right\}, \\
 y(n) &= \left\{ \frac{x_0}{y_0}, \frac{y_0^2}{x_0^2}, \frac{x_0^4}{y_0^4}, \frac{y_0^8}{x_0^8}, \frac{y_0}{x_0}, \frac{y_0^{15}}{x_0^{15}}, \frac{y_0^4}{x_0^4}, \frac{y_0^9}{x_0^9}, \frac{x_0}{y_0}, \frac{y_0^2}{x_0^2}, \frac{x_0^4}{y_0^4}, \frac{y_0^8}{x_0^8}, \frac{y_0}{x_0}, \frac{y_0^{15}}{x_0^{15}}, \frac{y_0^4}{x_0^4}, \frac{y_0^9}{x_0^9}, \dots \right\}.
 \end{aligned}$$

the solutions are shown to be 8-period.

The following Theorems 2, 3 and 4 can be obtained similarly to Theorem 1.

Theorem 2: Let (x_n, y_n) be a solution of equation (1) for

$$\begin{aligned}
 &1 < x_{-3} < x_{-2} < x_{-1} < x_0 < y_{-3} < y_{-2} < y_{-1} < y_0, & 1 < x_{-3} < x_{-2} < x_{-1} < x_0 < y_{-3} < y_{-1} < y_{-2} < y_0, \\
 &1 < x_{-3} < x_{-2} < x_{-1} < x_0 < y_{-2} < y_{-3} < y_{-1} < y_0, & 1 < x_{-3} < x_{-2} < x_{-1} < x_0 < y_{-2} < y_{-1} < y_{-3} < y_0, \\
 &1 < x_{-3} < x_{-2} < x_{-1} < x_0 < y_{-1} < y_{-3} < y_{-2} < y_0, & 1 < x_{-3} < x_{-2} < x_{-1} < x_0 < y_{-1} < y_{-2} < y_{-3} < y_0, \\
 &1 < x_{-3} < x_{-2} < x_{-1} < x_0 < y_{-3} < y_{-2} < y_0 < y_{-1}, & 1 < x_{-3} < x_{-2} < x_{-1} < x_0 < y_{-3} < y_{-1} < y_0 < y_{-2}, \\
 &1 < x_{-3} < x_{-2} < x_{-1} < x_0 < y_{-2} < y_{-3} < y_0 < y_{-1}, & 1 < x_{-3} < x_{-2} < x_{-1} < x_0 < y_{-2} < y_{-1} < y_0 < y_{-3}.
 \end{aligned}$$

Then for $n = 0, 1, \dots$ we have:

$$\begin{aligned}
 x(n) &= \left\{ \frac{y_0}{x_0}, \frac{x_0^2}{y_0^2}, \frac{y_0^4}{x_0^4}, \frac{1}{x_0}, \frac{y_0^8}{x_0^8}, \frac{y_0^2}{x_0^2}, \frac{y_0^5}{x_0^5}, x_0, \frac{y_0}{x_0}, \frac{x_0^2}{y_0^2}, \frac{y_0^4}{x_0^4}, \frac{1}{x_0}, \frac{y_0^8}{x_0^8}, \frac{y_0^2}{x_0^2}, \frac{y_0^5}{x_0^5}, x_0, \dots \right\}, \\
 y(n) &= \left\{ \frac{x_0}{y_0}, \frac{y_0^2}{x_0^2}, \frac{x_0^4}{y_0^4}, \frac{y_0^8}{x_0^8}, \frac{y_0}{x_0}, \frac{y_0^7}{x_0^7}, \frac{y_0^4}{x_0^4}, y_0, \frac{x_0}{y_0}, \frac{y_0^2}{x_0^2}, \frac{x_0^4}{y_0^4}, \frac{y_0^8}{x_0^8}, \frac{y_0}{x_0}, \frac{y_0^7}{x_0^7}, \frac{y_0^4}{x_0^4}, y_0, \dots \right\}.
 \end{aligned}$$

Theorem 3: Let (x_n, y_n) be a solution of equation (1) for

$$\begin{aligned}
 &1 < x_{-3} < x_{-2} < x_{-1} < x_0 < y_{-3} < y_0 < y_{-1} < y_{-2}, & 1 < x_{-3} < x_{-2} < x_{-1} < x_0 < y_{-3} < y_0 < y_{-2} < y_{-1}, \\
 &1 < x_{-3} < x_{-2} < x_{-1} < x_0 < y_{-2} < y_0 < y_{-1} < y_{-3}, & 1 < x_{-3} < x_{-2} < x_{-1} < x_0 < y_{-2} < y_0 < y_{-3} < y_{-1}, \\
 &1 < x_{-3} < x_{-2} < x_{-1} < x_0 < y_{-1} < y_0 < y_{-2} < y_{-3}, & 1 < x_{-3} < x_{-2} < x_{-1} < x_0 < y_{-1} < y_0 < y_{-3} < y_{-2}.
 \end{aligned}$$

Then for $n = 0, 1, \dots$ we have:

$$\begin{aligned}
 x(n) &= \left\{ \frac{y_0}{x_0}, \frac{x_0^2}{y_0^2}, \frac{y_0^4}{x_0^4}, \frac{x_0^8}{y_0^8}, \frac{y_0^{16}}{x_0^{16}}, \frac{y_0^2}{x_0^2}, \frac{y_0^{13}}{x_0^{13}}, \frac{y_0^8}{x_0^8}, \frac{y_0}{x_0}, \frac{x_0^2}{y_0^2}, \frac{y_0^4}{x_0^4}, \frac{x_0^8}{y_0^8}, \frac{y_0^{16}}{x_0^{16}}, \frac{y_0^2}{x_0^2}, \frac{y_0^{13}}{x_0^{13}}, \frac{y_0^8}{x_0^8}, \dots \right\}, \\
 y(n) &= \left\{ \frac{x_0}{y_0}, \frac{y_0^2}{x_0^2}, \frac{x_0^4}{y_0^4}, \frac{y_0^8}{x_0^8}, \frac{y_0^{15}}{x_0^{15}}, \frac{y_0^4}{x_0^4}, \frac{y_0^9}{x_0^9}, \frac{x_0}{y_0}, \frac{y_0^2}{x_0^2}, \frac{x_0^4}{y_0^4}, \frac{y_0^8}{x_0^8}, \frac{y_0^{15}}{x_0^{15}}, \frac{y_0^4}{x_0^4}, \frac{y_0^9}{x_0^9}, \frac{x_0}{y_0}, \dots \right\}.
 \end{aligned}$$

Theorem 4: Let (x_n, y_n) be a solution of equation (1) for

$$1 < x_{-3} < x_{-2} < x_{-1} < x_0 < y_{-1} < y_{-2} < y_0 < y_{-3}, \quad 1 < x_{-3} < x_{-2} < x_{-1} < x_0 < y_{-1} < y_{-3} < y_0 < y_{-2}.$$

Then for $n = 0, 1, \dots$ we have:

$$x(n) = \left\{ \frac{y_0}{x_0}, \frac{x_0^2}{y_0^2}, \frac{y_0^4}{x_0^4}, \frac{1}{x_0}, \frac{y_0^8}{x_0^7}, \frac{y_0^2}{x_0^2}, \frac{y_0^5}{x_0^4}; x_0; \frac{y_0}{x_0}, \frac{x_0^2}{y_0^2}, \frac{y_0^4}{x_0^4}, \frac{1}{x_0}, \frac{y_0^8}{x_0^7}, \frac{y_0^2}{x_0^2}, \frac{y_0^5}{x_0^4} x_0; \dots \right\},$$

$$y(n) = \left\{ \frac{x_0}{y_0}, \frac{y_0^2}{x_0^2}, \frac{x_0^4}{y_0^4}, \frac{y_0^8}{x_0^8}, \frac{y_0}{x_0}, \frac{y_0^7}{x_0^6}, \frac{y_0^4}{x_0^4}; y_0; \frac{x_0}{y_0}, \frac{y_0^2}{x_0^2}, \frac{x_0^4}{y_0^4}, \frac{y_0^8}{x_0^8}, \frac{y_0}{x_0}, \frac{y_0^7}{x_0^6}, \frac{y_0^4}{x_0^4}; y_0; \dots \right\}.$$

3. Examples

Example 1: If the initial conditions are selected in accordance with Lemma 1 and Theorem 1;

$$x_{-3} = 3; x_{-2} = 7; x_{-1} = 8; x_0 = 10; y_{-3} = 13; y_{-2} = 17; y_{-1} = 20; y_0 = 12,$$

$$x_n = \{1.2, 0.694444, 2.0736, 0.232568, 18.4884, 1.44, 10.6993, 4.29982,$$

$$1.2, 0.694444, 2.0736, 0.232568, 18.4884, 1.44, 10.6993, 4.29982, \dots\},$$

$$y_n = \{0.833333, 1.44, 0.482253, 4.29982, 1.2, 15.407, 2.0736, 5.15978,$$

$$0.833333, 1.44, 0.482253, 4.29982, 1.2, 15.407, 2.0736, 5.15978, \dots\},$$

solutions are obtained and the graphs of the solutions are shown below.

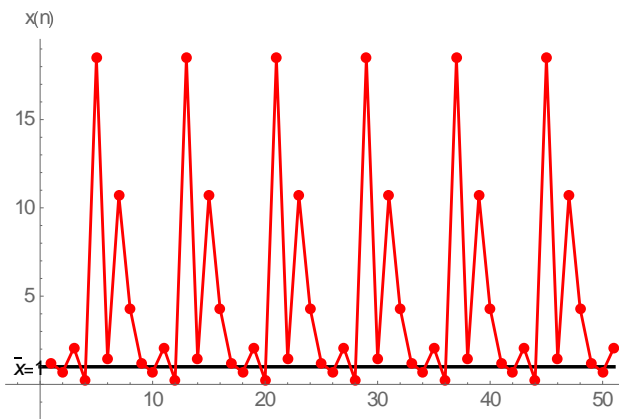


Figure 1. x_n solutions graph.

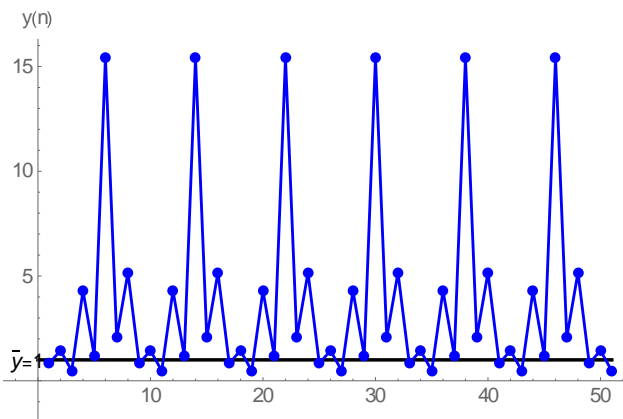


Figure 2. y_n solutions graph.

Example 2: If the initial conditions are selected in accordance with Lemma 2 and Theorem 2;

$$x_{-3} = 12; x_{-2} = 13; x_{-1} = 14; x_0 = 15; y_{-3} = 16; y_{-2} = 17; y_{-1} = 18; y_0 = 19,$$

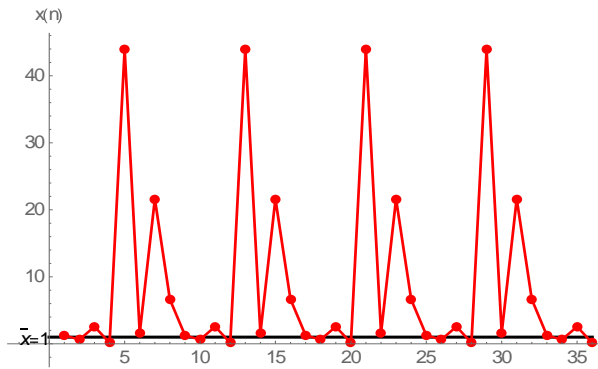
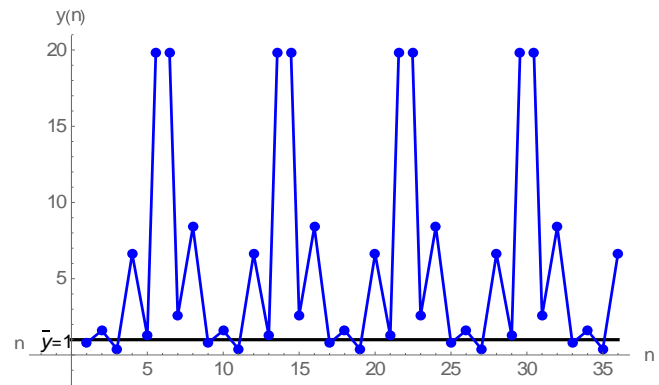
$$x_n = \{1.26667, 0.623269, 2.57424, 0.150904, 43.9134, 1.60444, 21.6078, 6.62672,$$

$$1.26667, 0.623269, 2.57424, 0.150904, 43.9134, 1.60444, 21.6078, 6.62672, \dots\},$$

$$y_n = \{0.789474, 1.60444, 0.388464, 6.62672, 1.26667, 34.6685, 2.57424, 8.39385,$$

$$0.789474, 1.60444, 0.388464, 6.62672, 1.26667, 34.6685, 2.57424, 8.39385, \dots\},$$

solutions are obtained and the graphs of the solutions are shown below.

Figure 3. x_n solutions graph.Figure 4. y_n solutions graph.

References

- [1]. Amleh A.M. "Boundedness Periodicity and Stability of Some Difference Equations", PhD Thesis, University of Rhode Island, (1998).
- [2]. Cinar C., Stevic S., Yalçinkaya I. "On the positive solutions of reciprocal difference equation with minimum", Journal of Applied Mathematics and Computing, 17, (1-2), (2005), 307-314.
- [3]. Elaydi S. "An Introduction to Difference Equations", Springer-Verlag, New York, (1996).
- [4]. Elsayed E.M., Stevic S. "On the max-type equation $x_{n+1} = \max\{A/x_n, x_{n-2}\}$ ", Nonlinear Analysis: Theory, Methods & Applications 71, (3-4), (2009), 910-922.
- [5]. Elsayed E.M., Iricanin B., Stevic S. "On the max-type equation $x_{n+1} = \max\{A_n/x_n, x_{n-1}\}$ ", Ars Combinatoria, 95, (2010), 187-192.
- [6]. Feuer J. "Periodic solutions of the Lyness max equation", Journal of Mathematical Analysis and Applications, 288, (1), (2003), 147-160.
- [7]. Gelişken A., Cinar C., Karataş R. "A note on the periodicity of the Lyness max equation", Advances in Difference Equations, 2008 (1), (2007), 651747.
- [8]. Gelişken A., Cinar C., Yalçinkaya I. "On the periodicity of a difference equation with maximum", Discrete Dynamics in Nature and Society, (2008), 820629.
- [9]. Gelişken A., Cinar C., Kurbanlı A.S. "On the asymptotic behavior and periodic nature of a difference equation with maximum", Computers & mathematics with applications, 59(2), (2010), 898-902.
- [10]. Iricanin B., Elsayed E.M. "On a max-type equation $x_{n+1} = \max\{A/x_n, x_{n-3}\}$ ", Discrete Dynamics in Nature and Society, 2010, (2010), 675413.
- [11]. Kulenevic M.R.S, Ladas G. "Dynamics of Second Order Rational Difference Equations with Open Problems and Conjecture", Boca Raton, London, (2002).
- [12]. Mishev D.P., Patula W.T., Voulov H.D. "A reciprocal difference equation with maximum", Computers & Mathematics with Applications, 43, (2002), 1021-1026.
- [13]. Moybe L.A., Difference Equations with Public Health Applications, New York, USA, (2000).
- [14]. Oğul B., Simsek D. "System Solutions of Difference Equations $x_{n+1} = \max(1/x_{n-4}, y_{n-4}/x_{n-4}), y_{n+1} = \max(1/y_{n-4}, x_{n-4}/y_{n-4})$ ", Kyrgyz State Technical University I. Razzakov Theoretical And Applied Scientific Technical Journal, 1(34), (2015), 202-205.
- [15]. Oğul B., Simsek D. "Maksimumlu Fark Denklem Sisteminin Çözümleri", Manas Journal of Engineering, 3(1), (2015), 35-57.
- [16]. Papaschinopoulos G., Hatzifilippidis V. "On a max difference equation", Journal of Mathematical Analysis and Applications, 258, (2001), 258-268.

- [17]. Papaschinopoulos G., Schinas J., Hatzifilippidis V. "Global behaviour of the solutions of a max-equation and of a system of two max-equation", *Journal of Computational Analysis and Applications*, 5(2), (2003), 237-247.
- [18]. Patula W.T., Voulov H.T. "On a max type recursive relation with periodic coefficients", *Journal of Difference Equations and Applications*, 10(3), (2004), 329-338.
- [19]. Simsek D., Camsitov, "Solutions Of The Maximum Of Difference Equations", *Manas Journal of Engineering*, 6, (2018), 14-25.
- [20]. Simsek D., Cinar C., Yalçinkaya I. "On the solutions of the difference equation $x_{n+1} = \max\{1/x_{n-1}, x_{n-1}\}$ ", *International Journal of Contemporary Mathematical Sciences*, 1(9), (2006), 481-487.
- [21]. Simsek D., Demir B., Kurbanlı A.S. " $x_{n+1} = \max\{(1/x_n), (y_n/x_n)\}$, $y_{n+1} = \max\{(1/y_n), (x_n/y_n)\}$ Denklem Sistemlerinin Çözümleri Üzerine", *Ahmet Keleşoğlu Eğitim Fakültesi Dergisi*, 28, (2009), 91-104.
- [22]. Simsek D., Demir B., Cinar C. "On the Solutions of the System of Difference Equations $x_{n+1} = \max\{(A/x_n), (y_n/x_n)\}$, $y_{n+1} = \max\{(A/y_n), (x_n/y_n)\}$ ", *Discrete Dynamics in Nature and Society*, (2009), 325-296.
- [23]. Simsek D., Kurbanlı A. S., Erdoğan M. E. " $x(n+1) = \max\{1 \setminus x(n-1) ; y(n-1) \setminus x(n-1)\}$; $y(n+1) = \max\{1 \setminus y(n-1) ; x(n-1) \setminus y(n-1)\}$ Fark Denklem Sisteminin Çözümleri", *XXIII. Ulusal Matematik Sempozyumu, Erciyes Üniversitesi*, 153, (2010).
- [24]. Simsek D., Dogan A. "Solutions Of The System Of Maximum Difference Equations", *Manas Journal of Engineering*, 2(2), (2014), 9-22.
- [25]. Simsek D., Erozu M., Oğul B. " $x(n+1) = \max(1/x(n), y(n)/z(n))$, $y(n+1) = \max(1/y(n), z(n)/x(n))$, $z(n+1) = \max(1/z(n), x(n)/y(n))$ Maksimumlu Fark Denklem Sisteminin Çözümleri", *Manas Journal of Engineering*, 4(2), (2016), 11-23.
- [26]. Simsek D., Oğul B. " $x(n+1) = \max(1/x(n-1), y(n)/x(n-3))$, $y(n+1) = \max(1/y(n-1), x(n)/y(n-3))$ Maximum of Difference Equations", *Manas Journal of Engineering*, 5(1), (2017), 14-28.
- [27]. Stefanidou G., Papaschinopoulos G. "The periodic nature of the positive solutions of a nonlinear fuzzy max-difference equation", *Information Sciences*, 176, (2006), 3694-3710.
- [28]. Stević S. "On the recursive sequence $x_{n+1} = \max\{c, x_n^p/x_{n-1}^p\}$ ", *Applied Mathematics Letters*, 21(8), (2008), 791-796.
- [29]. Teixeira C.T. "Existence Stability Boundedness and Periodicity of Some Difference Equations", PhD Thesis, University of Rhode Island, (2000).
- [30]. Valicenti S. "Periodicity and Global Attractivity of Some Difference Equations", PhD Thesis, University of Rhode Island, (1999).
- [31]. Voulov H.D. "On the periodic character of some difference equations", *Journal of Difference Equations and Applications*, (8), (2002), 799-810.
- [32]. Voulov H.D. "Periodic solutions to a difference equation with maximum", *Proceedings of the American Mathematical Society*, 131, (2003), 2155-2160.
- [33]. Yalçinkaya I., Iricanin B.D., Cinar C. "On a max-type difference equation", *Discrete Dynamics in Nature and Society*, (2007), 47264.
- [34]. Yalçinkaya I., Cinar C., Atalay M. "On the solutions of systems of difference equations", *Advances in Difference Equations*, (2008), 143943.